POLITECNICO DI MILANO
DIPARTIMENTO DI ENERGIA

DOCTORAL PROGRAM IN ENERGY AND NUCLEAR SCIENCE AND TECHNOLOGY

XXXII CYCLE (2016-2020)

MAINTENANCE MANAGEMENT BY CONDITION-BASED PRA WITH VOI-BASED OPTIMAL CONDITION MONITORING AND DATA ACQUISITION

(THE PH.D. THESIS)

DOCTORAL DISSERTATION OF: SEYED MOJTABA HOSEYNI

SUPERVISORS: PROF. FRANCESCO DI MAIO
PROF. ENRICO ZIO

TUTOR: PROF. FRANCESCO DI MAIO

COORDINATOR: PROF. VINCENZO DOSSENA

March 2021, Milan

This thesis is dedicated to my parents who sacrificed all their lives and loved their children unconditionally.

To my father, Seyed Reza Hoseyni, who gave me the vision to trust my capabilities and taught me to work hard.

To my mother, Kobra Nouri, who cherished me with love and taught me the way of living and being independent.

Every success I achieved is because of them.

May Allah bless their souls.

ACKNOWLEDGEMENTS

****** To my supervisors and PhD program ******

I would like to express my special appreciation and thanks to my supervisors:

Prof. Francesco Di Maio Prof. Enrico Zio, for their exemplary guidance, great technical supports, numberless insightful discussions throughout the course of this thesis.

I would like to specially thanks Prof. Zio for his friendliness. Besides being a professional supervisor, he was a true friend. He has been always supportive and helpful in my difficult moments of these 4 years.

I would like to express my sincere appreciation and gratitude to the Ph.D. program "Energy and Nuclear Science and Technology" in Department of Energy, Politecnico di Milano, for a four-year hosting.

I would like to thank Politecnico di Milano for awarding me the PhD scholarship, allowing me to pursue the study in Politecnico di Milano as PhD student.

I am grateful to the two anonymous reviewers and the defense committee members, whose comments have allowed improving the thesis significantly.

****** To my family ******

I would like to offer my sincerest and heartful thanks to my parents for giving me love, support and vision. You will always be in my heart.

I am grateful to my family. Thank you the loveliest:

Mohsen, Marziyeh, Elham, Morteza, Baharak and Ayhan.

[This page intentionally left blank.]

ABSTRACT

In the last few decades, the increase of energy demand has not been followed at the same pace by the installation of new energy generation facilities. As a result, the aging worldwide fleet of energy generation facilities will be capable of addressing the demand only if their life is extended. Digitization brings new opportunities for evaluating the viability of life extension and monitoring its effects on reliability and safety, thanks to the intelligent sensoring of Systems, Structures and Components (SSCs) through which monitoring data can be collected and used within risk assessment models to take risk-informed maintenance decisions that enable life extension.

In this context, the objective of the PhD thesis is to develop a computational framework for condition-based risk-informed decision-making, which includes: I. Value of Information (VoI)-based data acquisition, and II. Condition-Based Probabilistic Risk Assessment (CB-PRA) maintenance decision support.

Regarding I, a novel computational approach is introduced to identify the optimal positioning of sensors for condition monitoring of SSCs by VoI. VoI is a utility-based Figure of Merit (FoM), which quantifies the benefits of acquiring information for supporting the maintenance decision-making in a way to guarantee, at the same time, low cost, and valuable information. The VoI-based optimal sensors positioning is achieved by solving an optimization problem that maximizes the VoI among different sets of measurements using three different proposed optimization approaches namely, greedy, non-greedy and Subset Simulation (SS).

In terms of original contributions, the proposed advanced computational framework provides a simulation-based scheme for optimal condition monitoring and data acquisition for maintenance management and decision-making, as well as an innovative approach for developing condition monitoring guidelines, which have been traditionally relying only on operational experience.

With respect to II, an innovative framework is presented which makes use of the optimal condition monitoring data (obtained from I) within an innovative risk assessment framework (i.e., CB-PRA), for prioritizing the risk imposed on SSCs by different degradation mechanisms and taking the most proper decisions on the maintenance strategy to be adopted to control the degradation progression. This allows a proactive lifecycle asset management by allowing the decision-makers to taking real-time decisions on the optimal maintenance strategy for preventing accidents and balancing the maintenance budget expenditure.

The proposed framework of I is applied on a case study regarding the optimal sensors positioning on a Steam Generator (SG) of a Nuclear Power Plant (NPP) that is degrading under creep. Also, a SG Tube Rupture (SGTR) accidental scenario due to multiple degradation mechanisms is considered, to show the benefits gained by applying the framework in II.

KEYWORDS

Value of Information (VoI); Optimization; Sensors Positioning; Bayesian Statistics; Maintenance; Probabilistic Risk Assessment (PRA); Condition-Based PRA (CB-PRA); Condition-based; Risk-informed; Decision-making; Steam Generator (SG); Creep; Greedy Optimization; Non-greedy Optimization; Particle Swarm Optimization (PSO); Genetic Algorithms (GA); Subset Simulation (SS); Markov Chain Monte Carlo; Sub-modularity; Nuclear Power Plant (NPP); Steam Generator Tube Rupture (SGTR); Pitting; Stress Corrosion Cracking (SCC)

SOMMARIO

Negli ultimi decenni, l'aumento della domanda di energia non è stato seguito di pari passo dall'installazione di nuovi impianti di generazione di energia. Di conseguenza, l'invecchiamento della flotta mondiale di impianti di generazione di energia sarà in grado di soddisfare la domanda solo se la vita utile degli impianti esistenti verrà estesa. La digitalizzazione offre nuove opportunità per valutare la fattibilità dell'estensione della vita e monitorare i suoi effetti sull'affidabilità e sulla sicurezza, grazie alla sensorizzazione intelligente di Sistemi, Strutture e Componenti (SSC) attraverso la quale i dati di monitoraggio possono essere raccolti e utilizzati all'interno di modelli di valutazione del rischio per assumersi il rischio decisioni di manutenzione informate che consentono l'estensione della vita utile.

In questo contesto, l'obiettivo della tesi di dottorato è quello di sviluppare un framework computazionale a supporto di un processo decisionale informato, che includa: I. l'acquisizione dei dati basata sul Value of Information (VoI) e II. La presa di decisioni di manutenzione basati sulla sulla valutazione del rischio probabilistico on-condition (Condition Based Probabilisti Risk Assessment).

Per quanto riguarda la parte I, in questa tesi viene introdotto un nuovo approccio computazionale per identificare il posizionamento ottimale dei sensori per il monitoraggio delle condizioni di SSC tramite VoI. VoI è una Figura di Merito (FoM) che quantifica i benefici dell'acquisizione di informazioni per supportare il processo decisionale di manutenzione in modo da garantire, allo stesso tempo, di aver selezionato informazioni di valore al minor costo possibile. Il posizionamento ottimale dei sensori basato su VoI si ottiene risolvendo un problema di ottimizzazione che massimizza il VoI tra diversi set di misurazioni: in questa tesi vengono proposti tre diversi approcci di ottimizzazione per la risoluzione del problema, ovvero algoritmi di ottimizzazione greedy, non-greedy e Subset Simulation (SS).

In termini di contributi originali, il framework computazionale proposto fornisce uno schema basato sulla simulazione per il monitoraggio delle condizioni ottimali e l'acquisizione dei dati per

la gestione della manutenzione e il processo decisionale, nonché un approccio innovativo per lo sviluppo di linee guida per il monitoraggio delle condizioni, che tradizionalmente si sono affidate solo sull'esperienza operativa.

Rispetto alla parte II, in questa tesi viene presentato un framework innovativo che fa uso dei dati di monitoraggio delle condizioni ottimali (ottenuti da I) all'interno di un approccio di valutazione del rischio (chiamato CB-PRA), che consente di individuare le priorità (in termini di rischio) delle SSC, quando esposte a diversi meccanismi di degrado, e di prendere le decisioni più appropriate sulla strategia di manutenzione da adottare per controllare l'andamento del degrado. Ciò consente una gestione proattiva delle risorse del ciclo di vita consentendo ai responsabili di prendere decisioni in tempo reale sulla strategia di manutenzione ottimale per prevenire gli incidenti e bilanciare la spesa del budget di manutenzione.

Il framework proposto I viene applicato a un caso di studio riguardante il posizionamento ottimale dei sensori su un generatore di vapore (SG) di una centrale nucleare (NPP) che degrada a causa di creep. Inoltre, viene considerato uno scenario accidentale SG Tube Rupture (SGTR) dovuto a più meccanismi di degrado, per mostrare i benefici ottenuti applicando il framework in II.

PAROLE CHIAVE

Value of Information (VoI); Ottimizzazione; Posizionamento dei sensori; Statistica Bayesiana; Manutenzione; Probabilistic Risk Assessment (PRA); Condition Based Probabilistic Risk Assessment (CB-PRA); Generatore di vapore (SG); Greedy optimization; Non-greedy optimization; Particle Swarm Optimization (PSO); Algoritmi genetici (GA); Subset Simulation (SS); Markov Chain Monte Carlo; Centrale Nucleare.

CONTENTS

LIST OF TABLES

LIST OF FIGURES

[This page intentionally left blank.]

ABBREVIATIONS

CB-PRA	Condition-Based Probabilistic Risk Assessment
CDF	Core Damage Frequency
ET	Event Tree
FoM	Figure of Merit
FT	Fault Tree
GA	Genetic Algorithm
GP	Gaussian Process
IE	Initiating Event
MLE	Maximum Likelihood Estimation
NDT	Non-Destructive Test
NHPP	Non-Homogeneous Poisson Processes
NPP	Nuclear Power Plant
NRC	US Nuclear Regulatory commission
OD	Operator Depressurization
PDF	Probability Density Function
PFBR	Prototype Fast Breeder Reactor
PRA	Probabilistic Risk Assessment
PSO	Particle Swarm Optimization
PWR	Pressurized Water Reactor
RCS	Reactor Coolant System
RWST	Refill of the Water Storage Tank
SCC	Stress Corrosion Cracking
SG	Steam Generator
SGTR	Steam Generator Tube Rupture
SSC	Systems, Structures, and Component
SS	Subset Simulation
UTS	Ultrasonic Thickness Testing
VoI	Value of Information
WL-CC	Water Lancing and Chemical Cleaning

NOMENCLATURE

F	Random field model
$f(\bar{x})$	Random field at each spatial location $\bar{x}$
$\bar{f}(\bar{x})$	Multivariate random field vector that affect the behavior of the system at each location $\bar{x}$
$\bar{x}$	Location in the spatial domain
$\bar{X}$	Set of locations in the spatial domain Ω_x
$\bar{y}(\bar{x})$	Measurement
$\bar{Y}$	Set of measurements in the spatial domain Ω_y
$\bar{y}(\bar{x}^*)$	Optimal set of measurement
$\bar{y}_n{}^*$	Single sensor location that has the max VoI at the n^{th} iteration of the greedy method
i	Quantity of sensor locations in spatial domain Ω_x
k	Quantity of the realizations of measurement set $\bar{y}(\bar{x})$
$\bar{\varepsilon}$	Noise vector
$\bar{a}$	Action vector
$\bar{s}$	State vector
β	Reliability index
n	Quantity of optimal sensors
n_s	Quantity of sensor locations that share the same uncertainty and geometry
R	Matrix indicating which positions of the random field is observed
r	VoI per sensor
C_I	Coefficient of improvement
Ω_x	Spatial domain of sensors locations
Ω_y	Spatial domain of measurements
$\bar{p}_F$	Prior distribution of the random field $f(\bar{x})$
$\bar{p}_{F\|\bar{y}}$	Posterior distribution of the random field $f(\bar{x})$
$\bar{P}_F$	Prior probability of failure
$\bar{P}_{F\|\bar{y}}$	Posterior probability of failure
$\mathbb{E}L(\emptyset)$	Prior expected loss
$\mathbb{E}L(\bar{Y})$	Posterior expected loss
$\mathbb{E}_F$	Expected value over the prior field $\bar{p}_F$
$\mathbb{E}_{F\|\bar{y}}$	Expected value over the posterior field $p_{F\|\bar{y}}$
$\bar{\mu}_F$	Prior mean of the random variable $f(\bar{x})$
$\bar{\mu}_{F\|\bar{y}}$	Posterior mean of the random variable $f(\bar{x})$
$\bar{\mu}_{\bar{Y}}$	Mean of the random variable $f(\bar{x})$ derived from the measurement set
μ_g	Mean of the limit state
σ_g	Standard deviation of the limit state
Σ_F	Prior covariance matrix of the random variable $f(\bar{x})$
$\Sigma_{F\|\bar{Y}}$	Posterior covariance matrix of the random variable $f(\bar{x})$
$\Sigma_{\bar{Y}}$	Covariance matrix of the measurement
Σ_ε	Covariance matrix of the noise
C_f	Cost of failure
C_p	Cost of failure prevention
VoI_{UNI}	VoI obtained by UNI 11096 sensor positioning
n_{UNI}	Number of sensors as for UNI 11096 sensor positioning
r_{UNI}	VoI ratio for UNI 11096 sensor positioning
C	Cost of measurement
VoI	Value of information
B_{VoI}	Final benefit
$f_s(\bar{x})$	Strength random field
$f_t(\bar{x})$	Failure threshold field

$g(\bar{x})$	Limit state function
G	Target event for SS
q	Intermediate threshold values for SS
P	Probability of the occurrence of event G in SS
t	Inspection cycle
a	Crack size in axial direction
x_{pit}	Pit size in through-wall direction
K_s	Stress intensity factor
F_g	Geometric factor
d	Actual outer tube diameter
t_s	Actual thickness of the tube
ΔP	Actual pressure difference between the inner and the outer sides of the SG tube
m	Expected number of pits initiated within the two successive inspection cycles t and t+1
n_{pit}	Number of pits that are initiated during the t-th cycle
S_u	Ultimate tensile strength
S_y	Yield strength
T_m	Expected mission time of SG
P_b	Burst pressure of an unflawed virgin tube
m_b	Bulging factor
$\frac{da}{dt}$	Crack growth rate
f_{SGTR}	Frequency of SGTR occurrence
f_{TR}	Expected rupture frequency in cycle t
$N_{tb}(t)$	Number of available tubes at cycle t
d_{nom}	Nominal outside diameter of SG tube
$t_{s,nom}$	Nominal thickness of SG tube
ΔP_{nom}	Nominal pressure difference between the inner and the outer sides of the SG tube
W_{nom}	Nominal Power of the NPP
$P_{in,nom}$	Primary side pressure
$P_{out,nom}$	Secondary side pressure
a_{lim}	Plugging limit caused by SCC cracks
a_{cr}	Critical crack length
$\lambda(t)$	Power law intensity function
$\Lambda(t)$	Expected number of initiated pits per SG
$gr(x_{pit})$	Pit growth rate
TWD_{lim}	NRC Plugging limit with respect to Through Wall Depth
TWD	Through Wall Depth
TWD_{cr}	Failure threshold induced by pitting
B_c	Initial budget of each cycle
$S(t)$	Saved budget till cycle t
$B(t)$	Cumulative available budget at cycle t
$N_p(t)$	Number of tubes that should be plugged
$Ft(t)$	Number of tubes failed
$CDF_{SCC}\ (t)$	Core damage frequency if no plugging is enforced to counteract SCC
$CDF_P\ (t)$	Core damage frequency if no maintenance is enforced to counteract pitting
$CDF_{MD,SCC}$	Core damage frequency induced by SCC after maintenance decision is taken
$CDF_{MD,P}$	Core damage frequency induced by SCC after maintenance decision is taken
$CDF_{NRC,SCC}$	Core damage frequency from the enforcement of the NRC guidelines for maintenance
CDF_{static}	Core Damage Frequency calculated by the traditional PSA metho

SECTION I. GENERALITIES

This section of the dissertation describes the context of the PhD research, its relevance, the state-of-the-art methods, the challenges that are addressed, the overview of the developed framework and the description of the industrial applications carried out for the demonstration.

1. INTRODUCTION

Energy generation facilities are designed to operate for long periods of time (e.g., electric power plants for more than 50 years of operation [1]). Life extension of these facilities, beyond the designed life, are also required not only to meet the ever increasing energy demands [2, 3, 4] but also to respond to the high social and political pressures put in force to continue their operation due to the direct substantial replacement costs as well as the indirect incurred costs imposed by service disruption during replacement [5]. Indeed, life extension implies a substantial economic return (e.g., life extension of a 1000 MW Nuclear Power Plant (NPP) for 20 extra years may yield a saving of $1 billion) [6].

Life extension is not a trivial decision to undertake since aging exposes facilities to failures, that in turn, directly expose the environment and the society to significant risk [7] because the designed safety margins of Structures, Systems and Components (SSCs) of these facilities may not be adequate to deal with the stresses that challenge their integrity by life extension (for example, growing energy demand) [8, 9]. Therefore, life extensions should be achieved with caution, through maintenance, renovation and integration of new advanced technologies [10, 11] that enable time-dependent characteristics of the SSCs (due to aging) to be precisely monitored [12]. Digitization of the ongoing 4th industrial revolution brings new opportunities for condition monitoring by intelligent sensoring the SSCs [13]. Condition monitoring data, reflecting the current health condition of SSCs, can be indeed used for informing the risk assessment [14, 15, 16], as well as informing simulation models therein used with respect to the degradation mechanisms affecting the SSCs, to predict the SSC failure time and enable decision-makers to take risk-informed decisions regarding maintenance strategies, even whit budgetary constraints [17, 18, 19]. To achieve this, after collecting the condition monitoring data, Probabilistic Risk Assessment (PRA) models should be used to translate the acquired data into dynamic risk estimates that reflect the current health state of the SSCs and help the decision-maker taking risk-informed maintenance decisions [20, 21].

In this PhD thesis, with respect to the above-mentioned challenges, innovative solutions are provided to obtain optimal condition monitoring data in energy facilities by recommending the optimal sensors positioning that uses the Value of Information (VoI). Then, the innovative risk model of Condition-Based Probabilistic Risk Assessment (CB-PRA) [22] (briefly discussed in Section 1.2) is adopted in this thesis to provide dynamic risk estimates based on the previously collected optimal condition monitoring data which enables the decision-makers to, finally, make condition-based risk-informed maintenance decisions.

The novelty of the thesis work consists in: I. the proposed VoI-based data acquisition that uses greedy optimization, non-greedy optimization, and Subset Simulation (SS) to address the issue of optimal sensors positioning; and II. the proposed CB-PRA maintenance decision support, that adopts the CB-PRA to take condition-based maintenance decisions.

1.1. Research objectives of the thesis

The structure of this PhD thesis is summarized in Figure 1. First, the issue of optimal sensors positioning is addressed. Then, the innovative PRA approach (CB-PRA), capable of dynamically estimating the risk measures by updated condition monitoring data, is adopted to finally take condition-based risk-informed maintenance decisions, with respect to multiple degradation mechanisms for risk prioritization, accounting also for maintenance costs.

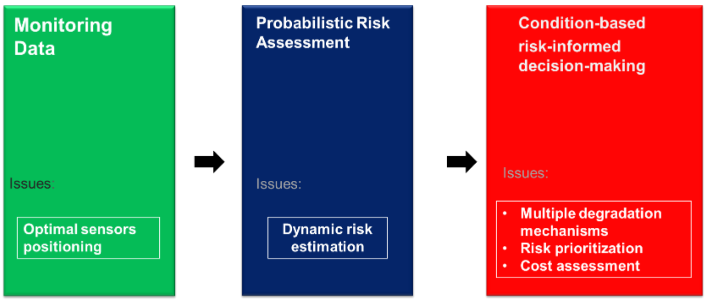

Figure 1: Schematic representation of the thesis framework

The novelty of the research consists in:

I) VoI-based data acquisition: a novel approach is presented to identify the optimal positioning of sensors for condition monitoring of SSCs by Value of Information (VoI) for supporting the decision making of maintenance, that guarantee, at the same time, low costs and valuable information.

II) CB-PRA maintenance decision support: an innovative framework is presented which makes use of the optimal condition monitoring data (addressed in task I) and of the CB-PRA methodology, to prioritize the risk of the different degradation mechanisms of SSCs, and support taking the most proper decision regarding the maintenance strategy to be adopted to control the degradation propagation and, therefore, extending the facility lifetime.

In other words, in a nutshell, using the optimal monitoring scheme of task I, and benefiting from the innovative approach of CB-PRA, a condition-based risk-informed decision-making support tool is achieved in task II.

In what follows, details will be provided on the research activities performed in this PhD thesis for addressing: Task I: "VoI-based data acquisition"; and Task II: "CB-PRA maintenance decision support". Table 1 lists subtasks details, along with the dissemination achievements.

Table 1: Tasks defined to achieve condition-based risk-informed decision-making

No.	Research tasks	Achievements
I	VoI-based data acquisition	2 Journals [J] and 3 Conference [C] papers
I.1	Optimal sensors positioning by greedy optimization method	1 [J] &1[C]
I.2	The sub-modularity issue in VoI based sensor positioning	1[C]
I.3	Optimal sensors positioning by non-greedy optimization method	1[C]
I.4	Optimal sensors positioning by subset simulation method	1 [J]
II	CB-PRA maintenance decision support	1 Journal paper [J] and 1 Book [B]
II.1	Modeling of multiple degradation mechanisms for Steam Generator (SG) of a NPP	1 [J] &1[C]
II.2	Risk prioritization	
II.3	Development of the maintenance decision tool for SG	

A brief discussion on the CB-PRA approach is provided in Section 1.2. Then, the two research tasks performed during the PhD thesis are introduced in Sections 1.3 and 1.4 (then, described in more details in Sections 2 and 3).

1.2. Condition-Based Probabilistic Risk Assessment (CB-PRA)

Risk assessment is one of the greatest concerns for many industrial systems because any failure could cause severe consequences with human fatalities and adverse impacts on economy, society, and environment [23]. Therefore, risk models able of modeling, simulating, and predicting the failure consequences are vital to any industry. In nuclear industry, dealing with the significant risk of nuclear radioactive materials, Probabilistic Risk Assessment (PRA) [24] is utilized as a useful tool for decision-makers to improve the safety and cover any available flaws during design and operation [25, 26].

Traditional PRA methods have a static nature and allow for a failure probability calculation based on the design (i.e., prior to operation) available information [27]. In current practice, risk measures such as Core Damage Frequency (CDF) in NPPs are calculated based on traditional static PRA methods like traditional Event Tree Analysis (ETA), Fault Tree Analysis (FTA) [28, 29]. Even though, PRA is believed to reflect the status of a specific plant, it is mostly obtained from generic data of other similar plants [30] which, in spite of the updates of the generic data with plant-specific data, gives a picture of prototypical plant, rather than a specific NPP [31]. In addition, aging and degradation may increase the probability of a failure that is often neglected and excluded throughout the assessment [32]. Therefore, traditional PRA methods only provide a static risk measure, without taking into account the new condition of degraded materials that, on the other hand might be easily inspected by numerous monitoring techniques [33]. As a result, remaining service life, and maintenance needs (calculated from such static reliability analysis methods) are generically based on the information of the design stage, generic data, codes, and expert judgments [34].

In light of this, a methodology called Condition-based PRA (CB-PRA) was proposed in [22] that utilizes data gathered from a plant by condition monitoring techniques that dynamically actualizes the related risk measures. The CB-PRA combines the traditional PRA with the intelligent condition monitoring tools to provide a powerful support to decision makers, being able to mine past, present and future data/information on environmental, operational and usage conditions of industrial equipment, for detecting degradation, diagnosing faults and predicting failures.

The innovative methodology has the potential to allow the decision makers to take real-time decisions to prevent accidents. These decisions will support effective and optimal operation, maintenance, and outage planning. In this PhD thesis, the CB-PRA methodology is adopted to take condition-based risk-informed maintenance decisions.

1.3. VoI-based data acquisition

Condition monitoring of SSCs has been fostered by sensors technology's rapid growth [35, 36]. By the exponential growth in computational capabilities of computers and by the availability of cheaper and more precise sensors, condition monitoring is more readily available, but the real challenge lies in acquiring optimal information [37]. Collecting useful condition monitoring data is the key point for cost-effective life extension of aging facilities since acquiring massive data, without exploiting it, has no benefit but unnecessary costs [38]. The main issue to be addressed is the positioning of the condition monitoring sensors in locations where they can collect the most beneficial data. This process is called the optimal sensors positioning [39, 40]. However, since sensors positioning and consequent actions taken, based on the data collected come with a cost, this must be justified in terms of safety improvements [41]. With the optimal sensors positioning, the optimal set of measurement that have the most beneficial information with the lowest cost can be identified [42, 43].

Till now, most of the recommendations of the norms on how to perform the health monitoring are drawn from the experiences gained during in-service inspections or from the structural analyses [44] which is a shortcoming that questions the accuracy and reliability of the suggested procedure when to be applied on new materials (or on the materials with short experience recorded) as well as new designed SSCs. In this research, a framework based on the computational techniques is proposed to give recommendations on optimal sensors positions that yielded the highest benefit from condition monitoring before installing the sensors. Therefore, it is also feasible to be applied on new design SSCs.

The rationale behind the proposed framework is that the positioning of sensors that measure specific properties f can be seen as an optimization problem that searches the maximum of Value of Information (VoI) metric [45, 46, 47, 48] by Bayesian decision theory [49]. The VoI is a utility-based Figure of Merit (FoM) which quantifies the benefits/losses of acquiring information that can be used to compare the benefit of taking a measurement regarding specific properties of the SSC in one position rather than another. A measurement is more beneficial than another if it has the larger VoI value. Therefore, VoI provides a clear indication on the benefits that may be gained (i.e., before sensors installation) by putting sensors in specific positions and finding the optimal sensors positions [50].

Let F be a spatial model of a system where each physical property f can be measured by random quantities $f(\bar{x})$ at each location $\bar{x}$ resulting in a vector $\bar{f}(\bar{x})$ representing a multivariate random field in which the various properties are jointly described. The set of measurement $\bar{y}(\bar{x})$ consists in a subset of all potential measurement sets $\bar{Y}$ that can be used to update the prior distributions of the multivariate random field $\bar{p}_F$ in the posterior distributions $\bar{p}_{F|\bar{y}}$, by the Bayesian inference method [49]. Based on the distributions, the decision maker can take actions $\bar{a}$ to counteract the degradation progression of the SSC that can cause a loss (i.e., a negative utility) described by a loss function $L(\bar{f}(\bar{x}), \bar{a})$.

VoI quantifies the loss reduction (i.e., the benefit) of decisions taken based on the posterior $\bar{p}_{F|\bar{y}}$, when the set of measurement $\bar{y}(\bar{x})$ would be collected. Taking measurements in different locations could bring different effects on the posterior and, ultimately, on the benefits on decision making. Therefore, measurement source locations (i.e., sensors positioning) are to be optimally identified. The maximum VoI would correspond to the optimal positioning for collecting the optimal set of measurements $\bar{y}(\bar{x}^*)$.

Solving the problem that finds the optimal set of measurements $\bar{y}(\bar{x}^*)$ by comparing all potential measurement sets $\bar{Y}$ brings complexity that is dramatically increased when the candidate positions of sensors are increased (i.e., all possible set of sensors should be investigated and compared to find the optimal solution by exhaustive search) making this search tedious and computationally intractable [51]. Therefore, optimization methods are proposed to find the solution in an efficient way. Two optimization methods, namely, greedy optimization, non-greedy optimization and one innovative approach by using Subset Simulation (SS) are proposed to find the VoI-based optimal sensors positioning.

In this PhD thesis, we tailor the VoI-based sensor positioning framework on ageing energy systems. Specifically, In Section 2.1, we propose a simulation-based framework that uses VoI for identifying the optimal spatial positioning of sensors on degrading energy systems. In Section 2.3, We apply the proposed framework for identifying the optimal spatial positioning of sensors on degrading pressurized equipment (i.e., a manifold of the SG of a Prototype Fast Breeder Reactor (PFBR)) under creep, whose sensors are typically positioned in line with recommendations of UNI 11096 [52]. In practice, we compare the optimized sensors positioning on the simulated case study with the normative recommendation. A Gaussian Process (GP) model is developed for the case study. The manifold is modeled as a rectangular plate of length L and width πD_e, whose surface is discretized into 160 squares all with dimension of 100×100 mm. Ultrasonic thickness gauges that measure the thickness of base material can be placed at the center of the squares. The thickness model of the manifold is assumed to be normally distributed coming from the GP. The less the thickness of the SG, the higher probability of creep failure. To Find the optimal sensors positioning, as discussed in Section 2.2, three different optimization approaches namely greedy optimization method, non-greedy optimization method and Subset Simulation (SS) are adopted. The objective of all these optimization methods is to find the optimal measurement set that accordingly provides the maximum VoI.

Greedy optimization method consists of looking for the optimal set of measurements $\bar{y}(\bar{x}^*)$ by iteratively adding one single sensor, until the optimal arrangement is reached by so doing [53, 54]. Results show that the VoI-based sensors positioning by greedy optimization, applied to the case study, allows reducing the number of sensors to be positioned with respect to UNI 11096 [52], while gaining the same VoI, meaning that guidelines can benefit from methodological and technical advancements (such as VoI and simulation) to provide end-users with cost-effective indications, overcoming, in this way the shortcomings of relying only on past operational experience.

Greedy optimization can guarantee optimal or near optimal results, for the metrics that satisfy the characteristics of sub-modularity that is, the larger the already identified set the lower the benefit of adding new measurements. For example, the metric M is sub-modular when its increase when it is evaluated at both locations a and b is smaller than when it is evaluated only at location b, (i.e., $[M(a\&b)- M(a)] \leq M(b)$). Incidentally, the VoI metric is not sub-modular making the VoI-based greedy optimization for sensors positioning not always effective [55, 56, 57]. In light of this, the sub-modularity issue in the case study is practically shown, and solutions are suggested to overcome this issue such as, non-greedy optimization methods (e.g., Particle Swarm Optimization (PSO) and Genetic Algorithm (GA)) that are not sensitive to non-sub-modularity of VoI. It is practically shown that, by using non-greedy methods, more optimal sensors positioning is provided which not only yields better VoI, but also provides more accurate risk estimates.

Despite both greedy and non-greedy methods can find a solution, each one comes with limitations and challenges: greedy optimization, as mentioned before, does not guarantee the optimal solution to be found due to the non-sub-modularity of VoI; non-greedy optimization, while being not sensitive to the non-sub-modularity, needs computationally expensive and tedious simulations to find the optimal solution. SS method which is typically used to find the failure probability in highly reliable SSCs is innovatively introduced to find the optimal sensors positioning. The proposed SS method not only does not have the greedy method's problem of the sensitivity to the non-sub-modularity of VoI but is also far more efficient than the non-greedy methods. The result of this computational work can be utilized to advance the process of data acquisition in safety related SSCs for a more profitable and reliable condition monitoring.

1.4. CB-PRA maintenance decision support

Since PRA does not reflect the actual status of the specific plant, but a generic prototypical plant [33], and it does not fully account for the time processes of aging and degradation for updated risk measures estimations [9], a methodology called Condition-based PRA (CB-PRA) was proposed in [22] that utilizes data gathered from a plant by condition monitoring techniques that dynamically actualizes the related risk measures. In this PhD thesis, a novel framework is proposed to make use of the advantages of CB-PRA for risk monitoring and taking risk-informed maintenance decisions. The dynamic provision of condition-based risk measures estimates enables ranking the contribution to risk of different failure mechanisms affecting a SSC and, consequently, taking real-time decisions to prevent accidents by prioritizing maintenance activities.

In Section 3.3, the framework has been applied on the spontaneous Steam Generator Tube

Rupture (SGTR) accident scenario in a Pressurized Water Reactor (PWR), considering the Steam Generator (SG) to be subjected to multiple degradation mechanisms. Different degradation mechanisms that affect the SG tubes integrity are considered [58], such as Stress corrosion cracking (SCC) and pitting, as being the mechanisms, most contributing to SGTR [59]. To counteract these degradation mechanisms, some maintenance strategies like tube plugging and Water Lancing and Chemical Cleaning (WL-CC) are commonly implemented [60] in line with the regulatory guideline, when corrosion reaches specific thresholds [61, 62]. This may result to be non-optimal [63]: numerous cases of unnecessary plugging have been reported worldwide [64]. Moreover, it has been reported that plugging is not always beneficial, since it increases the pressure difference between the inner and the outer sides of the SG tubes, that, in turn, increases the probability that microcracks reach the failure threshold [65]. Therefore, a method for prioritizing the risks due to multiple degradations, embedded into a decision framework, is proposed based on CB-PRA risk measures estimates. Based on this, an operator can dynamically choose, at each inspection cycle, the optimal maintenance action to be undertaken to trade-off the risk of any accident that might be induced by a SGTR and the related maintenance cost, without relying on the threshold-based on regulatory guidelines like NRC's NUREG guidelines [66].

The condition-based risk-informed maintenance decision provides maintenance strategies that are different from what US Nuclear Regulatory Commission (NRC) enforces [66]. If a realistic case of constrained budgetary resources is assumed, maintenance decisions taken by CB-PRA have lower risk than what is enforced by NRC guidelines.

The results show that the proposed maintenance decision support tool enables the decision maker to predict the degradation evolution, predict the tube failure time, calculate the risk of SGTR failure due to the multiple degradation mechanisms and prioritize the maintenance actions, under budget constraints. It is shown that the operators can optimally take the safest and most economic decision for maintenance, with respect to the NRC guidelines [66].

1.5. Case Studies

Without loss of generality and for demonstration purposes, the proposed computational framework is applied on the Steam Generator of two different NPPs. The SG of a of a Prototype Fast Breeder Reactor (PFBR) is selected to apply the VoI-based data acquisition. The SG of Zion NPP is selected to apply the maintenance decisions by CB-PRA. Subsections 1.5.1 and 1.5.2 are dedicated to a brief introduction of the considered case studies.

1.5.1. The SG of PFBR

The application of the VoI-based approach with respect to the optimization of sensors positioning is shown on a manifold of the SG of a Prototype Fast Breeder Reactor (PFBR) (See Figure 2), whose thickness can be measured by Ultrasonic Thickness Testing (UTS).

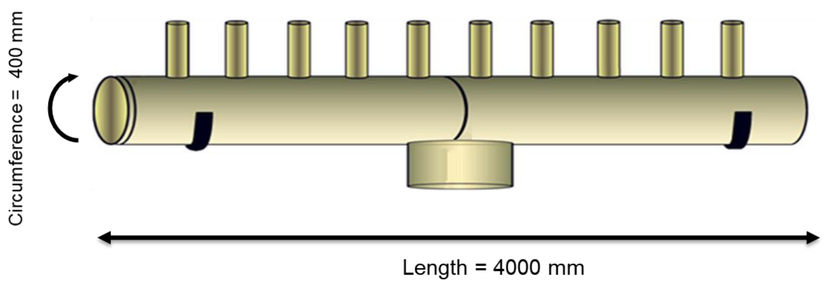

Figure 2:The manifold of a SG of a PFBR used as test case for the VoI-based approach for sensor positioning

Under the assumed operating conditions listed in Table 2, the manifold may suffer of creep due to the large design pressure and temperature, and long exposure time that may lead to failure.

Table 2: Operating conditions of the SG

Design pressure	189 barg
Design temperature	778 °K = 505 °C inlet 723 °K = 450 °C outlet
Material	9Cr-1Mo-V-Nb (Plate) ASME SA-387/SA-387M Grade 91
Percentage of life spent	35%
Operating hours	100,000 h
Tensile strength	475 MPa
Thickness	20 mm

Sensors can be positioned on the surface of the manifold to measure its thickness by Ultrasonic Thickness Testing (UTS). Positions where have smaller thickness are more susceptible to be damaged and ruptured by creep.

1.5.2. SGTR in Zion NPP

The SG of the Zion NPP is considered to apply the framework of CB-PRA maintenance decision. This is a typical Pressurized Water Reactor (PWR) SG which has 3.6 m of diameter and 21 m of height. Zion NPP's SG weights 800 t of weight. Total number of tubes is 3592 which are inverted U shaped. These tubes have an outside diameter of 22.23 mm, and the thickness of their walls are 1.27 mm [22]. The SG is modeled for 30 inspection cycles. Each inspection takes place every 2 years. The schematic view of the SG is shown in Figure 3.

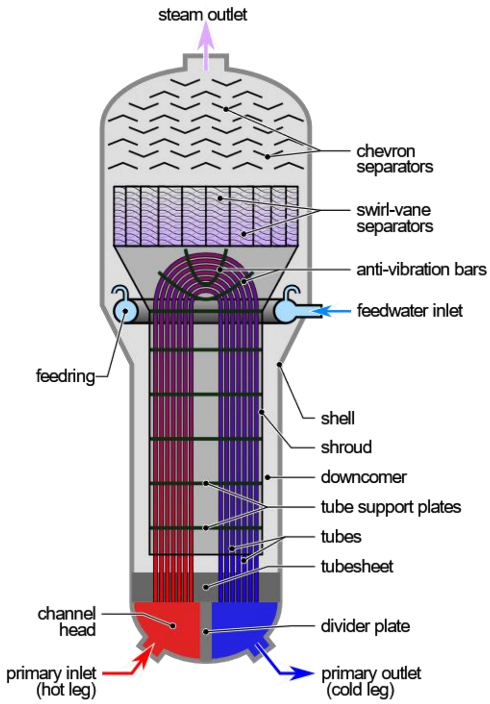

Figure 3: Schematic view of the SG of the case study

In this work, Stress Corrosion Cracking (SCC) and pitting degradation mechanisms are selected for further study and implementation of the CB-PRA framework. The effects of multi-degradation mechanism on spontaneous SG Tube Rupture (SGTR) accident scenario are studied to have comprehensive view on the decisions that must be taken on optimal maintenance strategies (i.e., tube plugging and Water Lancing and Chemical Cleaning (WL-CC)).

1.6. Thesis Structure

The structure of the thesis is shown in Figure 4. Chapters 2 and 3 are dedicated to the steps of the PhD research taken to achieve the research objectives introduced in Section 1.2. Chapter 4 draws the conclusions and future perspectives. At the end, a collection of the international peer-reviewed journals papers finalized during the PhD is included for further details.

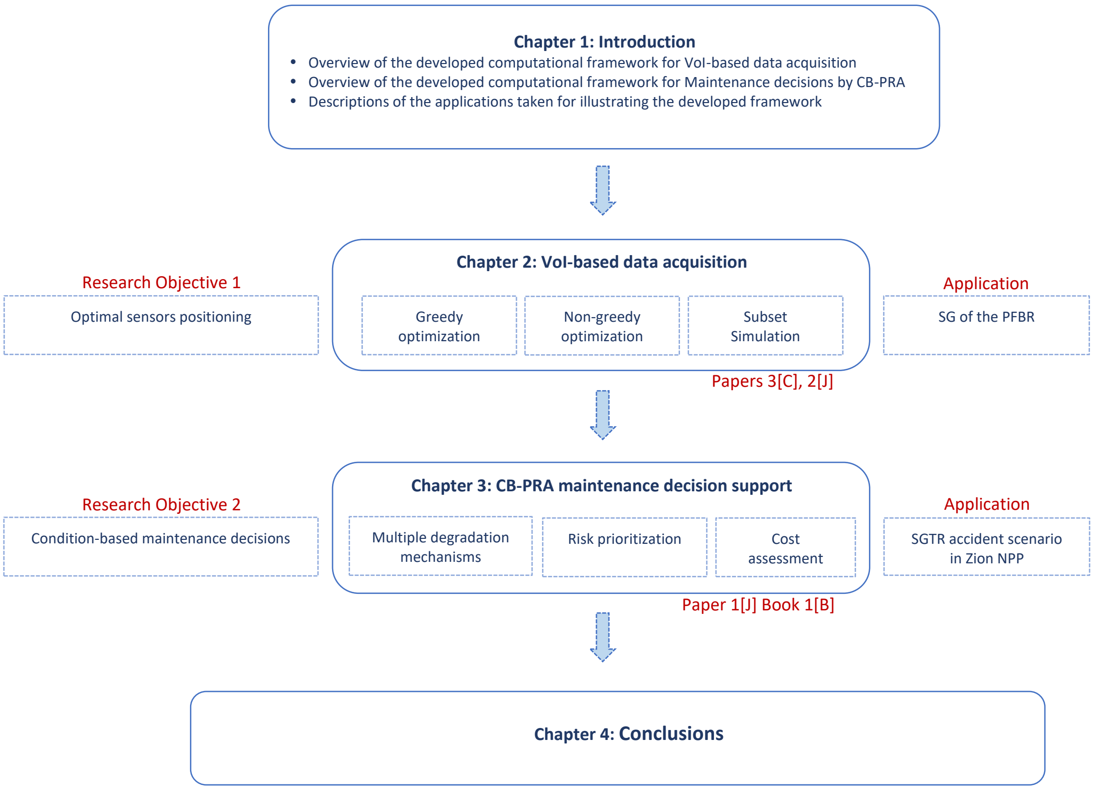

Figure 4: Sketch of the thesis structure

SECTION II. DETAILS OF THE DEVELOPED FRAMEWORK

This Section consists in 3 Chapters (i.e., Chapters 2: VoI-based data acquisition, Chapter 3: CB-PRA maintenance decision support, and Chapter 4: Conclusions) that describe in details the original contributions resulting from the PhD research work.

2. VoI-BASED DATA ACQUISITION

Contents of the Chapter have been adapted from the following publications disseminated from the PhD thesis (Along with the numbering, [J] represents Journal article, [C] represents Conference paper and [B] represents Book, e.g., 3[J] represents the 3rd published journal article):

1[J] *S.M. Hoseyni, F. Di Maio, E. Zio, "Optimal sensor positioning on pressurized equipment based on value of information". Proceedings of the Institution of Mechanical Engineers, Part O: Journal of Risk and Reliability, 1748006X21989661, January 2021.*

2[J] *S.M. Hoseyni, F. Di Maio, E. Zio, "Subset simulation for optimal sensors positioning based on value of information". In preparation*

1[C] *S.M. Hoseyni, F. Di Maio, E. Zio, "VoI-Based Optimal Sensors Positioning and the Sub-Modularity Issue". 4th International Conference on System Reliability and Safety (ICSRS 2019), Rome, November 2019.*

2[C] *S.M. Hoseyni, F. Di Maio, E. Zio, "Optimal Sensors Positioning for Condition-based Risk Assessment by Particle Swarm Optimization". 30th European Safety and Reliability Conference and the 15th Probabilistic Safety Assessment and Management Conference (ESREL2020-PSAM15), Venice, November 2020.*

3[C] *F. Di Maio, S.M. Hoseyni, E. Zio, "Stima probabilistica del rischio di rottura di componenti in pressione soggetti a creep e monitoraggio continuo delle condizioni" SAFAP 2018- Sicurezza ed affidabilità delle attrezzature a pressione, Bologna, Novembre 2018.*

In this Chapter of the PhD thesis, VoI-based data acquisition approach is discussed in detail to address the issue of optimal sensors positioning. First, in Section 2.1, the mathematical concept of VoI is provided. In Section 2.2., VoI-based optimal sensors positioning is discussed and 3 different approaches to find the optimal sensors positioning namely greedy method, non-greedy method, and Subset Simulation (SS) are proposed. In Section 2.3, these approaches are applied on a case study of SG undergoing creep. The advantages and disadvantages of each method are clearly compared, and the most suitable approach is proposed.

2.1. Value of Information

Value of Information (VoI) is a mathematical concept used in Bayesian statistical decision theory to quantify (in monetary terms) the gain that one could obtain by updating prior available information with new one, before adopting it [49]. Indeed, the process of acquiring information (here specifically consisting in measurements from sensors) may not always be justified because of the high cost, and one finds this out only after (the information is acquired by the measurements taken) [67, 68]. In other words, VoI predicts (by pre-posterior analysis) the economic benefit of collecting measurements in specific sensors locations, by accounting (in addition to the cost of the sensor and measurement acquisition chain) for the costs that the decision-maker might incur when adopting mitigative actions to counteract SSC degradation (or its failure in case no action is taken) based on the collected measurements. This provides a powerful tool for comparing different locations of measurement before physically placing the sensors on the SSCs (i.e., a location that has larger VoI value is more beneficial) and makes it possible to find the most beneficial set by solving an optimization problem that finds the observation that has the largest VoI.

The mathematical framework for quantifying the VoI is recalled in the following: In general terms, a spatial domain Ω_x can be defined over the SSC of interest and indicated by its spatial coordinates. For example, each location i on a 2-dimensional Ω_x can be indicated as $\bar{x}_i = \{x_1, x_2\}$. For practicality, the spatial domain Ω_x is discretized into a finite set of i locations $\bar{X} = \{\bar{x}_1, \bar{x}_2, \ldots, \bar{x}_i\}$. A spatial model $F= f(\bar{x})$, where hereafter $\bar{x}$ is generally assumed to represent a set of locations, can be introduced on the spatial domain Ω_x to measure a certain property of the SSC at each location $\bar{x}$ (e.g., for a pressurized vessel, a random field $f(\bar{x})$ of stress, at each location $\bar{x}$). If multiple random fields $\bar{f}(\bar{x})$ (e.g., stress, temperature, thickness and so on) insist on the SSC, $F = \bar{f}(\bar{x})$ can be defined as a multivariate random field, possibly with dependencies [48].

The spatial model can be described based on design values and operational experience (i.e., prior knowledge), eventually assigning prior distributions $\bar{p}_F$ of values to the relevant variables (e.g., the distribution of the internal stress in a pressurized vessel).

Similar to the spatial domain Ω_x, the measurements spatial domain Ω_y can be defined at the generic set of locations $\bar{x}$ where the measurements can be taken (i.e., $\Omega_y \subseteq \Omega_x$). The measurement set $\bar{y}(\bar{x})$ is the collection of measurements at the generic locations $\bar{x}$ (e.g., measurements of realizations of the multivariate random field $\bar{f}(\bar{x})$ at 3 locations $\bar{y}(\bar{x})=\{\bar{x}_2, \bar{x}_5, \bar{x}_{12}\}$):

$$\bar{y}(\bar{x}) = \boldsymbol{R}\bar{f}(\bar{x}) + \bar{\varepsilon} \tag{1}$$

where $\boldsymbol{R}$ is a row matrix with i elements indicating which locations in Ω_x are observed (i.e., $\boldsymbol{R}$ is a row matrix with zero value for the non-observed locations of $\bar{X}$ and 1 for the observed locations), and $\bar{\varepsilon}$ is a vector of random noise measurements, usually assumed to be distributed like a Gaussian with zero mean and covariance matrix Σ_ε [48]. When new information become available (new measurements are recorded), the distribution of the model $\bar{f}(\bar{x})$ can be updated. Specifically, Bayesian inference allows updating the prior distributions $\bar{p}_F$ to obtain the posterior distribution $\bar{p}_{F|\bar{y}}$.

Prior and posterior distributions, $\bar{p}_F$ and $\bar{p}_{F|\bar{y}}$ can be used by a decision-maker to decide an action from a set of possible actions $\bar{a}$. In particular, the SSCs prior probability of failure $\bar{P}_F(\bar{x})$ and posterior probability of failure $\bar{P}_{F|\bar{y}}(\bar{x})$ that can be inferred from $\bar{p}_F$ and $\bar{p}_{F|\bar{y}}$, respectively, can support, in a risk-informed perspective, a decision-maker choice of maintenance by balancing risk and actions costs, based on the most informative set that can be collected.

To this aim, a loss function $L(\bar{f}(\bar{x}), \bar{a})$ can be introduced as negative utility (i.e., loss) that may come from taking a decision. For example, in case a decision of action is taken based only on the prior knowledge $\bar{p}_F$ without relying on additional measurements ($\emptyset$), the prior expected loss $\mathbb{E}L(\emptyset)$ can be minimized to find the optimal action:

$$\mathbb{E}L(\emptyset) = min\{\mathbb{E}_F L(\bar{f}(\bar{x}), \bar{a})\} \tag{2}$$

On the other hand, if $\bar{y}(\bar{x})$ is available, the decision can be taken posteriori of collecting the information $\bar{y}(\bar{x})$, i.e., with respect to $\bar{p}_{F|\bar{y}}$, and minimizing the posterior expected loss $\mathbb{E}L(\bar{y}(\bar{x}))$:

$$\mathbb{E}L(\bar{y}(\bar{x})) = \mathbb{E}_Y \min\{\mathbb{E}_{F|\bar{y}} L(\bar{f}(\bar{x}), \bar{a})\} \tag{3}$$

For example, based on $\bar{p}_F$ (e.g. the prior knowledge on the field of stress on a plate with growing cracks, providing a failure probability estimate $\bar{P}_F(\bar{x})$ due to the load applied) a repair decision might be taken that differs from the one that would have been taken if the posterior probability of failure $\bar{P}_{F|\bar{y}}(\bar{x})$ would have been considered, if $\bar{P}_{F|\bar{y}}(\bar{x})$ were updated with the new measurements $\bar{y}(\bar{x})$ that have become available. For the pressurized vessel, $\bar{p}_{F|\bar{y}}$ reflects the updated distribution of the stress, conditioned on the collected information $\bar{y}(\bar{x})$: within the here proposed simulation-based approach, the measurement corresponds to random realizations in a specific location *i*. To account for this stochasticity, we assume that in each location, we simulate the collection of *K* alternative measurements, and $\bar{p}_F$ and $\bar{p}_{F|\bar{y}}$ are collected accordingly with their consequent losses as in Equations (2) and (3). *K* different stochastic realizations of $\bar{y}(\bar{x}_i)$ represent *K* different posterior expected losses $(\mathbb{E}L(\bar{y}(\bar{x}_i))_k$ which are averaged, by Monte Carlo simulation, to quantify the posterior expected loss conditioned on the measurement at a specific location *i* as:

$$\mathbb{E}L(\bar{y}(\bar{x}_i)) \cong \frac{\sum_{k=1}^{K}(\mathbb{E}L(\bar{y}(\bar{x}_i))_k}{K} \tag{4}$$

The difference between $\mathbb{E}\mathrm{L}(\emptyset)$ and $\mathbb{E}L(\bar{y}(\bar{x}))$ quantifies the benefit of taking decisions informed by the new information $\bar{y}(\bar{x})$, and is, thus, the VoI:

$$VoI(\bar{y}(\bar{x})) = \mathbb{E}L(\emptyset) - \mathbb{E}L(\bar{y}(\bar{x})) \tag{5}$$

2.1.1. VoI-based sensor positioning

As mentioned before, decisions are made optimal by the informativeness of $\bar{y}(\bar{x})$. The cost-effectiveness of $\bar{y}(\bar{x})$ holds when its cost $C(\bar{y}(\bar{x}))$ is less than (or equal) to the VoI gained (i.e., a measurement is cost-effective when $VoI(\bar{y}(\bar{x})) \geq C(\bar{y}(\bar{x}))$), and consequently, the total benefit utility $B_{VoI}(\bar{y}(\bar{x})) \geq 0$):

$$B_{VoI}(\bar{y}(\bar{x})) = VoI\ (\bar{y}(\bar{x})) - C(\bar{y}(\bar{x})) \tag{6}$$

The optimal set of measurement $\bar{y}(\bar{x}^*)$, i.e., the set which maximizes the utility B_{VoI} among all potential sets of measurements $\bar{Y}$, is determined by the optimal number of sensors *n* and their positioning. In principle, the optimal positioning of sensors can be found by simulating every possible set of measurement on $\bar{Y} \subseteq \Omega_Y$ (by a combinatorial and computationally impractical way of solving Equation (7):

$$\bar{y}^*(\bar{x}) = argmax_{\bar{Y}\subseteq\Omega_Y}\,(B_{VoI}(\bar{Y})) \tag{7}$$

To find the solution of Equation (7), one primitive yet non-efficient way is to perform the exhaustive search by calculating B_{VoI} for all potential sets of measurements $\bar{Y}$ and finding the optimal set which provides the maximum B_{VoI}. The exhaustive search is most of the time computationally intractable and this justifies the need for introducing more efficient solutions of optimization methods in this PhD thesis as: greedy and non-greedy method as wells as the Subset Simulation (SS).

2.1.2. VoI-based sensor positioning for Gaussian fields

A particular case of the sensor positioning procedure is the sensor positioning on Gaussian fields, which means that $\bar{f}(\bar{x})$ is normally distributed on Ω_x [69], with a mean function value $m(\bar{x})$, a standard deviation $\sigma(\bar{x})$, and covariance $k(\bar{x}, \bar{x}')$ with correlation $\rho(\bar{x}, \bar{x}')$ (i.e., $k(\bar{x},\bar{x}') = \sigma(\bar{x})\sigma(\bar{x}')\rho(\bar{x},\bar{x}')$) between locations $\bar{x}$ and $\bar{x}'$. This means, also, that when a measurement is taken at a given location (x_1, x_2), any other measurement at any other location (x_1', x_2') is correlated with (x_1, x_2) according to a correlation function. There are numerous correlation functions. In this work, for the case study of Section 2.3, an exponential correlation function is selected as it better represents the correlation of the locations in Gaussian fields [54]:

$$\rho(x_1, x_2, x_1', x_2') = exp\,(\,-\sqrt{\frac{((x_1-x_1')^2+(x_2-x_2')^2)}{\lambda^2}}) \tag{8}$$

where λ is called scale parameter (in the case study of Section 2.3, λ is taken equal to 100 mm in order to provide the maximum correlation among the adjacent sensors positions).

In various cases, spatially distributed systems can be assumed to be Gaussian [54] and, Bayesian inference for the sensors positioning can exploit the property of conjugate priors [70], as discussed hereafter.

Specifically:

- the multivariate field $\bar{f}(\bar{x})$ can be described by the mean vector $\bar{\mu}_F = \bar{m}(\bar{x})$ containing multivariate mean values $m(\bar{x})$ of different SSC properties and a covariance matrix $\Sigma_F = k(\bar{x}, \bar{x}')$, with a prior distribution $\bar{p}_F$:

$$\bar{f}(\bar{x}) \sim \bar{p}_F = \mathbb{N}(\bar{\mu}_F, \Sigma_F) \tag{9}$$

- the noise $\bar{\varepsilon}$ is modeled as an independent, identically distributed, zero mean Gaussian distribution covariance matrix Σ_ε can be described as distributed by a multivariate normal distribution so that the measurement set $\bar{y}(\bar{x})$ is Gaussian with $\bar{\mu}_{\bar{y}} = \mathbf{R}\bar{\mu}_F$ and $\Sigma_{\bar{y}} = \mathbf{R}\Sigma_F\mathbf{R}^T + \Sigma_\varepsilon$ (Equation (10)):

$$\bar{y}(\bar{x}) \sim \bar{p}_{F|\bar{y}} = \mathbb{N}\left(\bar{\mu}_{\bar{y}}, \Sigma_{\bar{y}}\right) \tag{10}$$

The conjugate posterior of $\bar{f}(\bar{x})$ is, thus, a Gaussian distribution [71]:

$$\bar{f} \mid \bar{y}(\bar{x}) \sim \mathbb{N}\left(\bar{\mu}_{F|\bar{y}}, \Sigma_{F|\bar{y}}\right) \tag{11}$$

with:

$$\bar{\mu}_{F|\bar{y}} = \bar{\mu}_F + \Sigma_F\mathbf{R}^T\Sigma_{\bar{y}}^{-1}\left(\bar{y}(\bar{x}) - \bar{\mu}_{\bar{y}}\right) \tag{12}$$

and

$$\Sigma_{F|\bar{y}} = \Sigma_F - \Sigma_F\mathbf{R}^T\Sigma_{\bar{y}}^{-1}\mathbf{R}\Sigma_F \tag{13}$$

being the posterior mean and covariance, respectively.

2.2. Optimal Sensors Positioning

Identifying the optimal set of sensors positions to be mounted on Safety-critical SSCs is crucial for maximizing the value of data collected and correctly informing the decision-making process regarding maintenance and risk management, yet very challenging in terms of the computational costs [72, 73, 74]. VoI, based on Bayesian statistics, is the utility used, in this PhD thesis, to quantify the value of data collected with a set of sensors positions, by estimating the benefits that can be gained, in monetary terms, by installing that set of sensors, prior to its installation [49, 75].

Beside the mathematical complexity of VoI, the real challenge is computational and comes when VoI computation has to be repeated among all candidate sets of sensors, to find the optimal positions set that gives the maximum VoI [76, 77]: if we assume that *n* sensors are to be positioned in a system that has *j* candidate sensors positions, $\binom{j}{n}$ VoI computations shall be conducted to consider all possible sets of sensors positions and, among these, find the optimal set that maximizes the VoI [56] (for example, *n*= 5 sensors in *j*=200 candidate positions = 2.54E+9 different sets of sensors positions). If we consider that in real applications, *j* can be very large and *n* unknown, the problem becomes intractable, from the computational point of view (e.g., for *j*=1000 candidate positions, $\sum_{n=1}^{j}\binom{j}{n}$ = 1.07e+301 possible set of sensors positions).

To overcome these issues, combinatorial optimization methods can be used to find the optimal solution not by comparing all potential solutions with an intractable exhaustive search but by smartly selecting a fraction of possible solutions that, eventually, lead us to the optimal solution [78, 79]. The combinatorial optimization methods that have been used for solving VoI-based sensors positioning problems [46, 56, 80] are here categorized in greedy and non-greedy methods. Moreover, an alternative novel approach, the SS method, is innovatively used to find the VoI-based optimal sensors positioning. The detailed description of these 3 approaches is provided at what follows.

2.2.1. Greedy method

A classical approach to find the optimal set of measurement is to use the greedy method [81]. To find the optimal set $\bar{y}(\bar{x}^*)$ comprised of *n* sensors (*n* is unknown usually) by greedy method, sensors are sequentially positioned one by one in *n* iterations until the objective of the optimization is reached by finding the set which has largest B_{VoI} (Equation (7)). More specifically, the first best single position is, firstly, identified. Then, for the remaining iterations, one other single sensor position with respect to previously positioned sensors are sequentially added until finding optimal set of measurement $\bar{y}(\bar{x}^*)$. This method is very efficient with respect to the dramatical reduction in the number of required VoI computations to find the optimal set [56] since $n \times j$ VoI computations are required.

The greedy optimization guarantees to achieve a solution with a metric value of at least $(1-\frac{1}{e})\cong 63\%$ of that of the true optimal solution obtained by exhaustive search for the problem that use sub-modular metrics [56], but VoI is a non-sub-modular metric [82]. Sub-modularity is discussed by detail in Section 2.2.1.1 below. Moreover, the non-sub-modularity of VoI metric will be practically shown in the case study of Section 2.3.

2.2.1.1. Sub-modularity

Greedy methods guarantee the optimal result for optimization problems that use sub-modular metric. More specifically, the larger a set of measurement, the less beneficial is adding new measurements. In mathematical terms, consider $\bar{y}_1(\bar{x})$ to be a smaller set of measurement than $\bar{y}_2(\bar{x})$ and $\bar{y}_s(\bar{x})$ a specific measurement set added to both these sets. Metric M is sub-modular when for every $\bar{y}_1(\bar{x}) \subseteq \bar{y}_2(\bar{x}) \subseteq \Omega_Y$, $\bar{Y}_1 \subseteq \bar{Y}_2 \subseteq \Omega_Y$, $\bar{y}_s(\bar{x}) \in \Omega_Y$ and $\bar{y}_s(\bar{x}) \notin \bar{y}_2(\bar{x})$:

$$M\big(\bar{y}_1(\bar{x}) \cup \bar{y}_s(\bar{x})\big) - M\big(\bar{y}_1(\bar{x})\big) \geq M\big(\bar{y}_2(\bar{x}) \cup \bar{y}_s(\bar{x})\big) - M\big(\bar{y}_2(\bar{x})\big) \tag{14}$$

The sub-modularity of metric M in Equation (14) implies that when a specific set $\bar{y}_s(\bar{x})$ is added to a smaller set $\bar{y}_1(\bar{x})$, the improvement in the metric value is more than that of adding the same set $\bar{y}_s(\bar{x})$ to a bigger set $\bar{y}_2(\bar{x})$ (i.e., the bigger set $\bar{y}_2(\bar{x})$ also contains the smaller set $\bar{y}_1(\bar{x})$). When the metric M is non-sub-modular, the greedy method may not well perform the process of sensors positioning. Table 3 shows, as a demonstrative example, the benefits of information acquisition by sensors positioning in a system that n=2 sensors are to be positioned in j=3 candidate positions {a,b,c}. Two different generic metrics M_1 and M_2 are used to show the benefits of data acquisition (where M_1 is sub-modular, while M_2 is not). As shown in Table 3, both metrics show equal benefits for adding single sensors and two sensors positions of {a,b} and {a,c}. However, for {b,c}, there is diminishing return for the sub-modular metric (M_1) and non-diminishing return for non-sub-modular metric (M_2). If greedy method is used for both problems with M_1 and M_2, first {a} will be selected and then {b} will be added to form the optimal set{a,b}. By this numerical example, it is obvious that when the metric is sub-modular, the greedy methods easily identifies the optimal set while, otherwise, fails to identify the optimal set {b,c}.

Table 3:Comparison of sub-modular metric (M1) and non-sub-modular metric (M2)

		Sensors positions					
		a	b	c	a,b	a,c	b,c
Metric Value	M_1	4	3	2	6	5	4
	M_2	4	3	2	6	5	7

It is worth mentioning that, using non-sub-modular metrics does not mean that greedy method always fails to identify the optimal solution, but there is the possibility to encounter cases similar to the example shown in Table 3. Therefore, letting the greedy method to find the optimal solution by chance of not encountering such an example is not wise.

2.2.2. Non-greedy method

The non-greedy methods are generally called to the optimization methods that do not follow greedily selecting the optimal set of measurement by sequentially adding single sensor position to the $\bar{y}(\bar{x}^*)$ but by smartly searching in all possible configuration of sensors positions and finding the optimal set $\bar{y}(\bar{x}^*)$. The non-greedy methods can span among lots of combinatorial optimization methods like Genetic Algorithm (GA) [83], Particle Swarm Optimization (PSO) [84], Differential Evolution (DE) [85] and so on.

Despite the greedy method which is sensitive to non-sub-modularity of VoI because it adds the single positions one by one to build up the $\bar{y}(\bar{x}^*)$ and, therefore, may fail to find the optimal result (e.g., similar to M_2 in Table 3), the search space for non-greedy methods involves all possible configurations of sensors positions making it not sensitive to the non-sob-modularity of VoI (e.g., in searching the optimal solution for n=2 sensors in the same example of j=3 candidate sensors positions abovementioned for the non-sub-modular metric M_2 in Table 3, the optimal set {b,c} would be found by non-greedy method by smartly searching in all sets with n=2 sensors position while greedy method would find {a,b} that is not the optimal solution.)

The main drawback of VoI-based non-greedy optimization is its computational cost as VoI computation is mathematically complex by itself, and it becomes very burdensome when the VoI evaluation has to be repeated for a large number of times, evolving towards the optimal solution.

2.2.3. Subset simulation

Subset Simulation (SS) is an adaptive stochastic simulation procedure, originally developed by Au and Beck [86], that can efficiently estimate small probability of rare events, when crude Monte Carlo Simulation (MCS) fails. In other words, SS is an improved MCS method that is adaptively improved to find the probability of rare events where crude MCS can barely estimate or is very demanding in terms of computational cost. SS, due to its high efficiency, have been applied in different fields of engineering, not only for probability estimation, but adapted to also address optimization problems [87].

SS for optimization consists in iteratively generating samples of solutions of the optimization problem towards a target event G (i.e., the optimal solution), assuming $G_1 \supset G_2 \supset \ldots \supset G_m = G$ to be a sequence of nested intermediate events (i.e., suboptimal solutions) where $G_k = \bigcap_{i=1}^{k} G_k$, k= 1,2,…,m. By conditioning on the sequential events G_i, the probability of event G is defined as:

$$P(G) = P(G_m) = P(G_1) \,.\, \prod_{i=1}^{m-1} P(G_{i+1}|G_i) \tag{15}$$

meaning that $P(G)$ in Equation (15) is quantified by conditional probabilities G_i of intermediate events (i.e., the quantification of $P(G)$ passes through the quantification of the probabilities of a series of conditional events $G_{i+1}|G_i$ that are more frequent and have larger probabilities of occurrence. MCS is used to quantify $P(G_1)$ and the conditional samples in $G_{i+1}|G_i$ are generated by Markov Chain MC (MCMC) [88].

In this work, SS for optimization is proposed for finding the optimal sensors positions by searching for the set of measurements locations that satisfy Equation (16) (i.e., no other set of measurements can have a benefit greater than the benefit of the optimal set of measurement $\bar{y}(\bar{x}^*)$. Therefore, the probability of event G which is the probability of $B_{VoI}\big(\bar{y}(\bar{x})\big) > B_{VoI}(\bar{y}(\bar{x}^*))$ is equal to zero):

$$P(G) = P\big(B_{VoI}\big(\bar{y}(\bar{x})\big) > B_{VoI}(\bar{y}(\bar{x}^*))\big) = 0 \quad (16)$$

where $B_{VoI}\big(\bar{y}(\bar{x})\big)$ is the benefit of acquiring information by the set of measurement $\bar{y}(\bar{x})$ quantified by Equation (6), while $\bar{y}(\bar{x}^*)$ is the optimal set of measurement and $B_{VoI}(\bar{y}(\bar{x}^*))$ is its associated benefit.

The probability of target event G (i.e., $P(G)$) can be defined as product of a sequence of conditional probabilities $P(G_{i+1}|G_i)$ as shown in Equation (15) (Suo, et al., 2017). In solving the optimization problem by SS, a series of intermediate threshold values q_i with i=1,2,3,…,mm are adaptively selected, in each iteration i, to make the conditional probability of intermediate events equal to $P(G_{i+1}|G_i)$:

$$P(G_1) = P\big(B_{VoI}\big(\bar{y}(\bar{x})\big) \geq q_1\big) \quad (17)$$

$$P(G_{i+1}|G_i) = P\big(B_{VoI}\big(\bar{y}(\bar{x})\big) \geq q_{i+1} \mid B_{VoI}\big(\bar{y}(\bar{x})\big) \geq q_i\big) \quad (18)$$

where q_1 is the first threshold value used to compute the probability of event G_1 and $\{q_2 \dots q_{mm}\}$ are the intermediate threshold values. In the optimization problem, the algorithm will progressively move toward the optimal set of measurements as $P(G)$ moves toward zero (i.e., $q_i \rightarrow B_{VoI}(\bar{y}(\bar{x}^*))$ as $P(G) \rightarrow 0$).

The conditional probabilities $\{P(G_{i+1}|G_i)\colon\ i = 1, 2, 3, \dots, mm - 1\}$are affected by how the threshold values $\{q_i$: i=1,2,3,…,mm } are selected as arbitrarily choosing q_i values may end up in inability to control the conditional probabilities values being too small or too large. Small $P(G_{i+1}|G_i)$ values will put, once again, the problem in the loop of finding rare events and large values will increase the computational efforts (Li & Au, 2010). Therefore, q_i values are chosen adaptively in order to make the conditional probabilities always be equal to a fixed value p_0 (i.e., $\forall\ i = 1, 2, 3, \dots, mm$, $P(G_{i+1}|G_i)$= p_0) (Pedroni & Zio, 2017).

In summary, to perform the optimization, first N_p samples are generated by crude MCS. Then, q_1 value is adaptively selected in a way that N_t=p_0N_p number of samples have $B_{VoI}\big(\bar{y}(\bar{x})\big) \geq q_1$

making $P(G_1)$ of Equation (17) equal to p_0. These N_t samples are kept for the next iteration as seed samples. Using MCMC, $(1- p_0)N_p$ new conditional samples are generated from the seed samples to make the number of samples, once again, equal to N_p. Then, q_2 value is adaptively selected as N_t=p_0N_p samples have $B_{VoI}\big(\bar{y}(\bar{x})\big) \geq q_2$ to set $P(G_2|G_1)$ of Equation (18) equal to p_0. These N_t top samples are, again, selected as seed samples to be fed to the next iteration i, and generate by MCMC, another $(1- p_0)N_p$ new conditional samples. This loop will continue until $P(G) \to 0$ meaning that $q_i \to B_{VoI}(\bar{y}(\bar{x}^*))$ and the optimal solution $\bar{y}(\bar{x}^*)$ is identified.

2.3. Case Study: SG Undergoing Creep

The manifold of Steam Generator (SG) of a Prototype Fast Breeder Reactor (PFBR), with the properties described in Figure 2 and Table 2, is considered as the case study to show the application of VoI-based sensors positioning by greedy, non-greedy and SS methods. Sensors are installed on the manifold to measure its thickness by Ultrasonic Thickness Testing (UTS) [52]. The thickness measurement is used to monitor the health condition of the manifold to prevent any failure caused by creep. The schematic view of the manifold is shown in Figure 5.

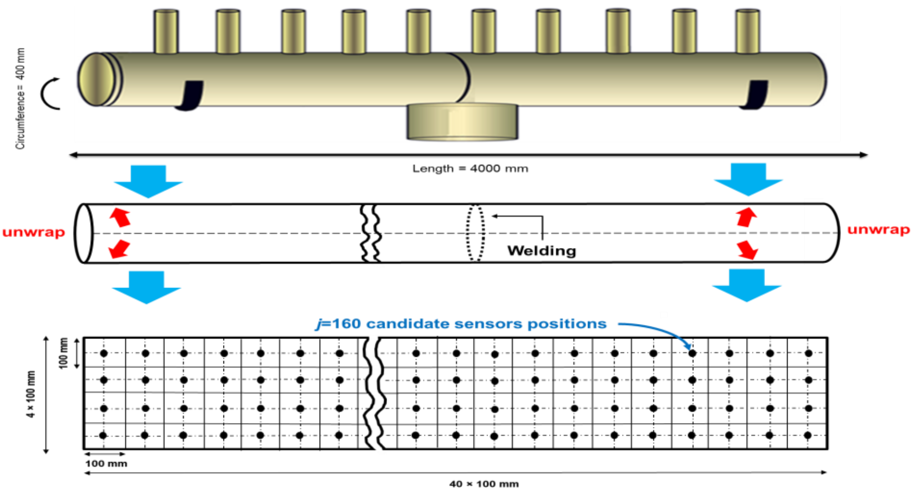

Figure 5: The schematic view of a SG of a PFBR used for the VoI-based sensors positioning and the candidate sensors positions

As can be seen in Figure 5, for modelling purpose, the manifold is unwrapped in a form of rectangular plate and is discretized into j=160 candidate sensors positions where sensors can be installed (Shown as black circles).

Failure would occur at location $\bar{x}$ if the thickness (i.e., the Gaussian strength random field $f_s(\bar{x})$) is smaller than a threshold thickness, here assumed equal to a constant value of 16.9 mm on the whole Ω_x (i.e., the failure threshold field $f_t(\bar{x})$ calculated in [89] in line with [90] using the NIMS creep database [91], that contains creep data collected in experiments related to pressurized equipment of NPP of the same material and operating under the same conditions of the manifold considered in our case).

Since $f_s(\bar{x})$ is a Gaussian field and $f_t(\bar{x})$ is a constant, the limit state function $g(\bar{x}) = f_s(\bar{x}) - f_t(\bar{x})$ is a Gaussian $g(\bar{x}) \sim N(\mu_g(\bar{x}), \sigma_g(\bar{x}))$, which implies a probability of manifold failure $\bar{P}(\bar{x})$ (i.e., the probability that $g(\bar{x})<0$) equal to:

$$\bar{P}(\bar{x}) = \Phi(-\beta(\bar{x})) \tag{19}$$

where $\Phi(.)$ is the standard normal cumulative distribution function, and β is the reliability index equal to:

$$\beta(\bar{x}) = \frac{\mu_g(\bar{x})}{\sigma_g(\bar{x})} \tag{20}$$

The actual thickness $f_s(\bar{x})$ may vary, due to the manifold production process. The following common cases are considered (see Figure 6 where dashed lines show the welding):

1. Circumferential welding of two extruded manifolds.
2. Longitudinal welding of a rectangular plate.
3. Circumferential welding of two manifolds resulting from a longitudinal welding of two rectangular plates.
4. Manifold extrusion.

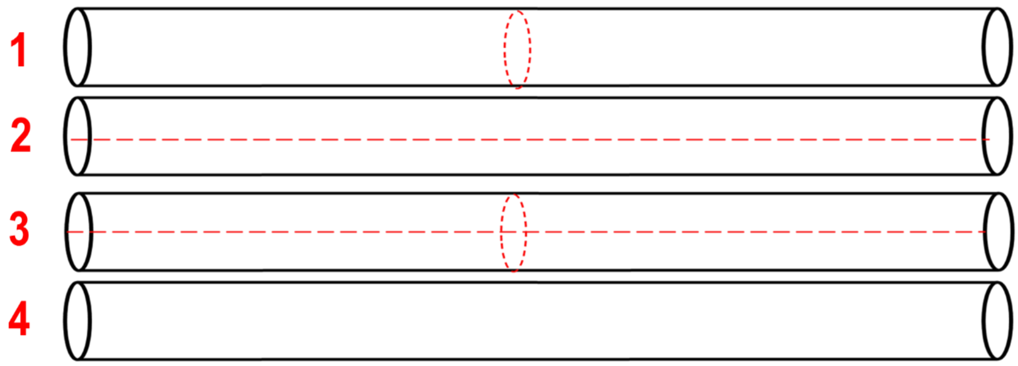

Figure 6: schematic view of the four case studies.

In all these cases, the $f_s\,(\bar{x})$ is modeled with a Gaussian model $\bar{p}_F(\bar{x}) = \mathbb{N}$ (20mm, 1mm) except for the Welding and Heat Affected Zone (WHAZ), where $\bar{p}_F(\bar{x})$ of $f_s\,(\bar{x})$ is $\mathbb{N}$ ~ (20mm, 2mm). Figure 7 shows the standard deviation of $f_s\,(\bar{x})$ for all the cases (the lighter the color, the larger the standard deviation).

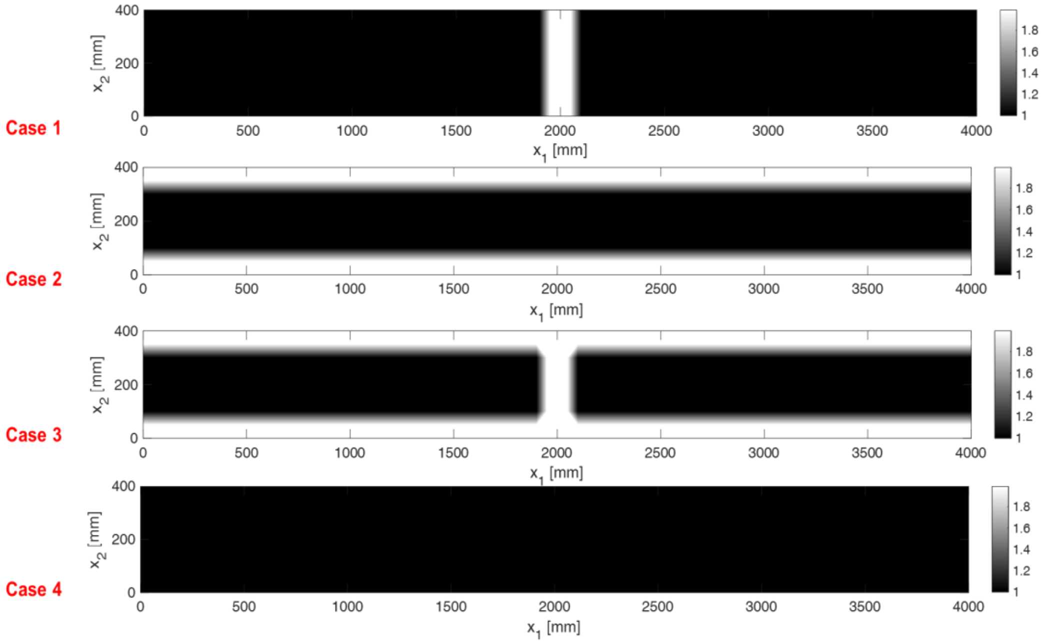

Figure 7: Standard deviation of fs ($\bar{x}$) for the four case studies

Knowing that $f_t\,(\bar{x})$ is equal to 16.9 mm, the prior probability of failure $\bar{P}_F\,(\bar{x})$ can be calculated at any location $\bar{x}$ of the manifold, as plotted in Figure 8 (the warmer the color, the larger the probability of failure).

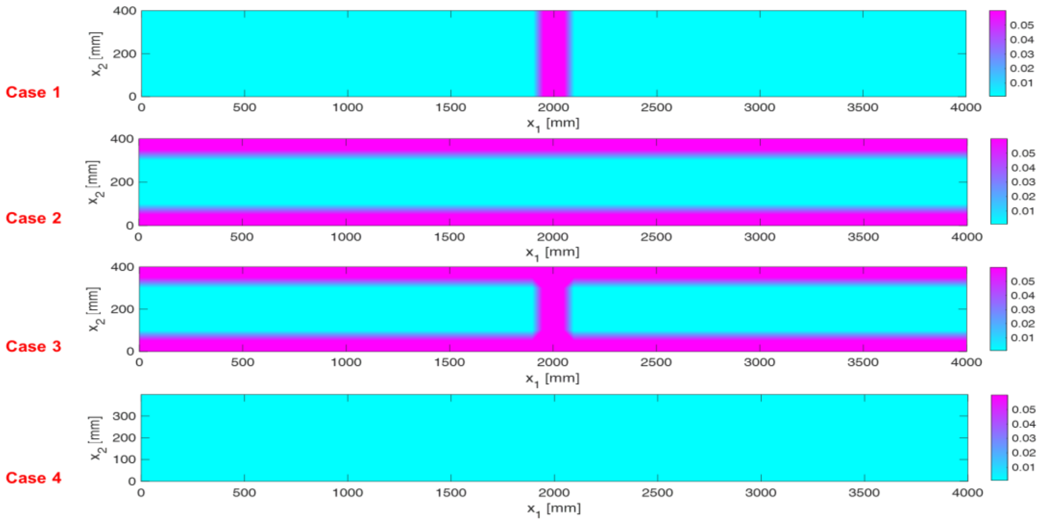

Figure 8: Prior probability of failure $\bar{P}F\ (\bar{x})$ for the four case studies

At this point, it can be decided to: 1. do nothing (a = 0) with zero cost, or 2. mitigate degradation (a = 1) (for, example, for mitigating creep, one can either reduce the operational stress (i.e., lowering pressure, temperature, …), or sleeve the risky area, or perform a weld repair [92], or any combination of these with cost C_m). Depending on the true state ($\bar{s}$) of the manifold, unknown to the decision maker, (i.e., severely degraded (s = 0) that would entail failure cost of C_f, or intact (s = 1)), one sets the loss function value:

$$L\big(\bar{f}(\bar{x}), \bar{a}\big) = \begin{Bmatrix} 0 & \text{if } s = 1 \text{ and } a = 0 \\ C_f = 200K€ & \text{if } s = 0 \text{ and } a = 0 \\ C_m = 5K€ & \text{if } a = 1 \end{Bmatrix} \tag{21}$$

In other words, if no mitigation action is performed (a = 0) and the true state is intact (s = 1), then the decision comes with zero cost; otherwise, if the actual state is severely degraded (s = 0), then, a wrong decision comes with cost C_f. It is assumed that, regardless of the true state of the manifold, if a failure mitigation action is undertaken, the payoff is the cost C_m.

For the proposed application, the prior expected loss $\mathbb{E}L(\emptyset) = \sum_{i=1}^{160} \mathbb{E}L_i(\emptyset)$ is quantified by simultaneously accounting for all the 160 prior expected losses, where, for the i-th location, the prior expected loss is:

$$\begin{aligned} \mathbb{E}L_i(\emptyset) &= min\{\mathbb{E}_F L_i\big(\bar{f}(\bar{x}_i),\ \bar{a}_i\big)\} = min\{\mathbb{E}_F L_i\big(\bar{f}(\bar{x}_i), 0\big), \mathbb{E}_F L_i\big(\bar{f}(\bar{x}_i), 1\big)\} \\ &= min\{C_f \times P_F\,(\bar{x}_i), C_m\,\} \end{aligned} \tag{22}$$

being $\mathbb{E}_F L_i\big(\bar{f}(\bar{x}_i), 0\big)$ the failure cost C_f = 200 $K€$ weighted by the probability of failure $P_F(\bar{x}_i)$ (if no action is taken, a=0), and $\mathbb{E}_F L_i\big(\bar{f}(\bar{x}_i), 1\big)$ corresponds to the cost $C_m = 5K€$ (if maintenance action is taken, a=1). Figure 9 shows the process of $\mathbb{E}L_i(\emptyset)$ calculation by the logic of Equation (22) in the form of a decision tree.

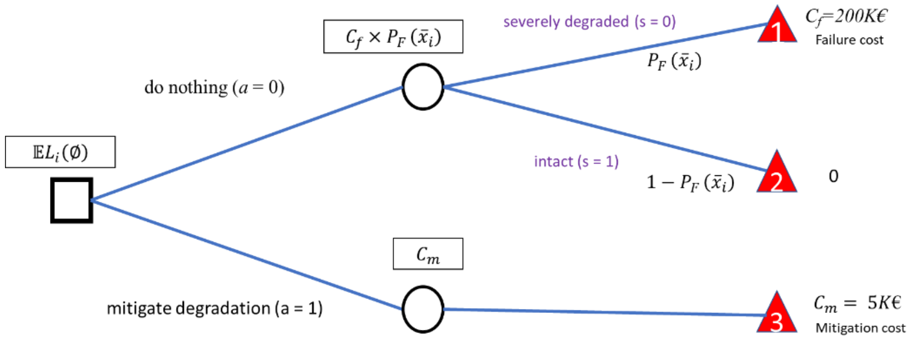

Figure 9:Decision tree used to calculate $\mathbb{E}L_i(\emptyset)$

Also the posterior expected loss $\mathbb{E}L(\bar{y}(\bar{x})) = \sum_{i=1}^{160} \mathbb{E}L_i(\bar{y}(\bar{x}))$ is quantified by simultaneously accounting for all the 160 posterior expected losses where, for the i-th location, the posterior expected loss conditional on the measurement set $\bar{y}(\bar{x})$ is:

$$\mathbb{E}L_i(\bar{y}(\bar{x})) = min\{C_f \times P_{F|\bar{y}}(\bar{x}_i), C_m\} \tag{23}$$

being $P_{F|\bar{y}}(\bar{x}_i)$ the posterior probability of failure of location $\bar{x}_i$.

It is worth mentioning that $\mathbb{E}L(\emptyset)$ and $\mathbb{E}L(\bar{y}(\bar{x}))$ have been calculated as the sum of all the prior and posterior losses, $\mathbb{E}L_i(\emptyset)$ of Equation (22) and $\mathbb{E}L_i(\bar{y}(\bar{x}))$ of Equation (23) respectively, from all the i locations (i.e, $\mathbb{E}L(\emptyset) = \sum_{i=1}^{160} \mathbb{E}L_i(\emptyset)$ and $\mathbb{E}L(\bar{y}(\bar{x})) = \sum_{i=1}^{160} EL_i(\bar{y}(\bar{x}))$), because we assumed the system as a cumulative system where the total cost is the cumulative cost for managing all i locations.

In Figure 10, the $\bar{P}_F$, the prior $\bar{a}$ and the prior expected loss of each i_{th} location $\mathbb{E}L_i$ for the case 1 (circumferential welding of two extruded manifolds) are plotted resulting in a total prior expected loss $\mathbb{E}L(\emptyset) = \sum_{i=1}^{160} \mathbb{E}L_i(\emptyset)$, which can be interpreted as the utility value of taking decisions $\bar{a}$ on the prior belief $\bar{p}_F$, when due account is given to all the 160 prior expected loss values $\mathbb{E}L_i$ of each i_{th} discretized locations $\bar{x}$.

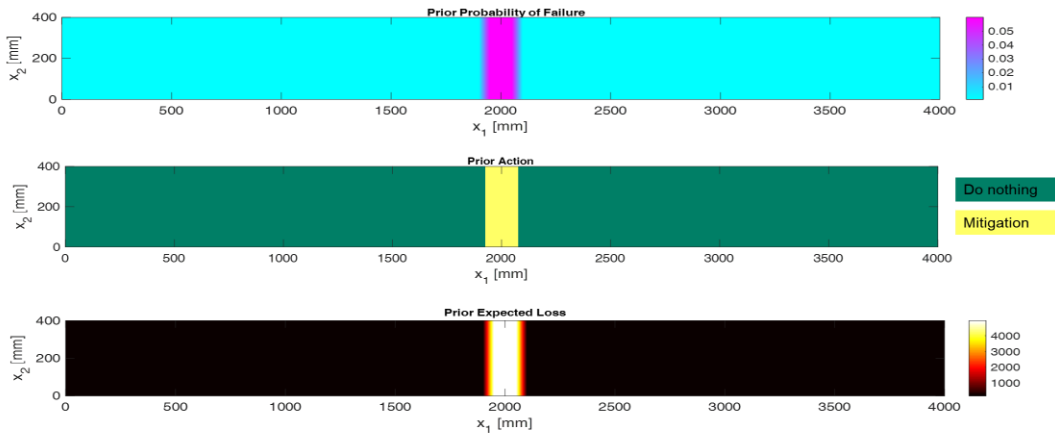

Figure 10: Prior probability, prior actions and the prior expected loss for the case study 1

When a new measurement $\bar{y}(\bar{x})$ is taken, it reduces the uncertainty of $f(\bar{x})$. In each realization, $\bar{p}_F$ is to be updated in $\bar{p}_{F|\bar{y}}$ to calculate the posterior probability of failure $\bar{P}_{F|\bar{y}}$, the posterior actions ($\bar{a}$) and the posterior expected loss $\mathbb{E}L_i(\bar{y}(\bar{x}))$ for each i_{th} location (see Figure 11, where the posterior expected loss field is plotted conditioned on a specific observation at location $\bar{x}_o$ shown by the circle). Finally, $VoI(\bar{y}(\bar{x}))$ is calculated using Equation (5) and $\mathbb{E}L(\bar{y}(\bar{x})) = \sum_{i=1}^{160} EL_i(\bar{y}(\bar{x}))$.

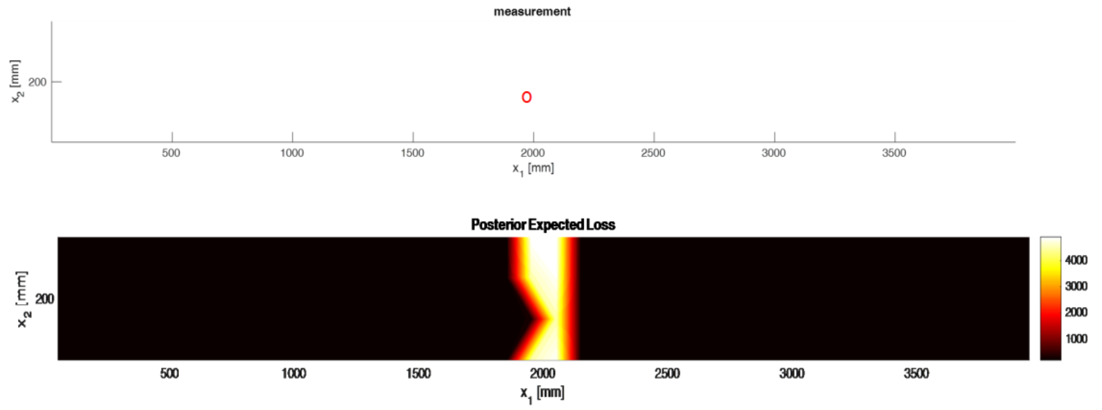

Figure 11: The plot of the posterior expected loss field, conditioned on a specific observation at location $\bar{x}_o$

The above-mentioned descriptions showed the detailed steps of the computation of the VoI value for a measurement set $\bar{y}(\bar{x})$. In the following sections the VoI-based optimal sensors positioning by greedy, non-greedy and SS for the case studies are provided where to find the optimal set of measurement multiple VoI computations shall be conducted.

2.3.1. Sensors positioning by greedy method

In this Section, we use the concept of VoI-based greedy optimization to find how to optimally position ultrasonic thickness gauges on the pressurized equipment, for largest benefit in terms of reduced costs and increased data accuracy. The greedy optimization that finds the optimal set of sensors positions is compared with the sensors positioning recommendations of the Italian guideline ISPESL n. 48/2003 [90] and, specifically, the norm (UNI 11096, 2012) [52] where are derived from past operational experiences. The novelty of this work lies in use of the VoI-based sensors positioning framework for comparing the outcomes with standards/recommendations/guidelines for monitoring of energy SSCs issued by regulatory bodies, to confirm their validity or suggest improvements. Results show that the VoI based sensor positioning allows reducing the number of sensors to be positioned with respect to the guidelines in [52], while achieving the same VoI. This shows that guidelines can benefit from VoI and simulation to obtain cost-effective solutions that overcome the shortcomings of relying only on past operational experience.

The technical procedure in the Italian guideline ISPESL n. 48/2003 [90] and, specifically, the norm (UNI 11096, 2012) [52] is used as benchmark for the sensors positioning. In line with [52], 32 thickness gauges are placed in the locations (*) of Figure 12, among 160 locations available. Notice that holes of subchannels within the manifold are neglected in line with [52].

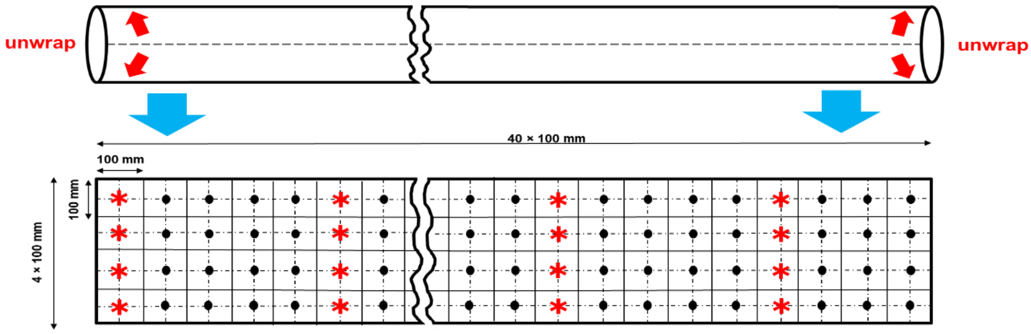

Figure 12: Schematic view of the unwrapped manifold with sensor locations ($\bar{x}$), in line with (UNI 11096, 2012)

In this case study, VoI_{UNI} is the standard value to be reached by the inspection scheme assuming that the inspection costs are neglected (i.e., $C(\bar{y}(\bar{x}))=0$). As a result, the largest VoI of the case study comes from the set of measurement that fills all the i=160 candidate locations with sensors. Instead, we are looking for a set that its benefit exceeds that of the standard value VoI_{UNI} to evaluate the proposed simulation-based methodology's capabilities and compare it with the experience-based standard in recommending better sensors positioning strategy.

The optimal n sensors locations $\bar{y}(\bar{x}^*)$ can be found with the greedy optimization method whose flowchart, tailored on the specific case study, is given in Figure 13.

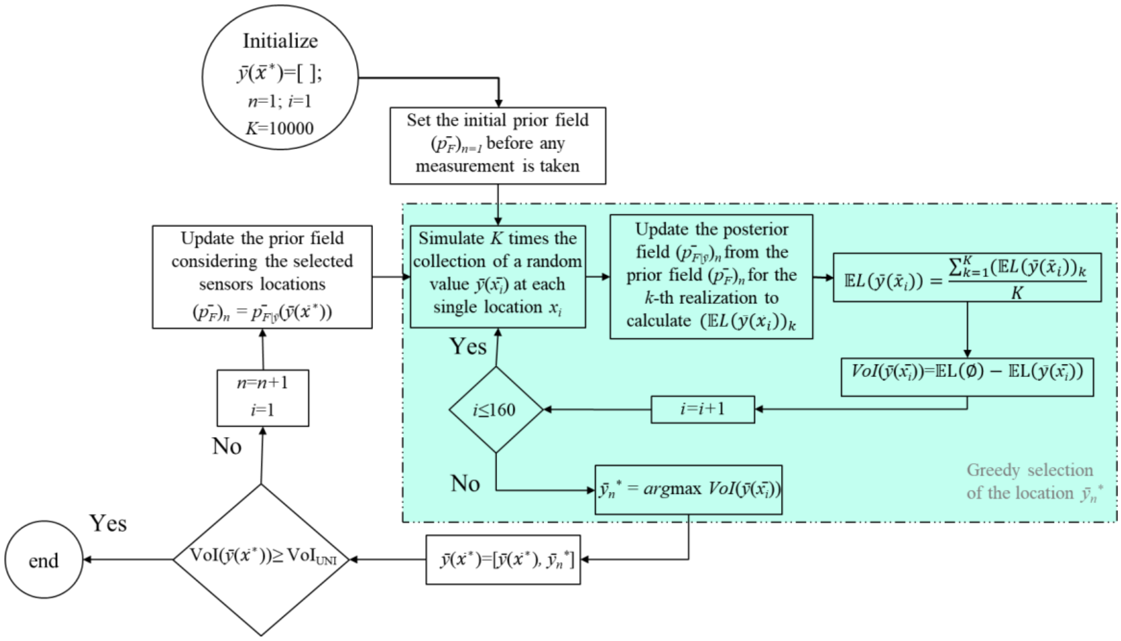

Figure 13: Flowchart for VoI-based greedy optimization

At each n-th iteration, we aim at positioning one sensor among the 160 candidate positions. The posterior field $(\bar{p}_{F|\bar{y}})_n$ is calculated K=10000 times to simulate K different stochastic realizations of $\bar{y}(\bar{x}_i)$ (i.e., to consider the stochasticity of the measurement, instead of assuming one possible realization, K=10000 realizations of a measurement are considered). The posterior expected loss $\mathbb{E}L(\bar{y}(\bar{x}_i)) = \frac{\sum_{k=1}^{10000}(\mathbb{E}L(\bar{y}(\bar{x}_i))_k}{10000}$ (Equation (4)) is calculated and VoI($\bar{y}(\bar{x}_i)$ is quantified; the sensor position $\bar{y}_n^*$ that yields the largest VoI($\bar{y}(\bar{x}_i)$) value among the 160 candidate positions is added to the optimal set $\bar{y}(\bar{x}^*)$ and the prior belief $(\bar{p}_F)_n$ of the next iteration becomes the posterior field, informed by $\bar{y}(\bar{x}^*)$ (i.e., $(\bar{p}_F)_n = \bar{p}_{F|\bar{y}}(\bar{y}(\bar{x}^*))$. In other words, a sensor position is added to $\bar{y}(\bar{x}^*)$ in each iteration and the effects of adding this single sensor position in the next iteration's search to another single sensor position is considered by considering the n-th iterations prior field $(\bar{p}_F)_n$ equal to previous field's posterior $\bar{p}_{F|\bar{y}}(\bar{y}(\bar{x}^*))$. The search of the optimal location sets stops when the set $\bar{y}(\bar{x}^*)$ yields a VoI value greater than or equal to VoI_{UNI} that represents the positioning of 32 sensors in the 32 locations identified by (*) in Figure 12 (as supported by the technical procedure in the Italian guideline ISPESL n. 48/2003 [90] and, specifically, the norm (UNI 11096, 2012) [52], assuming that inspection costs are negligible with respect to C_m and C_f).

Figure 14 shows the contour plots of VoI at the first iteration of greedy optimization, where the circle identifies the location where the max VoI would have been reached if the sensors were positioned there.

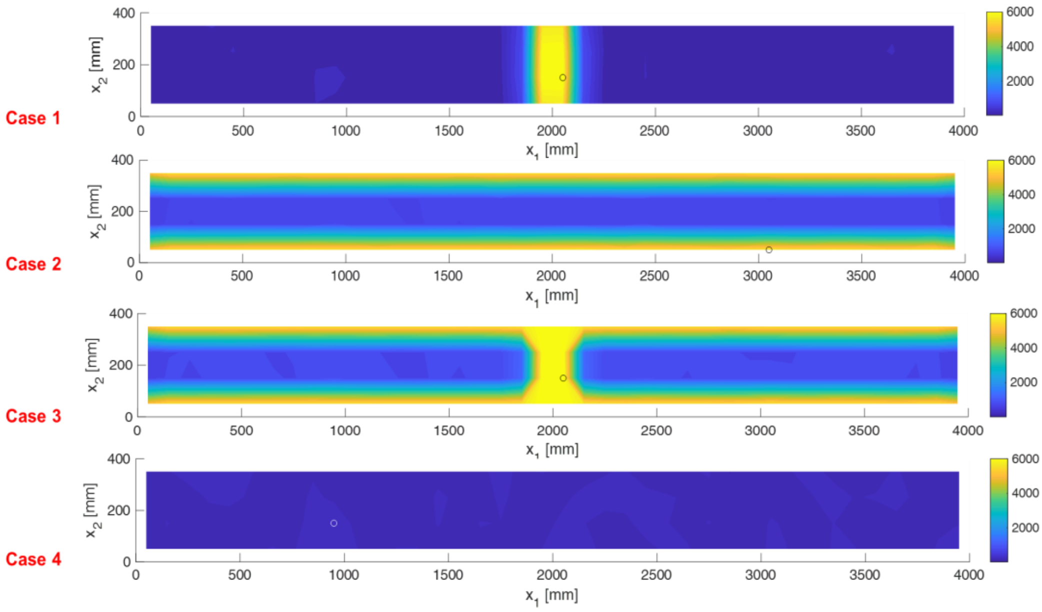

Figure 14: VoI contours for the four case studies at the first iteration n=1

It can be seen that locations close to the WHAZ (with larger uncertainty) also have larger VoI; a further proof comes from the case study 4, for which all locations have the same $\bar{p}_F$ and, therefore, the VoI for any *i*-th location is almost identical with all other locations (i.e., slight difference in VoI is due to the stochasticity of the random field characterization). Additionally, the chance of a location to be selected as the single location that has the max VoI value in WHAZ area, from an engineering point of view, should be equal as the uncertainty is the same (e.g., all locations of WHAZ area shown in yellow in case 2 have the same chance to be selected as the point with max VoI and their VoI is slightly different due to the stochasticity of the analysis.)

Figure 15 shows the optimal sensors positions $\bar{y}(\bar{x}^*)$ for each of the case studies. The number of sensors n required to exceed VoI_{UNI} is 5, 17, 18, 32, respectively (where the numbers indicate the order of positions selected by the optimization strategy).

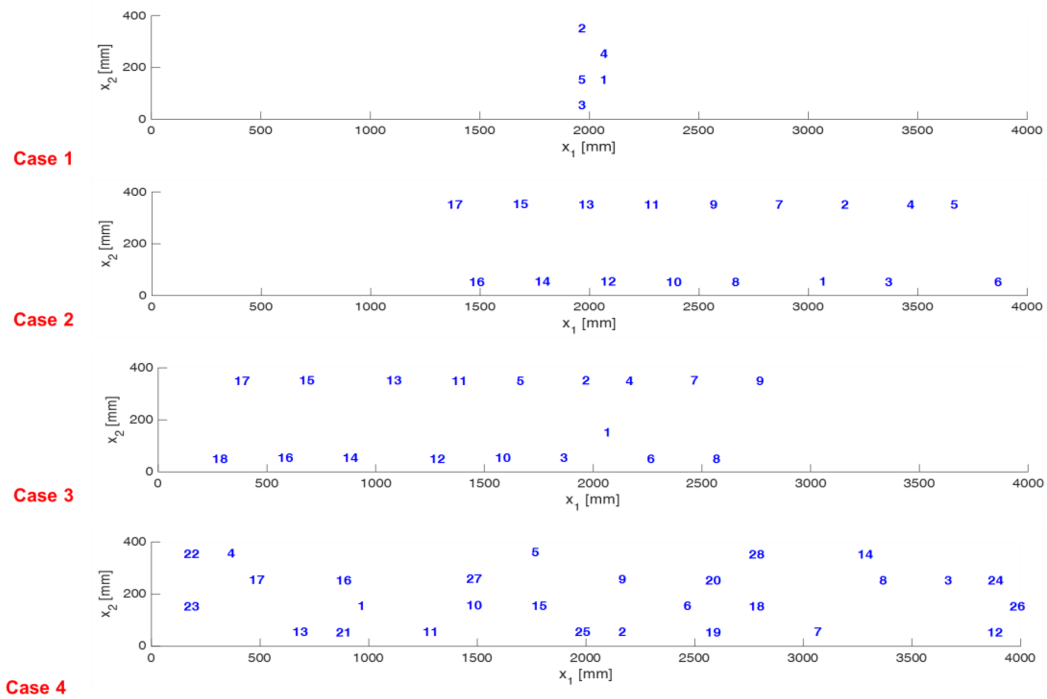

Figure 15: Sensor positioning using the greedy optimization algorithm for the four case studies

In all cases, $n < n_{\mathrm{UNI}}=32$ and the ratio $r = \frac{VoI}{n}$ is defined to show the VoI-per-sensor in each case study. Similarly, $r_{UNI} = \frac{\mathrm{VoI_{UNI}}}{n_{\mathrm{UNI}}}$ shows the VoI-per-sensor obtained by positioning by the [52] guidelines with $n_{\mathrm{UNI}}=32$. Table 4 compares quantitatively the VoI, number of sensors n, and the VoI-per-sensor ratio r in the different case studies, with their corresponding values of the (UNI 11096, 2012) sensors positioning. The VoI-per-sensor ratio r of the case studies are compared with their associated r_{UNI} values, with the coefficient of improvement C_I showing how much the VoI-per-sensor ratio r is improved using the suggested framework ($C_I = \frac{r}{r_{UNI}}$).

Table 4: Comparison between the UNI 11096 and the proposed method for sensor positioning

Case Study	*VoI*	*n*	*r*	*VoI*$_{UNI}$	n_{UNI}	r_{UNI}	C_I
1	2.6495e+04	5	5299	2.6386e+04	32	824.56	6.43
2	9.9772e+04	17	5868.94	9.4014e+04	32	2937.94	2.00
3	1.0727e+05	18	5959.44	1.0420e+05	32	3256.23	1.83
4	6.1561e+03	28	219.86	5.9847e+03	32	187.02	1.18

It can be seen that the VoI-based sensor positioning strategy in all cases gives a better VoI-per-sensor than following the normative recommendation of [52].

2.3.1.1. Considerations on Geometrical Symmetry

Due to the symmetry of the manifold geometry and thickness distribution, one might argue that positioning sensors in locations n_s with the same uncertainty should not imply differences in VoI. To test this hypothesis, let us consider case study 1, in which n_s=8 potential sensors locations fall in the WHAZ area with large uncertainty (i.e., elements in the frame highlighted in Figure 16) and they may be equally selected as one of the optimal location of each greedy optimization iteration (i.e., $\bar{y}_n^*$). These locations are sketched in Figure 16 (top).

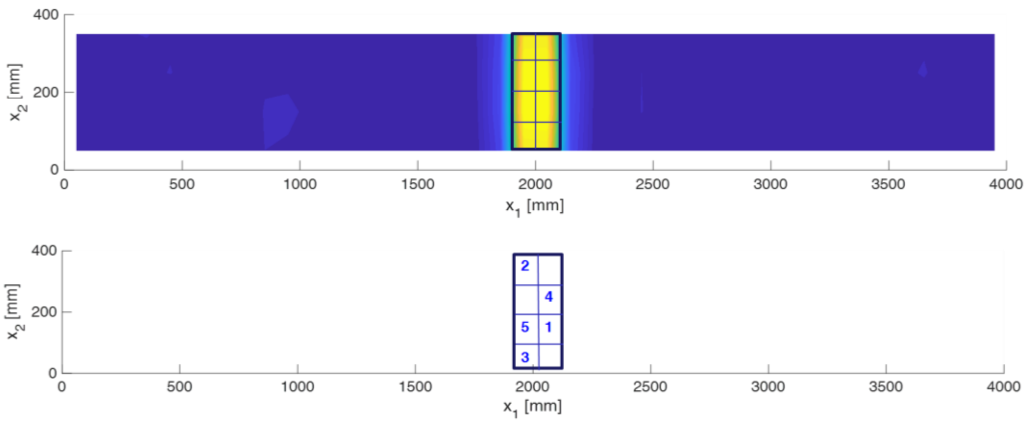

Figure 16: Sensor positioning for case study 1

As mentioned in Section 2.3.1, to exceed the VoI_{UNI} value of case study 1, a measurement set $\bar{y}(\bar{x}^*)$ comprised of n=5 sensors were needed (shown in Figure 16 (bottom)). However, if the sensor positioning approach is repeated 1000 times to find $\bar{y}(\bar{x}^*)$ and the probability that each one of these n_s locations being selected as one of the n optimal sensors of $\bar{y}(\bar{x}^*)$ is calculated, the results shown in Figure 17 are obtained, showing that the probability of each location being selected as one of the n optimal sensors positionings is 62±5% (the fluctuation is due to the randomness inherent in the Monte Carlo simulation and in the realizations of the measurements), which proves that the locations n_s sharing the same uncertainty and geometrical properties have almost equal probability to be selected as one of the optimized locations for sensor positioning of the optimal set $\bar{y}(\bar{x}^*)$.

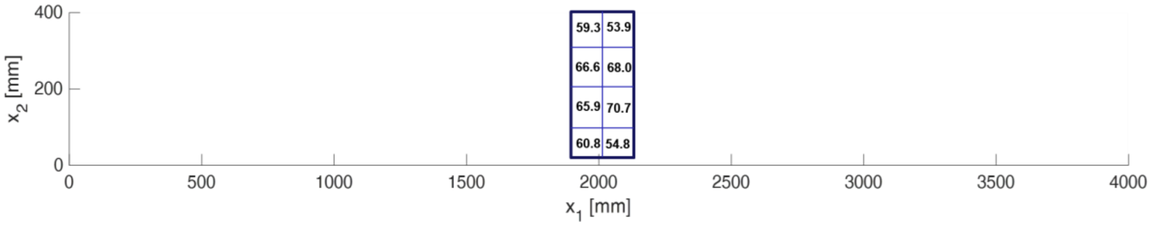

Figure 17: Probability of the sensors locations to be selected as one of the optimal positions (%)

2.3.1.2. Practical example for non-sub-modularity of VoI

In this Section, the greedy method is conducted on the manifold of case study 1. Instead of trying to exceed the VoI_{UNI}, the procedure of greedy optimization is here assumed to continue iteratively, until the VoI improvements are less than a predefined negligible benefit (here arbitrarily taken equal to 4000 €), resulting in the set of 5 sensors locations, shown in Figure 18.

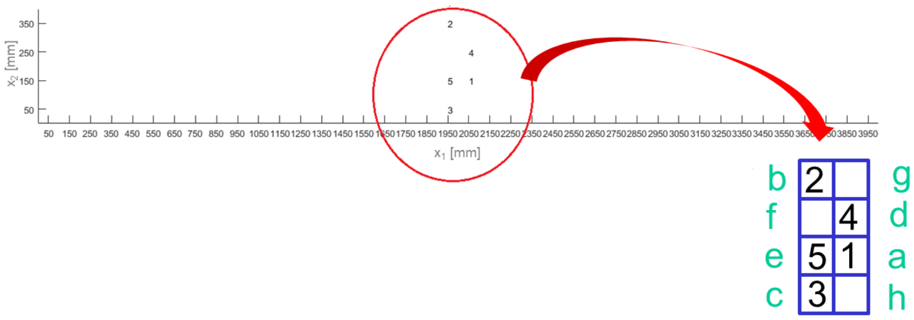

Figure 18: The arrangement of sensors positioning by greedy optimization

It is worth mentioning that, as expected, all the n=5 sensors are placed in WHAZ locations with larger uncertainty on the thickness (labeled with a to h as in Figure 18): this is to say that acquiring information under this condition provides the highest benefit (i.e., VoI), because it allows reducing the posterior uncertainty. The detailed VoI value of these single sensor locations are presented in Table 5. For example, positioning sensor in *b* provides a VoI equal to 5691 €, compared to the benefit of no measurement. It is worth mentioning that, due to symmetry of the pipe and equal uncertainty in WHAZ area, VoI values of Table 5, from an engineering point of view, should be the same and the difference is due to the stochasticity in measurement realizations.

Table 5: VoI for single sensor locations

	Sensors							
	a	***b***	***c***	***d***	***e***	***f***	***g***	***h***
VoI	6203	5691	5693	6132	6177	6091	5701	5682

The sensor location labeled as *a* has the maximum VoI value as a single sensor configuration and is selected as the first sensor location by greedy optimization. The values of the VoI in the step-by-step iterations followed by the greedy method are given in Table 6. As it can be seen, since the VoI improvements in the sixth iteration are less than 4000 € (i.e., 30043-26495=3548 €), the first n=5 sensors locations are selected as the final optimal set.

Table 6: VoI for greedy sensor positioning in each iteration

	Sensors					
Iteration	***1***	***2***	***3***	***4***	***5***	***6***
Location	***a***	***a, b***	***a, b, c***	***a, b, c, d***	***a, b, c, d, e***	***a, b, c, d, e, f***
VoI	6203	12463	17745	22464	26495	30043

In this Section, we practically show the sub-modularity issue in the case study. As shown in Table 6, when at the second iteration, location *b* is added to *a,* the resulting benefit (i.e., VoI({a,b})-VoI({a})=12463- 6203 = 6260 €) is larger than the VoI value of *b* alone (shown in Table 5 (i.e., 5691)). This implies that the inequality of (14), with $\bar{y}_1(\bar{x})$ =∅ $\bar{y}_2(\bar{x})$ =$\{a\}$ and $\bar{y}_s(\bar{x})$ =$\{b\}$, is not satisfied since adding *b* to *a* result in an increasing return, rather than in a diminishing return (see Figure 19). This increasing return property of the non-sub-modular VoI metric that causes VoI(*a*,*b*)>VoI(*a*)+ VoI(*b*) could be explained by the advantageous benefit that a 2 configuration sensors positions set provides on the measurement of adjacent areas due to the correlation of these 2 sensors in comparison to that of two separate single configurations.

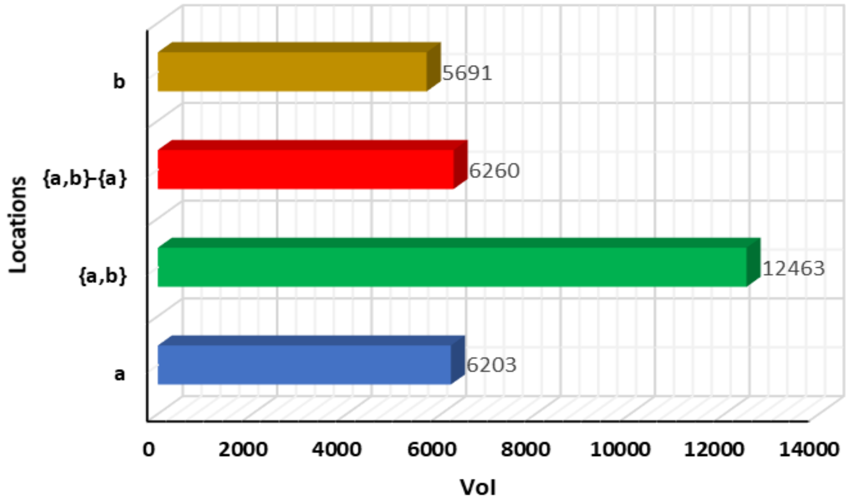

Figure 19: Sub-modularity issue with a subset of locations

This shows that the VoI metric is not sub-modular, causing the sensor positioning not to be optimal (but still, sub-optimal). If we rely on a non-greedy optimization method such as Particle Swam Optimization (PSO) to optimize the sensors positioning constrained by the requirement that in j=160 candidate locations only a set of n=5 sensor locations are to be selected, a different result is obtained as shown in Table 7.

Table 7: VoI of 5 sensor locations by greedy and non-greedy methods

Optimization method	**Greedy**	**Non-Greedy**
Sensors selected	*a, b, c, d, e*	*a, b, c, f, g*
VoI	26495	26926

The non-greedy optimization results in a VoI 2% larger (26926) than that of the greedy optimization result (26495), since locations *f* and *g* are selected instead of *d* and *e*. Figure 20 compares the VoI values obtained with the non-greedy optimization (dot) and those obtained by greedy optimization adding one location at a time (line).

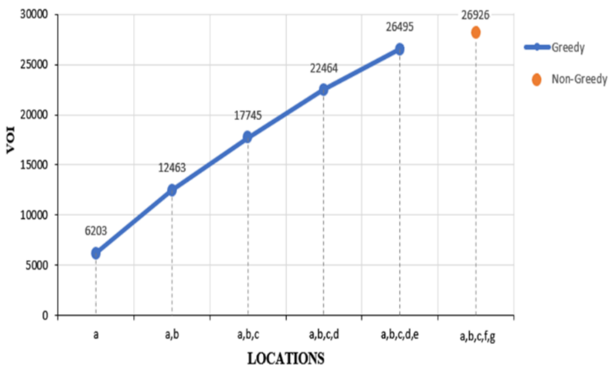

Figure 20: Comparison of the VoI values in greedy and non-greedy optimizations

2.3.1.3. Considering the inspection cost

In this section, for case 1, it is assumed that taking measurement comes with a cost $C(\bar{y}(\bar{x}))$ that depends on the measurement set $\bar{y}(\bar{x})$ and comprises of a fixed cost of measurement chair system installation equal to 3 K€ plus a cost proportional to the number of sensors in the set $n(\bar{y}(\bar{x}))$ where each sensor costs 250 €:

$$C(\bar{y}(\bar{x})) = 3000 + 250 \times n(\bar{y}(\bar{x})) \tag{24}$$

Using Equations (1)-(5) and the specific loss function defined in Equation (21) we will quantify the VoI.

Greedy method is here used to find the optimal set of measurement $\bar{y}(\bar{x}^*)$ that yields the maximum benefit by solving the optimization problem of Equation (7). To this end, as discussed by details in Section 2.2.1, single best sensor positions are sequentially quantified and added one by one until the maximum benefit is reached. In this section, we continue the iterations until the cost of sensors positioning suppresses the benefit gained meaning that $B_{VoI}(\bar{y}(\bar{x}))$ in iteration n+1 is less than its value in iteration n. Table 8 shows the VoI, total benefit and selected sensors positions ID number (i.e., ID number is defined for all 160 sensors positions starting from 1 at bottom left to 160 at top right as shown in Figure 21) quantified by greedy method.

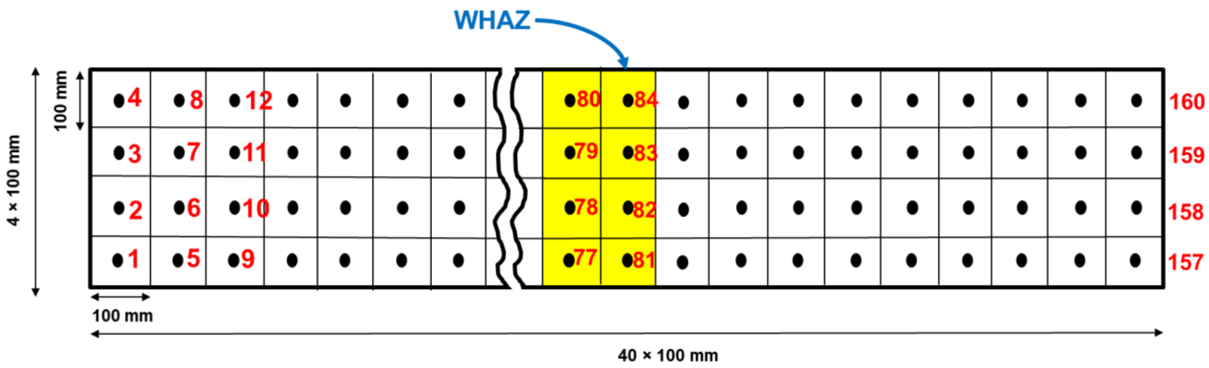

Figure 21: Schematic view of numbering the ID numbers of sensors positions

As can be seen, at the 10th iteration $B_{VoI}(\bar{y}(\bar{x}^*))$ is smaller than its value at the 9th step, meaning that the cost of an additional sensor is not justified by the increase in VoI. Therefore, the optimal set $\bar{y}(\bar{x}^*)$ is the one resulted at the 9th iteration with B_{VoI} $(\bar{y}(\bar{x}^*))$ = 32547.62 €.

Table 8: Details quantities of greedy method in 10 iterations

n	$\bar{y}(\bar{x}^*)$	**VoI** $(\bar{y}(\bar{x}^*))$	$C(\bar{y}(\bar{x}^*))$	B_{VoI} $(\bar{y}(\bar{x}^*))$
1	82	6203.85	3250	2953.85
2	82, 80	12463.17	3500	8963.17
3	82, 80, 77	17745.91	3750	13995.91
4	82, 80, 77, 83	22464.18	4000	18464.18
5	82, 80, 77, 83, 78	26495.20	4250	22245.20
6	82, 80, 77, 83, 78, 84	30403.15	4500	25903.15
7	82, 80, 77, 83, 78, 84, 81	34115.92	4750	29365.92
8	82, 80, 77, 83, 78, 84, 81, 79	37535.84	5000	32535.84
9	82, 80, 77, 83, 78, 84, 81, 79, 38	37797.62	5250	32547.62
10	82, 80, 77, 83, 78, 84, 81, 79, 38, 71	38037.97	5500	32537.97

To confirm the result, in Figure 22, we show the curve of total benefit solving the optimization problem by the greedy method for all iterations until covering all the160 candidate sensor: As can be seen, the benefit B_{VoI} $(\bar{y}(\bar{x}))$ rapidly increases from 1st to 8th iteration, then there is a small increase in 9th iteration and after that it is decreasing until 160th iteration, showing once more that the optimal solution lays in the 9th iteration.

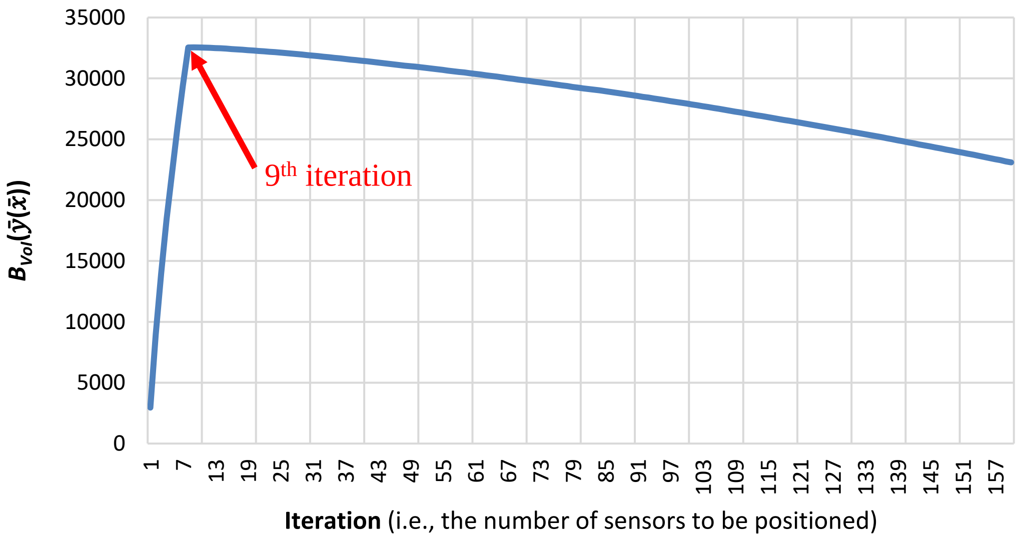

Figure 22: The total benefit of sensors positioning by greedy method

An in-depth analysis of the selected set of positions {82, 80, 77, 83, 78, 84, 81, 79, 38} highlights that all these 8 sensors positions located at WHAZ area (in yellow at Figure 21) characterized by a larger uncertainty on the random field $f(\bar{x})$ of thickness are among the selected 9 sensors positions; this means that taking measurements in positions with larger uncertainty yields larger benefits (according to VoI) because this helps reducing it, whereas larger uncertainty, consequently would provide larger benefits. Positions with smaller uncertainty would provide less benefit in gaining accurate knowledge on the field $f(\bar{x})$ and their positioning is, therefore, not justified by their costs.

2.3.2. Sensors positioning by non-greedy method

Two non-greedy optimization methods namely, Genetic Algorithm (GA) and Particle Swarm Optimization (PSO) [93] are used to find the $\bar{y}(\bar{x}^*)$ for the case study 1 while considering the inspection cost like Section 2.3.1.3. In contrast to the greedy method which finds the optimal set by sequentially adding single sensors positions, the non-greedy method finds the optimal set by smartly searching into all potential measurement sets with different number of sensors positions n (i.e., $1\leq n\leq 160$). Using GA and PSO, the optimal set is searched among all the possible sets of measurement that may have 1 to 160 members. Non-greedy methods concluded the same result of greedy method, in Section 2.3.1.3, with n=9 sensors positions (i.e., {82, 80, 77, 83, 78, 84, 81, 79, 38}). However, this calculation almost took 8 hours by non-greedy method instead of 5 minutes of the greedy method with our typical computer.

In this case study, the optimal set $\bar{y}(\bar{x}^*)$) obtained by greedy and non-greedy methods were finally identical and the non-sub-modularity of VoI metric did not affect the final result. The detailed plot of the iterations of PSO method used to find the optimal set with $B_{VoI}(\bar{y}(\bar{x}^*))$ value equal to 32547.62 after 106 iterations is shown in Figure 23. Unlike the greedy method, the number of sensor *n* in each iteration is not equal to the iteration number itself and the number of sensors position in each iteration *n* could be any number between 1≤ *n*≤160. In other words, regardless of the number of sensors position *n* in the optimal set $\bar{y}(\bar{x}^*)$, non-greedy method searches into all configurations of sensors positions in each iteration and finds the one with the largest B_{VoI} value which, in the case study $\bar{y}(\bar{x}^*)$ has *n*=9 sensors positions with $B_{VoI}(\bar{y}(\bar{x}^*))$=32547.62.

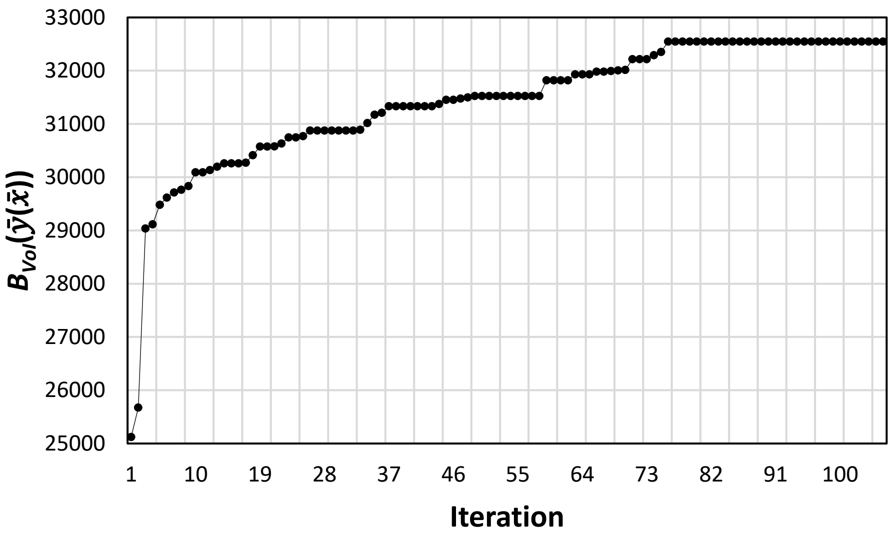

Figure 23: The plot of total benefit in each iteration of the PSO method

There are cases where the non-sub-modularity of the VoI metric may cause the greedy method to fail to find the optimal solution. However, there is no guarantee to find the optimal solution even with sub-modular metrics. To practically show this, the following examples are provided:

GA and PSO are utilized to solve 9 separate optimization problems and find 9 sets of $\bar{y}(\bar{x}^{*})$ where each sets number of sensors positions n is restricted to a certain value, namely n=1,2,3,4,…,9. In other words, in this approach, the number of sensors positions in the optimal set $\bar{y}(\bar{x}^{*})$ is deliberately restricted to n and the non-greedy optimization method in each of the 9 optimization problems search only among candidate sensors positions that have n members. For example, at 4th optimization problem where n=4, the non-greedy method searches into all possible configurations of 4 sensors positions and finds the one which yields the largest benefit. Therefore, at the end of these 9 optimizations, there are 9 optimal set $\bar{y}(\bar{x}^{*})$ each representing the set with largest benefit in n sensors positions configuration and their resulted sensors positions as well as B_{VoI} $(\bar{y}(\bar{x}^{*}))$ are compared with those of the greedy optimizations results as shown in Table 9.

Table 9: Detailed comparison of greedy and deliberately constrained non-greedy optimization

n	Greedy		Non-greedy	
	$\bar{y}(\bar{x}^{*})$	B_{VoI} $(\bar{y}(\bar{x}^{*}))$	$\bar{y}(\bar{x}^{*})$	B_{VoI} $(\bar{y}(\bar{x}^{*}))$
1	82	2953.85	82	2953.85
2	82, 80	8963.17	80, 82	8963.17
3	82, 80, 77	13995.91	80,81,83	14034.65
4	82, 80, 77, 83	18464.18	77,79,82,84	19171.76
5	82, 80, 77, 83, 78	22245.20	77,79,80, 82,84	22671.81
6	82, 80, 77, 83, 78, 84	25903.15	77,79,80, 81,82,84	26165.96
7	82, 80, 77, 83, 78, 84, 81	29365.92	82, 80, 77, 83, 78, 84, 81	29365.92
8	82, 80, 77, 83, 78, 84, 81, 79	32535.84	82, 80, 77, 83, 78, 84, 81, 79	32535.84
9	82, 80, 77, 83, 78, 84, 81, 79, 38	32547.62	82, 80, 77, 83, 78, 84, 81, 79, 38	32547.62

As can be seen in Table 9, the non-greedy method where n is equal to 3,4,5 or 6, finds different $\bar{y}(\bar{x}^{*})$ than the greedy method where also has larger B_{VoI}. In other cases, the results of both optimizations approaches are identical. These examples, practically, show the cases that the greedy method, due to the non-sub-modularity of VoI, fails to find the optimal solution.

2.3.3. Sensors positioning by subset simulation

The SS method is here used to find $\bar{y}(\bar{x}^{*})$ that satisfies the condition $P(G)$=0 of the event G={$B_{VoI}\left(\bar{y}(\bar{x})\right) > B_{VoI}(\bar{y}(\bar{x}^{*}))$}, as defined in Equation (7) and (8) with the following steps:

1. Generate N_p=200 independent and identically distributed samples of measurement sets $\bar{y}(\bar{x})$ (with random number of sensors positions *n* and random positioning)
2. Quantify $B_{VoI}\left(\bar{y}(\bar{x})\right)$ of the N_p samples and sort in increasing order
3. Select N_t=p_0N_p=100 top solutions as seed samples to be fed to the MCMC (i.e., p_0 is the conditional probability (being constant in all intermediate events *i* and, in this work, is assumed to be equal to 0.5)
4. Generate by MCMC (1- p_0)N_p new conditional samples from the selected N_t seed samples, by using modified Metropolis-Hastings algorithm (Au & Beck, 2001) and stochastically generating samples (i.e., seed samples plus the conditional MCMC samples consist in N_p possible measurement sets solution of the optimization problem and for each of N_t seed samples a Markov chain with 1/p_0 length is generated). The proposal distribution is the conditional distribution and algorithm stops when the maximum sample standard deviation is less than the target tolerance here assumed to be equal to 1e-4.
5. Repeat steps 3 and 4 until the convergence of the optimization in Equation (8) is satisfied (i.e., $P(G)$ = 0)

As shown in Figure 24, after 50 iterations in 1 hour and 57 minutes, the optimal set with $B_{VoI}(\bar{y}(\bar{x}^*))$ = 32547.62 euros with the same set of sensors positions configuration obtained by greedy and non-greedy method (i.e., $\bar{y}(\bar{x}^*)$ = [82, 80, 77, 83, 78, 84, 81, 79, 38]) is obtained. It is worth mentioning that this 9-sensors configuration (found by greedy, non-greedy and SS) is also the true optimal solution that can be found by exhaustive search. After all 8 sensors positions of WHAZ area is filled with sensors (i.e., 8 sensors positions with max VoI), the 9th sensors position of the 9-sensors configuration can be easily found by searching among 152 remained sensors positions which is the location with ID number 38.

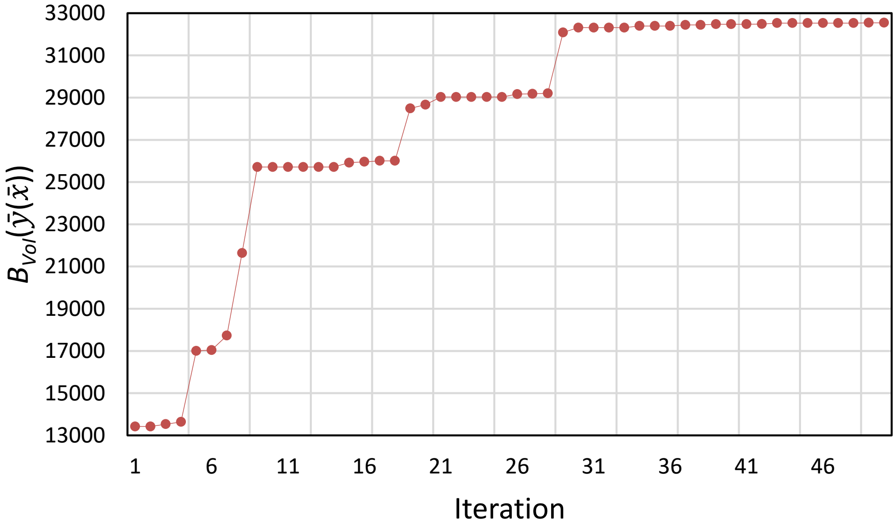

Figure 24: The iterations of SS method and the path toward finding $\bar{y}(\bar{x}^*)$

The SS method, as proved in the case study, can find the optimal solution four times faster than the non-greedy method. Additionally, it does not have the drawbacks of greedy method for the non-sub-modular VoI. To prove this, the 9 optimizations performed by the non-greedy method with the approach of restricted number of sensors positions *n* (described in Table 3) are conducted using the SS method. Results are shown in Table 4 and are identical to the non-greedy method whereas *n*=3,4,5, and 6, the SS method yielded better result than the greedy method.

Table 10: Detailed comparison of greedy and deliberately constrained SS optimization

n	Greedy		SS	
	$\bar{y}(\bar{x}^*)$	B_{VoI} $(\bar{y}(\bar{x}^*))$	$\bar{y}(\bar{x}^*)$	B_{VoI} $(\bar{y}(\bar{x}^*))$
1	82	2953.85	82	2953.85
2	82, 80	8963.17	80, 82	8963.17
3	82, 80, 77	13995.91	80,81,83	14034.65
4	82, 80, 77, 83	18464.18	77,79,82,84	19171.76
5	82, 80, 77, 83, 78	22245.20	77,79,80, 82,84	22671.81
6	82, 80, 77, 83, 78, 84	25903.15	77,79,80, 81,82,84	26165.96
7	82, 80, 77, 83, 78, 84, 81	29365.92	82, 80, 77, 83, 78, 84, 81	29365.92
8	82, 80, 77, 83, 78, 84, 81, 79	32535.84	82, 80, 77, 83, 78, 84, 81, 79	32535.84
9	82, 80, 77, 83, 78, 84, 81, 79, 38	32547.62	82, 80, 77, 83, 78, 84, 81, 79, 38	32547.62

2.4. Conclusions

In this part of the PhD thesis, the framework for VoI-based data acquisition is proposed to find the optimal sensors positioning with three different methodologies namely, greedy method, non-greedy method, and subset simulation with a case study of sensors positioning of a SG of PFBR under creep.

The sensors positioning obtained in Section 2.3.1 using the proposed greedy framework is compared with the sensors positioning recommendation of the standard [52] and gives results that not only justify the positioning of the standard, but also require less sensors to reach the VoI that would be obtained by duly implementing the current guidelines/norms. This proposed advanced computational framework can be used for supporting the development of guidelines based on past operational experience and could be particularly useful for those ones with limited past operational records. Then, the main limitation of greedy approach, non-sub-modularity of VoI, is practically shown in Section 2.3.1.2 and non-greedy and SS methods are proposed to overcome this.

The pros and cons of each method in solving the problem of sensors positioning is summarized in Table 11 which compares the characteristics of each method used to solve the problem of optimal sensors positioning, namely, the sensitivity to the non-sub-modularity of VoI metric, the elapsed time dedicated to run the method in a typical computer and a qualitative judgment on difficulties associated with settings and coding of the methods.

Table 11: Detailed comparison of the methods used on optimal sensors positioning

Optimization method	Sensitive to the non-sub-modularity of VoI	Elapsed time	Difficulty in settings
Greedy	Yes	< 1 hour	Intermediate
Subset Simulation	No	2 hours	High
Non-greedy, GA	No	8 hours	High
Non-greedy, PSO	No	8 hours	High

The greedy method has the lowest time and effort required to set the method and run the optimization. However, due to the non-sub-modularity of VoI, as practically shown in Tables 9

& 10 and in Section 2.3.1.2, greedy method cannot be trusted to always achieve the optimal result. The non-greedy methods (both GA and PSO), despite being not sensitive to the non-sub-modularity of VoI, are difficult to set and require huge computational effort to find the optimal solution. The SS method, at the other hand, can be trusted as a powerful efficient method that does not have the drawbacks of greedy (i.e., not sensitive to non-sub-modularity of VoI) and non-greedy method (i.e., SS is 4 times faster than non-greedy) and is the recommended method for the optimal sensors positioning. Finally, it is concluded that the obtained results by greedy method can give a rough estimate for the sensors positioning, but it can never be considered as the optimal solution. For a precise trustworthy solution, it is always required to search by non-greedy methods or SS for the optimal sensors positions, preferably with the latter as it demands less computational efforts. The result of this computational work can be utilized to advance the process of data acquisition in safety related SSCs for a more profitable and reliable condition monitoring.

3. CB-PRA MAINTENANCE DECISION SUPPORT

Contents of the Chapter have been adapted from the following publications disseminated from the PhD thesis (Along with the numbering, [J] represents Journal article, [C] represents Conference paper and [B] represents Book, e.g., 3[J] represents the 3rd published journal article):

3[J] S.M. Hoseyni, F. Di Maio, E. Zio, "Condition-based probabilistic safety assessment for maintenance decision making regarding a nuclear power plant steam generator undergoing multiple degradation mechanisms". Reliability Engineering & System Safety. 2019 Nov 1;191:106583.

1[B]F. Antonello, P. Bragatto, F. Di Maio, S. M. Hoseyni, E. Zio, "Stima adattiva del rischio di rottura di attrezzature in pressione, sulla base dei dati di monitoraggio", Quaderni INAIL, 2019, ISBN: 978-88-7484-174-5.

Condition-Based Probabilistic Risk Assessment (CB-PRA) developed in [22], makes use of inspections and monitoring information on SSCs to update risk quantities. CB-PRA is adopted in this PhD thesis, to show the benefits of exploiting the optimal condition monitoring data, addressed in Chapter 2, to provide condition-based estimates for taking maintenance decisions on a SSC undergoing multiple degradation mechanisms even with budgetary constraints.

The methodology is presented with respect to a spontaneous Steam Generator Tube Rupture (SGTR) accident scenario that may occur in a Pressurized Water Reactor (PWR) [22]. Different degradation mechanisms that affect the SG tubes integrity are considered [58]. Stress corrosion cracking (SCC) and pitting are eventually mentioned as the mechanisms most contributing to SGTR [59]. To counteract these degradation mechanisms, some maintenance strategies like tube plugging and Water Lancing and Chemical Cleaning (WL-CC) are commonly implemented [60]. These maintenance strategies are usually enforced according to regulatory guideline when corrosion reaches specific thresholds of developments [61, 62]. These strategies are found to be non-optimal [63]: numerous cases of unnecessary plugging have been reported worldwide [64] arguing that the risk related to possible NPP accidental scenarios generated by SG degradation is neither optimally controlled nor cost-efficient. In this study, we propose a decision framework, based on CB-PRA risk measures estimates for the operators to dynamically choose, at each inspection cycle, the optimal maintenance action to be undertaken to trade-off the risk of any accident that might be induced by a SGTR and the related maintenance cost. Indeed, realistic case of constrained budgetary resources is assumed, challenging for the operator choice on the maintenance strategy to be adopted (i.e., not only beneficial for safety but also economically affordable). The results show that the proposed framework enables the decision maker to predict the degradation evolution, predict the tube failure time, calculate the risk of SGTR failure due to the multiple degradation mechanisms and prioritize the maintenance actions, under budget constraints [20]. It is shown that the operators can optimally take the safest and most economic decision for maintenance, with respect to the state-of-practice NUREG report [66].

In Section 3.1, the methodology is presented with respect to a spontaneous Steam Generator Tube Rupture (SGTR) accident scenario that may occur in a Pressurized Water Reactor (PWR). In Section 3.2, the methodology of CB-PRA maintenance support tool is discussed. To show the application of the methodology, the SG of Zion NPP is selected as details are provided in Section 3.3. Results of a case study regarding SGTR show that the decisions based on the risk estimates provided by a CB-PRA approach allow controlling the SGTR risk at minimum maintenance cost.

3.1. The Spontaneous SGTR Accident Scenario

The SGTR accident scenario is one of the most significant accidents in NPPs that can lead to core damage [58]. SG tube rupture can not only lead to a modest release of radioactive material to the environment, but also, if not properly controlled, to severe core damage and substantial release of radioactive material. In this study, without loss of generality, spontaneous SGTR accident scenario in a typical PWR (i.e., the Zion NPP) is analyzed. It is assumed that tube ruptures are caused by multiple degradation mechanisms, specifically SCC and pitting, which are the main contributors to tube ruptures [63].

In a traditional level 1 PRA, the SGTR accident scenario is modeled by an Event Tree (ET) [94] (see Figure 25), where the core damage is one of the possible end states reached after the Initiating Event (IE) of SGTR is triggered, with frequency f_{SGTR} estimated as:

$$f_{SGTR} = \frac{N + 1/2}{T} \tag{25}$$

where $N = 3$ is the number of SGTR occurrences in $T = 499$ years of similar NPPs operations, irrespectively of the failure mechanism that has induced the SGTR (the interested readers are invited to refer to [98, 99] for further information). A simplified event tree with a spontaneous SGTR initiating event potentially leading to core damage is shown in Figure 25. Some safety functions/systems are considered and modelled to mitigate the SGTR effects, namely: the operator driven plant depressurization (OD), the Reactor Water Storage Tank (RWST) refill and, finally, the Reactor Coolant System (RCS) heat removal. If all the safety functions/systems are operational, the plant end state would result to be safe, whereas if any of them fails, core damage occurs. In the ET of Figure 25, the frequency of IE is computed from Equation (25), resulting in a value of 7.01×10^{-3} per reactor year and the probabilities of failure of operator depressurization OD, RWST and RCS are taken equal to 1.8×10^{-4}, 2.4×10^{-8}, 5.6×10^{-5} per reactor year, respectively, from [97]. The ET (static) approach of Figure 25 provides a Core Damage Frequency CDF_{static} (constant in time) equal to 3.92×10^{-7} per reactor year.

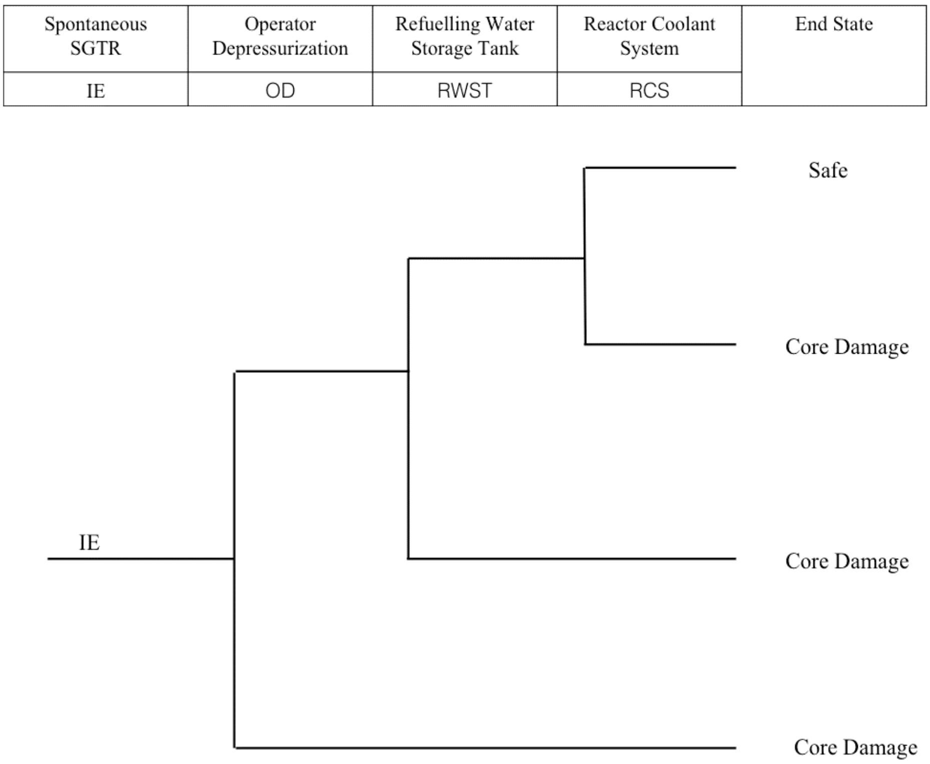

Figure 25: Simplified event tree for a spontaneous SGTR

In CB-PRA, we rely on models of the multiple degradation mechanisms (i.e., SCC and pitting, in this case) to calculate f_{SGTR}: onset, formation, and propagation models of SCC, besides models of initiation and growth of the pits, are used to predict the degradation progression and, finally, to update the values of f_{SGTR} and CDF.

3.1.1. The steam generator

We consider the Zion PWR NPP, with SGs of 3.6 m of diameter and 21 m of height. Each SG weighs 800 tons and consists of a bundle of N_{tb} =3592 inverted U-shaped tubes with nominal outside diameter of d_{nom} equal to 22.23 mm. Nominal thickness $t_{s,nom}$ is equal to 1.27 mm to withstand a nominal pressure difference on the tube wall equal to ΔP_{nom} =8.3 MPa. Details on the Zion NPP parameters are provided in Tables 12 and 13, together with their uncertainties [98, 22]. It is worth mentioning that these random variables are independent.

Table 12: Parameters of the Zion NPP [97]

NPP Operating Conditions	
Nominal Power W_{nom}	1110 MW_e

Primary side pressure $P_{in,nom}$	15.2 MPa
Secondary side pressure $P_{out,nom}$	6.9 MPa
SG Parameters	
Number of tubes N_{tb}	3592
Material	Alloy 600MA
Ultimate tensile strength (UTS) S_u	713 MPa
Yield strength (YS) S_y	362 MPa

Table 13: Uncertainty in tubes parameters [22]

Parameter	**Nominal Value**	**Uncertainty [uniform distribution]**
Outside diameter d_{nom}	22.23 mm	+/- 0.5 mm
Thickness $t_{s,nom}$	1.27 mm	+/- 12.5%
Nominal pressure difference ΔP_{nom}	8.3 MPa	+/- 1 MPa

3.1.2. The SGTR degradation mechanisms

The most significant degradation mechanism that can affect the SG during its expected mission time (T_m = 60 years) is SCC, which contributes to 60 to 80 percent of tubes defects requiring plugging. Pitting and fretting collectively account for 15 to 20 percent [99]. In this work, we complement the analysis in [22] by considering the simultaneous effects of multiple degradation mechanisms on the spontaneous SGTR accident scenario and investigating the maintenance activity to be performed at each *t*-th inspection cycle, here taken equal to two years, when inspection of the SG is also allowed due to core refueling. Degradation in tubes is inspected with techniques that are assumed to be perfectly reliable. For the prevention of tube rupture, it is assumed that plugging and WL-CC are performed as maintenance strategies to counteract SCC and pitting, respectively. Alternatively, instead of plugging the tubes with medium-sized cracks, sleeving can be selected as another option of maintenance. However, since sleeving imposes higher operational costs than plugging [63], it is opted out of this research.

In this research, two different separate approaches are used to model the two main degradation mechanisms affecting SG performance, that are SCC and pitting. While the axial growth rate of the stress corrosion cracks is modeled by the Scott model [100], the through-wall penetration rate of the pits is modeled by the Turnbull model [101]. Both degradation models describe a one-dimensional damage to SG tubes, modelling axial crack length growth and pit depth growth, respectively for SCC and pitting. The models describing for SCC and pitting are briefly presented in the following Sections.

3.1.2.1 Stress corrosion cracking

The tube cracking process induced by SCC can be divided into three phases: onset, formation, and propagation [22]. Crack onset and formation are modelled based on the real data collected in the Zion NPP (see [97]).

To estimate the onset probability of cracks in the SG, a Maximum Likelihood Estimation (MLE) approach is used to fit the available data collection (see [97] for further details) to a Weibull distribution, with Probability Density Function (PDF) of Equation (26) whose parameters b and λ are equal to 0.3654 and 30.1609, respectively:

$$f(t) = \frac{b}{\lambda^b} t^{b-1} e^{(\frac{-t}{\lambda})^b} \tag{26}$$

For cracks formation, it is assumed that in about 9.3 years (with standard deviation of 3.2 years), at the operating temperature of 330 °C, axial microcracks reach a critical length of 0.1 mm at which propagation becomes faster [103]. Following the Scott model [103], which is an empirical model that depends on the material property, tube dimension and pressure difference of the tube bundles, the crack growth rate $\frac{da}{dt}$ which grows in the axial direction is modeled as in Equation (27):

$$\frac{da}{dt} = \alpha_s . (K_s - K_{th})^{\beta_s} \tag{27}$$

where α_s, β_s and K_{th} are constant values, and the stress intensity factor K_s is derived from Equation (28):

$$K_s = F_g \frac{\Delta P.d}{2t_s}\sqrt{\frac{\pi a}{2}} \tag{28}$$

where F_g is a geometric factor, ΔP is the actual pressure difference between the inner and the outer sides of the SG tube, d is the actual outer tube diameter, and t_s is the thickness of the tube (see Table 2 for the nominal values of these parameters ΔP_{nom}, d_{nom}, and $t_{s,nom}$). The nominal values of the crack growth parameters are listed in Table 14:

Table 14: Parameters of crack growth used in the Scott model [22]

Parameter	Minimum	Maximum	Nominal
α_s	2.5e-2	3.1e-2	2.8e-2
K_{th} (MPa $\sqrt{m}$)	8	10	9
β_s	1.07	1.25	1.16
F	-	-	0.93

According to NUREG report [66], when a reaches a_{lim} = 1.52 mm, the tube where that crack has propagated must be plugged as soon as it is detected when inspected, to avoid reaching the critical crack length a_{cr} (i.e., the spontaneous SGTR is induced). It is worth mentioning that a_{cr} is calculated from Equation (29):

$$\Delta P = \frac{P_b}{m_b} = \frac{P_b}{0.614 + 0.481\phi + 0.386e^{-1.25\phi}} \tag{29}$$

where P_b is the burst pressure of an unflawed virgin tube, m_b is the bulging factor, and $\phi = \frac{1.82\, a_{cr}}{\sqrt{2d - t_s}}$ [105]. The critical crack length a_{cr}, therefore, changes in time depending on the actual workload of the plant and the pressure difference, W and ΔP, respectively (that, incidentally, also influences K, and in turn, $\frac{da}{dt}$). Therefore, we can claim that plugging may not be always the optimal decision, because costly and not always effective for controlling the SGTR occurrence [60]: Indeed, plugging reduces the heat transfer surface and the primary system mass flow rate, and increases the actual ΔP (facilitating the crack propagation as shown in [22]); large amount of plugging also reduces the reactor nominal power and generates economic losses [103]. This problem is overlooked by regulation but can be improved by the application of CB-PRA to support maintenance decisions, as we shall see in what follows. In practice, the optimized condition-based plugging strategy introduced in [22], consists in plugging tubes when the identified crack at inspection time t is calculated to exceed a_{cr} within the t-th cycle and t+1-th cycle of length 2 years with more than 1% probability (see [22] for further details), instead of when the cracks exceed the plugging limit a_{lim}, as regulation would suggest.

3.1.2.2. Pitting

Pitting is a local corrosion mechanism which typically occurs at the tube surface where pre-existing defects are incidentally generated by surface machining and whose growth is accelerated by impurities [104]. Pitting can be modeled as a two steps stochastic process: pit initiation and pit growth [105, 106]. Pit initiates when breakdown occurs in the passive layer of the metal surface and consequent metal dissolution takes place, whereas pit growth occurs when corrosion radially penetrates the tube wall and creates small holes [107, 101].

For pit initiation, stochastic models are proposed based on Non-Homogeneous Poisson Processes (NHPP): let the number of initiated pits $N(t)$ at time t (for all the SG tubes surface area) follow a NHPP [108, 109, 110] with a power law intensity function $\lambda(t) = \alpha t^{\beta-1}$, where α and β are the scale and shape parameters taken equal to 0.0014 and 4.526, respectively, as in [108] where the pitting initiation process is modeled for a SG that has similar specifications (height, length, surface area, …) and properties (material, working pressure and temperature, …) to those of Zion NPP. The expected number $\Lambda(t)$ of initiated pits at time t is:

$$\Lambda(t) = \int_0^{2t} \lambda(s)ds = \frac{\alpha}{\beta}(2t)^{\beta} \tag{30}$$

and the expected number m of pits initiated within the two successive inspection cycles t+1 and t (of length 2 years):

$$m = \Lambda(t+1) - \Lambda(t) = \frac{\alpha}{\beta}\left((2(t+1))^{\beta} - (2t)^{\beta}\right) \tag{31}$$

The number n_{pit} of pits that are initiated during the t-th cycle follows a Poisson distribution:

$$Pr\{N(t+1) - N(t) = n_{pit}\} = exp\left(-[\Lambda(t+1) - \Lambda(t)]\right)\frac{[\Lambda(t+1) - \Lambda(t)]^{n_{pit}}}{n_{pit}!} \tag{32}$$

Figure 26 shows the cumulative number of pits initiated at each inspection cycle t, and the 5% and 95% percentiles (i.e., a two-sided 90% confidence interval).

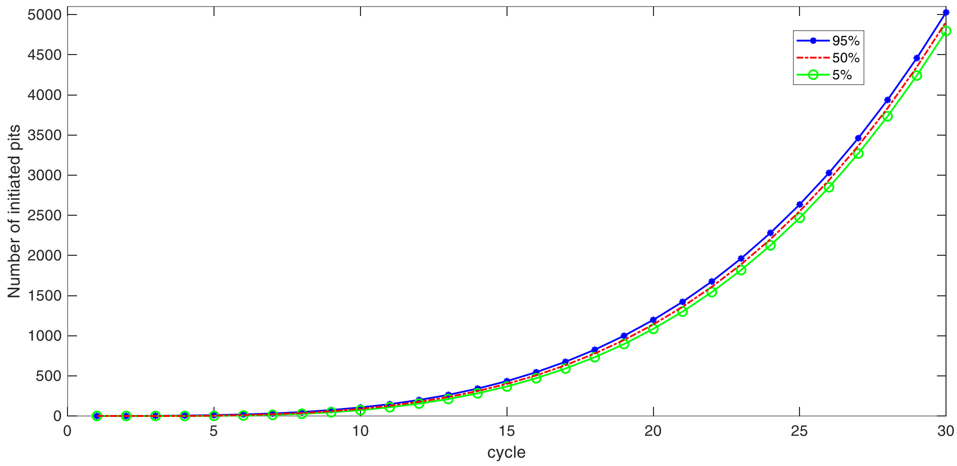

Figure 26: A two-sided 90% confidence interval for the number of initiated pits, at each SG inspection cycle

Following the initiation of a small pit, we use the model in [101] to simulate the pit growth in time. The pit growth is modelled as a one-dimensional radial degradation in the wall depth direction. As soon as the through-wall depth of the pit exceeds a specific threshold, failure of the tube will occur [108]. The radial growth rate $gr(x_{pit})$ of the pit size x_{pit} [m] in through-wall direction is equal to:

$$\frac{dx}{dt} = gr(x) = \delta\gamma^{\frac{1}{\delta}}x^{(1-\frac{1}{\delta})} \qquad (33)$$

$$x_{pit} = \gamma t^{\delta} \qquad (34)$$

where γ and δ are fitting parameters experimentally calculated: γ is assumed to be distributed as a truncated positive normal distribution with mean value equal to 0 and standard deviation equal to 1.36e-5, and δ is taken as a constant equal to 0.064, [111]).

With reference to the operational experience in [108], plugging must be enforced when the Through Wall Depth (TWD), $x_{pit}/t_{s,nom}$ reaches 51%, meaning that plugging is done when x_{pit} penetrates 51% of the tube thickness $t_{s,nom}$ to avoid it reaches the failure threshold TWD_{cr} = 95%: a small pit that may exceed the failure threshold TWD_{cr} would trigger a SGTR accident scenario [66]. Moreover, regulation recommends performing Water Lancing and Chemical Cleaning (WL-

CC) at least once in T_m, not only for reducing the corrosive environment during SG operation, due to the large concentration of chlorides and sulfites in deposit, but also for improving the heat transfer rate of the tubes [60]. By WL-CC, sludges are removed and, consequently, pits initiation is temporarily slowed down to 80% [64, 108, 109]. However, there is no theoretical evidence that changes to the SG operational conditions can modify the growth parameters [106], although cracks formed by pitting propagate slower than those induced by SCC. Then, in this work, we assume pitting is controlled only by WL-CC (and not also by plugging).

3.2. Maintenance Support Tool

SG degradation can be counteracted by plugging the tubes [58] or by WL-CC [112]. These strategies can be enforced at each inspection time t, but at a cost. We denote the budgetary constraint as B_c for each cycle and as $B(t)$ for the cumulative available budget at cycle t. The risk measures updated at each inspection by the CB-PRA are utilized to evaluate the risk due to the different degradation mechanisms and prioritize the activities of maintenance. On the basis of the CDF estimates relative to SCC and pitting provided by CB-PRA at each inspection, the operator chooses the balance of plugging and WL-CC to perform on the SG tubes, so as to trade off cost (up to the maximum affordable cost $B(t)$) and risk at each t-th cycle.

The cost of WL-CC is assumed to be 5 times the initial budget (B_c) of each cycle [113]; the plugging cost depends on the number of tubes that must be plugged: if the number of plugged tubes is smaller than 300 tubes it is equal to $0.2B_c$, otherwise the cost is $0.6B_c$ [63].

The novel framework (sketched in Figure 27) for simultaneously considering pitting and SCC and deciding on the most proper budget of maintenance activities, consists of four nested steps, namely degradation modelling, risk prioritization, cost assessment and decision making. In practice, starting from inspection cycle t = 1

1. Set the operational conditions that are expected to be experienced by the SG up to the next cycle t+1, i.e., the number of available tubes N_{tb}, the actual pressure difference ΔP, the water chemistry and the sludge content (that affect α and β of Equation (30));

    - **a: Degradation Modeling (SCC)**

- **a.1.** Define a_{cr}, depending to the operational conditions (see Equation (29));
- **a.2.** Simulate the SCC microcracks generation and their propagation up to the next cycle t+1 (see Equations (26) & (27)): First, the probability of a crack onset and formation (i.e., the probability that the crack length reaches the limit beyond which it propagates) is calculated by the convolution of the two distributions of onset (Equation (26)) and formation (N ~ (9.3, 3.2) years). Then, the crack is propagated by Equation (27) up to the next cycle t+1;
- **a.3.** Simulate the SCC progression of the existing cracks up to the next cycle t+1 (see Equation (27));
- **a.4.** Calculate the number of tubes $N_p(t)$ that should be plugged, according to the optimized condition-based plugging strategy presented in [22] (i.e., tubes are plugged only if the crack length x exceeds a_{cr}, with probability larger than 1%);
- **a.5.** Calculate the number of tubes $Ft(t)$ with cracks exceeding a_{cr} if no plugging is enforced and the corresponding $CDF_{SCC}(t)$, as follows [22]:

$$CDF_{SCC}(t) = f_{SGTR}(t) \times \frac{CDF_{static}}{f_{SGTR}} \tag{35}$$

Assuming $N_{tb}(t)$ is the number of tubes available at cycle t, and these tubes are independent, $f_{SGTR}(t)$ is the frequency of SGTR occurrence at cycle t:

$$f_{SGTR}(t) = 1 - \prod_{N_{tb}(t)} (1 - f_{TR}(t)) \tag{36}$$

where f_{TR} is the expected tube rupture frequency between cycles t and t +1:

$$f_{TR}(t) = \frac{Ft(t) + \frac{1}{2}}{t \cdot N_{tb}(t)} \tag{37}$$

$f_{TR}(t)$ is a function of the number of available tubes $N_{tb}(t)$ at cycle t and the number of tubes $Ft(t)$ with cracks exceeding a_{cr}. Since $Ft(t)$ and $N_{tb}(t)$ are changing in time based on the maintenance strategy that is enforced, the value of $f_{TR}(t)$ should be accordingly updated, which results in the change of $f_{SGTR}(t)$ in time.

- **b: Degradation Modeling (Pitting)**
- **b.1.** Define TWD_{cr} depending on the operational conditions;

- **b.2.** Simulate pits initiation and their stochastic growth up to the next cycle t+1 (see Equation (0-32));
- **b.3.** Simulate the progression of the existing pits up to the next cycle t+1 (Equation (33));
- **b.4.** Calculate the number of tubes $Ft(t)$ with pits exceeding TWD_{cr} if no WL-CC is enforced and compute the $CDF_P(t)$, as follows:

$$CDF_P(t) = f_{SGTR}(t) \times \frac{CDF_{static}}{f_{SGTR}} \quad (38)$$

where $f_{SGTR}(t)$ is calculated as in Equations (36-37) and is updated in each cycle based on the current properties of the tubes, as explained in section a.5.

c. Risk Prioritization

c.1. Compare $CDF_{SCC}(t)$ and $CDF_P(t)$ for risk prioritization:

- **c.2.** If $CDF_{SCC}(t) \leq CDF_{static}$ or $CDF_P(t) \leq CDF_{static}$, there is no need to perform plugging or WL-CC, respectively.

✓ if $CDF_{SCC}(t) \geq CDF_P(t)$ and $CDF_{SCC}(t) > CDF_{static}$, priority goes to plugging to counteract SCC;

- **d. Cost Assessment**
- **d.1.** if $N_p(t) \geq 300$, then the maintenance cost is $C(t)$=0.6B_c.
- **d.2.** else if $N_p(t) < 300$, then $C(t)$ = 0.2B_c.
- **d.3.** set saved budget $S(t) = B(t)$-$C(t)$, if it is decided to perform plugging; then, if $S(t) \geq 5.0B_c$, WL-CC can be performed.

✓ else if $CDF_{SCC} < CDF_P$ and $CDF_P > CDF_{static}$, then priority goes to WL-CC to counteract pitting.

- **d. Cost Assessment**
- **d.4.** Set $C(t)$=5B_c
- **d.5.** set $S(t) = B(t)$- $C(t)$, if it is decided to perform WL-CC.
- **d.6.** Then, if $N_p(t) \geq 300$ and $S(t) \geq 0.6B_c$, plugging can be

performed.

- **d.7.** else if $N_p(t) < 300$ and $S(t) \geq 0.2B_c$, plugging can be performed.

e. Decision Making

e.1. Take decision:

- ✓ If priority is for plugging and $B(t) \geq C(t)$, then perform plugging and set $S(t) = B(t) - C(t)$.
  - Then, if no WL-CC has been performed before, and $S(t) \geq 5B_c$, perform WL-CC, and set $S(t) = S(t) - 5B_c$ and $C(t) = C(t) + 5B_c$.
- ✓ If priority is for WL-CC and $B(t) \geq C(t)$ and no WL-CC has been performed before, then perform WL-CC and set $S(t) = B(t) - C(t)$.
  - then, if $N_p(t) \geq 300$ and $S(t) \geq 0.6B_c$, perform plugging, and set $S(t) = S(t) - 0.6B_c$ and $C(t) = C(t) + 0.6B_c$.
  - else, if $N_p(t) < 300$ and $S(t) \geq 0.2B_c$, plugging can be performed, and set $S(t) = S(t) - 0.2B_c$ and $C(t) = C(t) + 0.2B_c$.

There may be cases when the budget is not sufficient for performing maintenance. Therefore, the maintenance is postponed to the next inspection cycle, accepting the risk of not performing maintenance.

2. At the end of each inspection cycle t, set $B(t+1) = S(t)+B_c$ and $t=t+1$ to repeat the framework for the next cycles, depending on the decisions taken, by setting:

- the number of available tubes N_{tb} (as in Equation (39)) if plugging is performed.

$$N_{tb}(t+1) = N_{tb}(t) - N_p(t) \tag{39}$$

where $N_p(t)$ is the number of plugged tubes.

- the pressure difference ΔP (as in Equation (40)) if plugging is performed.

$$\Delta P\ (t+1) = P_{in}(1 + \frac{N_p(t)}{N_{tb}(t)} \times 0.4)P_{out,nom} \tag{40}$$

because ΔP increases when the number of plugged tubes $N_p(t)$ increases.

- the number of initiated pits based on the improved environment after cleaning, which affects α and β of Equations (30) and (31) if WL-CC is performed

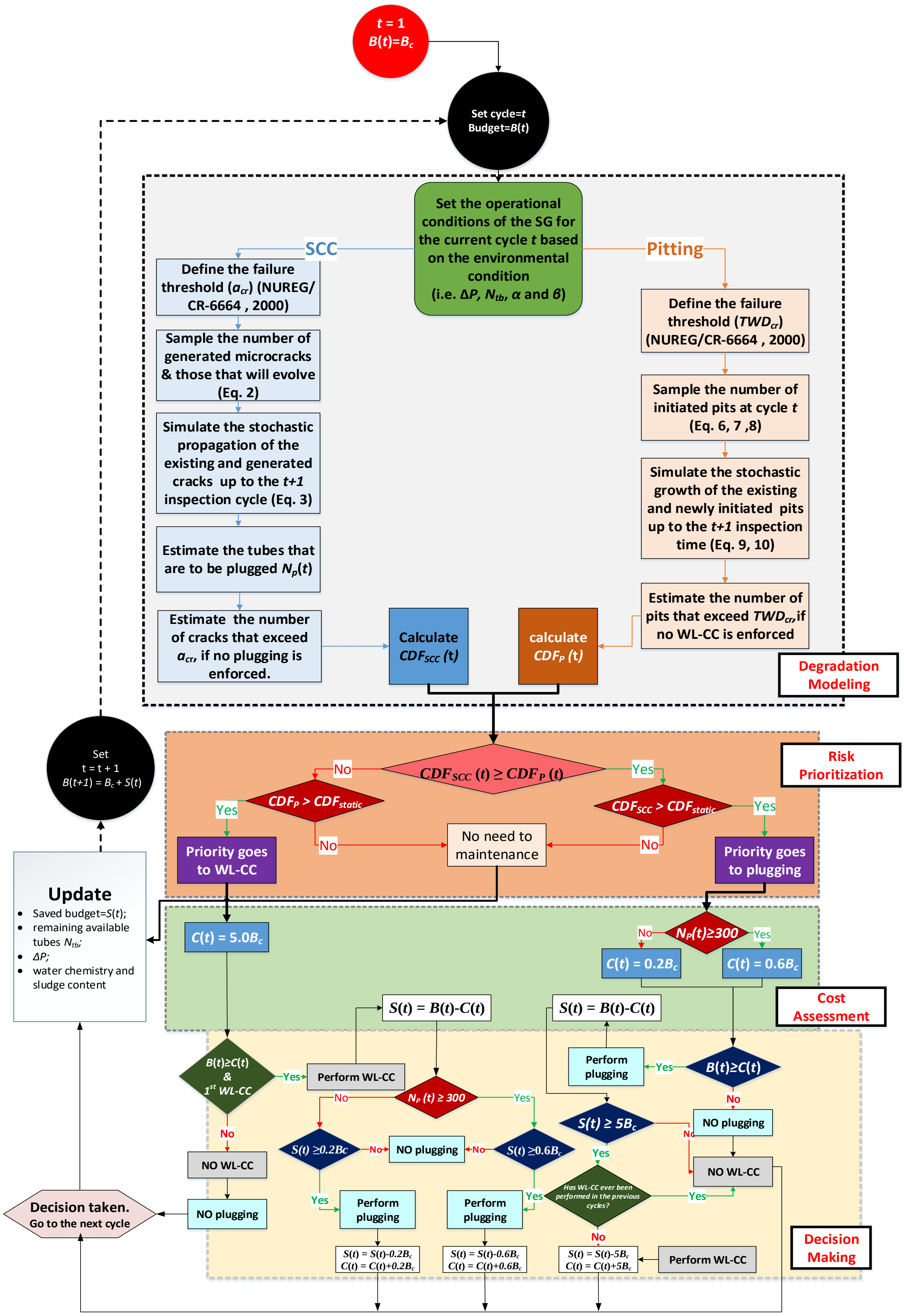

Figure 27: Flowchart of the risk-informed maintenance decision strategy

3.3. Case Study: SG of Zion NPP

The SG of the Zion NPP with the properties described in Section 3.1 is considered. At each cycle, (inspection time) t, starting from t = 1, with the operational conditions of the SG in Tables 12 and 13, the failure thresholds of a_{cr} and TWD_{cr} are set. The generation of microcracks and their growth progression are simulated up to the next cycle t+1 for SCC. At the same time, the pit initiation and stochastic growth of pits are stochastically simulated up to cycle t+1. The CDF estimates obtained at each inspection cycle, with the maintenance managed as explained in Section 3.1, are plotted in Figure 28: the bold continuous line is the estimated $CDF_{SCC}(t)$ and the dashed line is $CDF_P(t)$. For comparison, CDF_{static} is plotted in the dashed-dotted line. The values of $CDF_{SCC}(t)$ and $CDF_P(t)$ are calculated for each cycle to prioritize the maintenance activity, and the associated costs are used to inform the decision maker regarding the maintenance to be performed to counteract the most dangerous degradation. It should be noted that the value of $CDF_{SCC}(t)$ increases in time until the 7th cycle and, then, decreases until it reaches an almost constant value at the last cycles. This is due to the fact that most of the cracks due to SCC are generated at the earliest cycles of the SG operation, as shown in Figure 3 of [22] and, then, the probability of crack onset in a given cycle reduces with time. Therefore, as the operational time increases, the probability of crack onset and formation reduces as well. On the other hand, tubes that were plugged do not impair the SG integrity, resulting, as a whole, in the $CDFscc(t)$ decreasing in time.

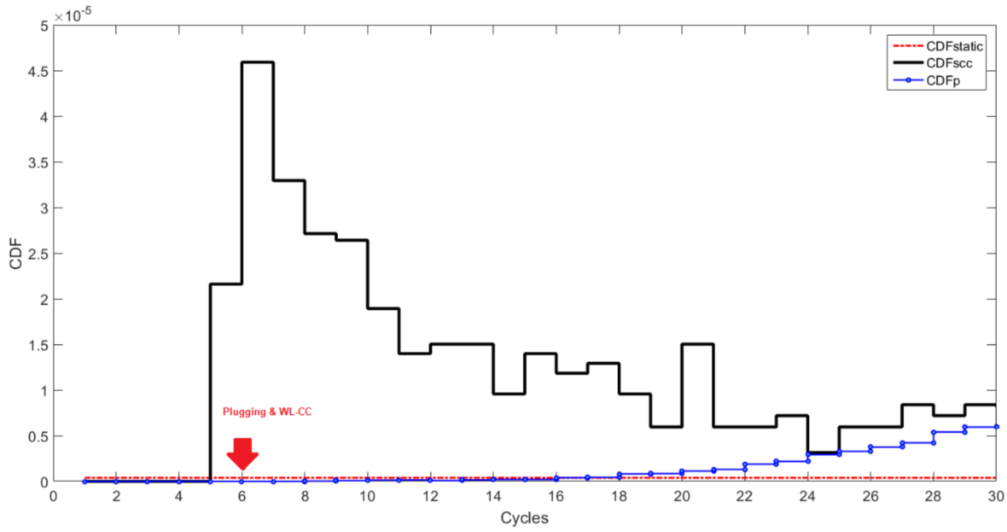

Figure 28: CDF estimates when CB-PRA estimates are used to prioritize maintenance

From inspection cycle t=1 to t=4, $CDF_{SCC}(t) < CDF_{static}$ and $CDF_P(t) < CDF_{static}$; therefore, there is no need to perform any maintenance. On the other hand, at inspection time t=5, $CDF_{SCC}(t) > CDF_P(t)$ making plugging the prioritized maintenance to counteract SCC. At cycle t=6, plugging is still the preferred maintenance activity, but since the available budget $B(t=6)=5.8B_c$ is enough for both plugging and WL-CC (cost $C(t=6)=5.2B_c$), both maintenances activities are performed, reducing the savings to $S(t=6)=0.6B_c$ as shown in Figure 29 where the total maintenance cost for each cycle $C(t)$ (continuous line), the cumulative savings $S(t)$ accumulated up to the current cycle t (dashed line), and the available budget of each cycle $B(t)$ (dotted line) are shown. At any following cycles plugging is performed.

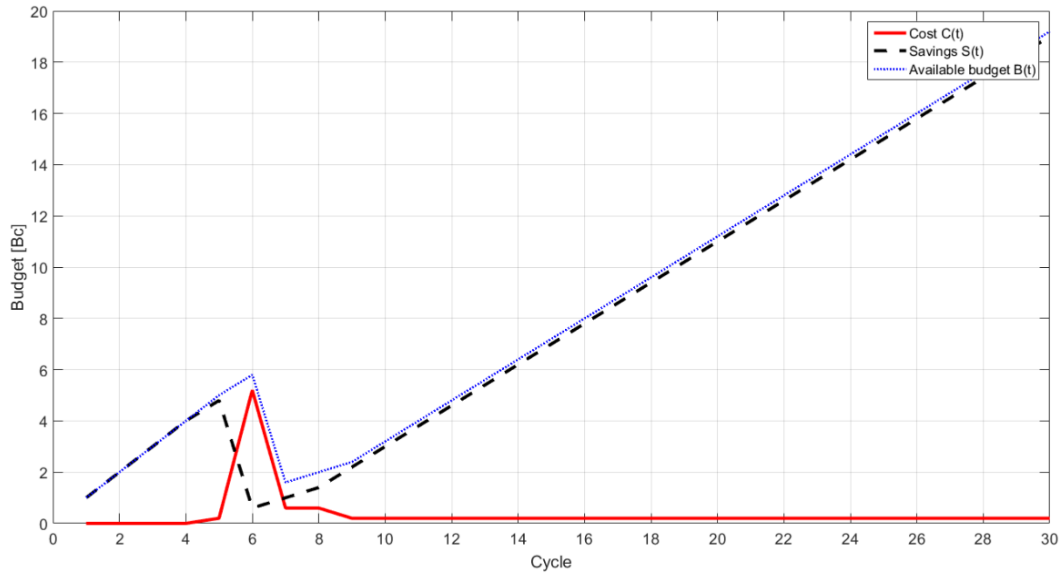

Figure 29: Comparison of the total cost of maintenance for each cycle $C(t)$ (continuous line), the cumulative saved money accumulated from previous cycles $S(t)$ (dashed line) and the available budget of each cycle $B(t)$.

Figure 30 shows the ratio between $C(t)$ and $B(t)$ (continuous line) and $S(t)$ and $B(t)$ (dashed-dotted line). At cycle 6, 90% of the available budget $B(t)$ is spent for maintenance. This budget is the result of savings accumulated in the first 5 cycles and is more than 90% of the available budget (dashed-dotted line from t=1 to 5).

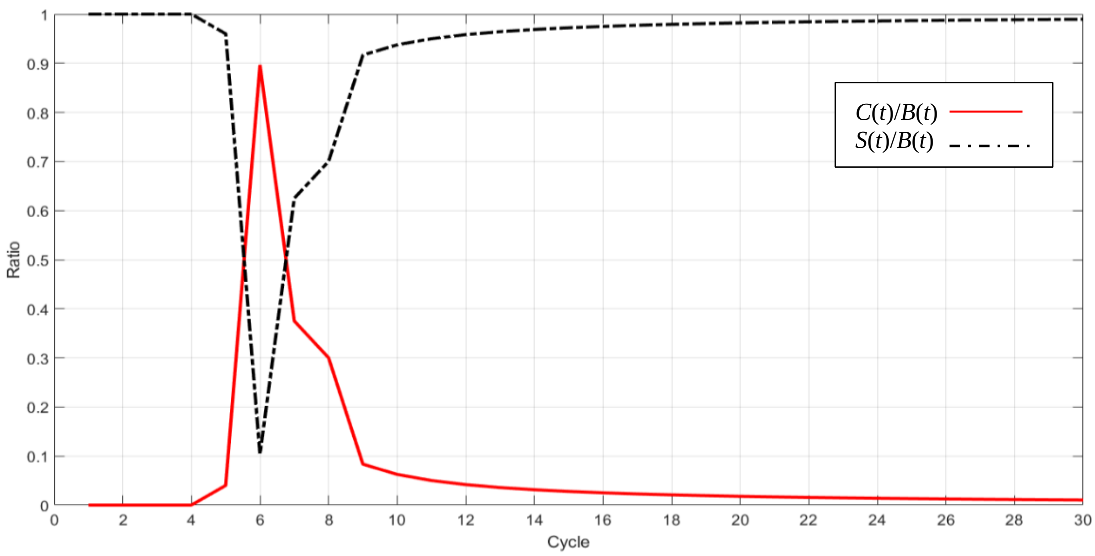

Figure 30: The ratio of risk-informed maintenance cost to available budget $C(t)/B(t)$ (continuous line) and savings *per available budget $S(t)/B(t)$* (dashed-dotted line).

Figure 31 shows the resulting $CDF_{MD,SCC}$ of SCC (i.e., CDF estimated by taking the Maintenance Decisions by CB-PRA to counteract SCC shown with dashed line with crosses) and $CDF_{MD,P}$ (dashed line) of pitting upon enforcement of the optimal maintenance at each cycle t and compares it with the traditional CDF_{static} (dashed-dotted line), the $CDF_{NRC,SCC}$ (continuous line), that would result from the enforcement of the NRC guidelines for plugging (i.e., exceeding the crack length of 1.52 mm in case of SCC) and the $CDF_{NRC,P}$ (continuous line with circles) resulting from performing one WL-CC in the lifetime of the SG at cycle 15. It can be seen that: i) $CDF_{MD,SCC}$ is zero at all cycles because of implementing plugging that never lets a crack to reach the failure threshold a_{cr}, ii) $CDF_{MD,P}$ initially increase and, then, decreases at cycle 11 thanks to the WL-CC performed at 6th cycle, iii) the positive effect of WL-CC at the 15th cycle for the NRC method is visible in $CDF_{NRC,P}$, after the 20th cycle, iv) $CDF_{NRC,P}$ and $CDF_{NRC,SCC}$ are larger than CDF_{static}, because they are the realistic risk measures updated by the plant conditions after each inspection cycle, v) for SCC, the $CDF_{MD,SCC}$ values with maintenance performed based on the CB-PRA results is always lower than its corresponding value $CDF_{NRC,SCC}$, where maintenance follows the NRC recommendations. For pitting, $CDF_{MD,P}$, is always lower than its corresponding value $CDF_{NRC,P}$, until the 25th cycle, and almost equal to it at the next cycles. These evidences show the beneficial effects of the proposed CB-PRA framework for maintenance decision making.

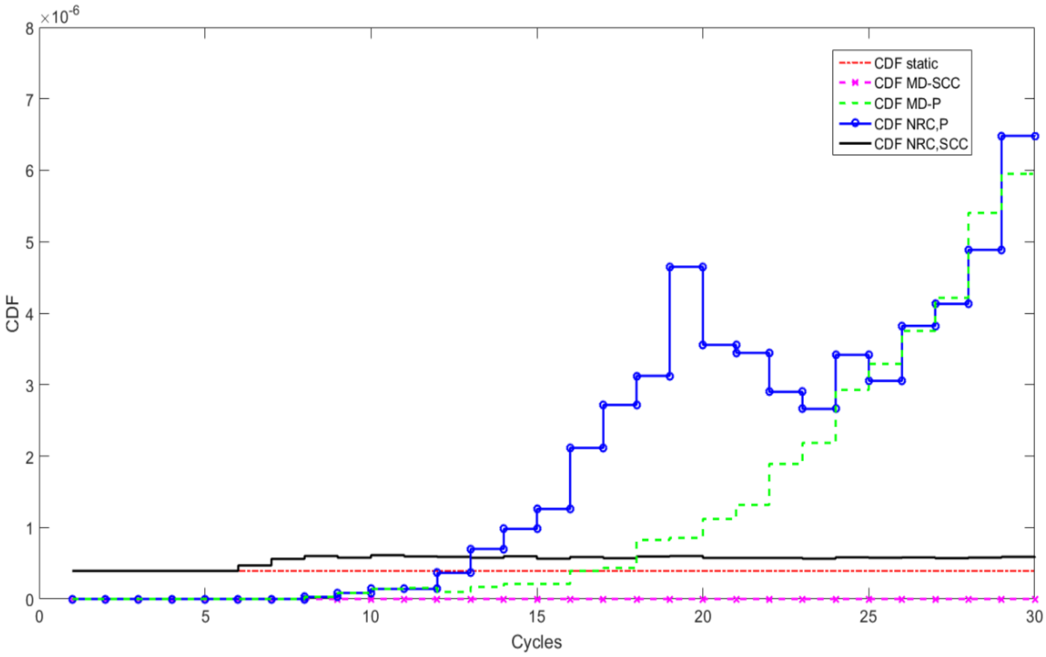

Figure 31: Comparison of CDF for multiple degradation mechanisms with different maintenance strategies.

Figure 32 shows the cumulative CDF when both pitting and SCC are considered as SGTR initiating events, and NRC procedures [66] (solid line) or CB-PRA driven maintenance decisions (dashed line) are followed. The proposed methodology controls better the escalation of the CDF as the NPP ages (CDF_{NRC} is larger than CDF_{MD}). It should also be noted that CDF_{NRC} is dynamically changing and at most cycles is larger than CDF_{static} (dashed-dotted red line), because the CDF is estimated with updated plant conditions. As previously shown in [22], risk measures are underestimated by the traditional static method (i.e., CDF_{static}).

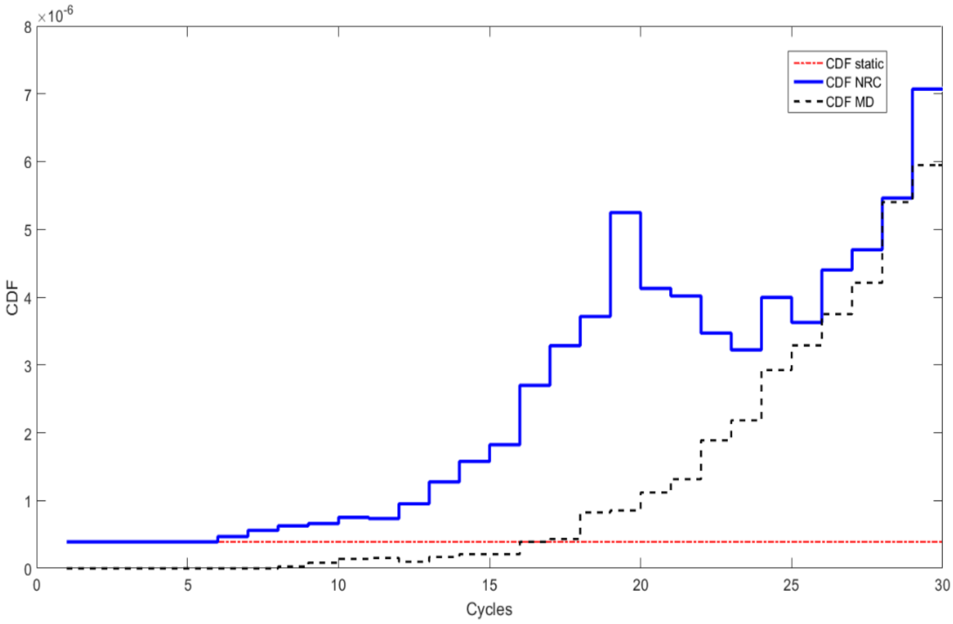

Figure 32: Comparison of CDF of the NRC procedure (solid line) with the CB-PRA driven maintenance decisions (dashed line).

Moreover, following the NRC guidelines [66]: i) the tubes should be plugged when the cracks exceed the failure threshold for both degradation mechanisms of pitting and SCC and ii) at least one WL-CC is recommended within the lifetime of the SG (here set to be performed at cycle 15). The advantage of the proposed methodology over the conventional NRC method, in terms of cost, is presented in Figure 33, where enforcing the NRC method gives 65% higher total cumulative maintenance cost $\sum_{t=1}^{30} C(t)$ at the end of the NPP life in comparison to our proposed maintenance methodology. Therefore, the proposed method not only leads lower risk than the NRC requirement (see Figure 32), but also smaller cost.

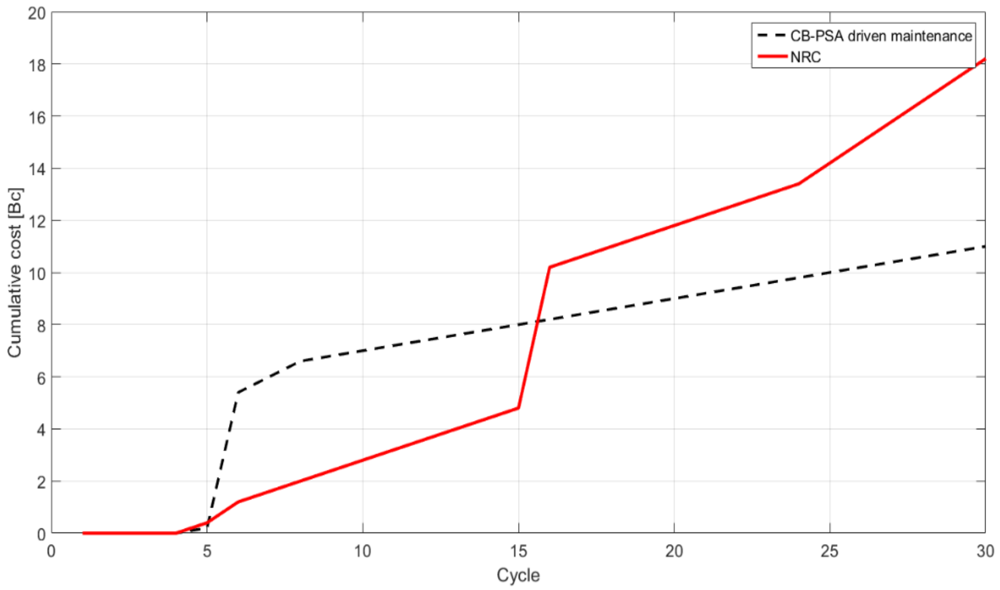

Figure 33: Comparison between the cumulative cost of maintenance in CB-PRA driven maintenance and NRC enforcement.

3.3.1. Sensitivity analysis

In this Section, we analyze the effects of different hypotheses of the cost model as summarized in Table 15.

Table 15: Different cost hypotheses

Maintenance type	Smallest cost	Average cost	Largest cost
WL-CC	5.0 B_c	7.5 B_c	10.0 B_c
Plugging more than 300 tubes in a cycle	0.6 B_c	0.8 B_c	1.0 B_c
Plugging less than 300 tubes in a cycle	0.2 B_c	0.35 B_c	0.5 B_c

A combination of 27 possible cost models are generated and used as hypotheses within the framework of maintenance decision making described in Section 3.2.

Figure 34 shows the cost of maintenance for the 27 cases. The Figure shows the ratio of the cumulative cost at cycle t ($\sum_{i=1}^{t} C(i)$) to the cumulative budget at cycle t ($B_c \times \sum_{i=1}^{t} i$). Generally speaking, it can be seen that the sooner WL-CC is performed the lower probability of SGTR failure due to pitting, although WL-CC is only affordable for 6 out of the 27 cost models at nearest eligible time which is cycle 6 (i.e., those with cheapest WL-CC cost equal to 5.0 B_c (solid lines)).

In particular, as shown in Figure 34, for two cases WL-CC is affordable at cycle 7 (diamond-lines), for one case at cycle 9 (green circled-lines), continuing postponing it (dashed lines), cycle by cycle, until the most expensive case where the WL-CC can be performed only at cycle 18 (line with crosses).

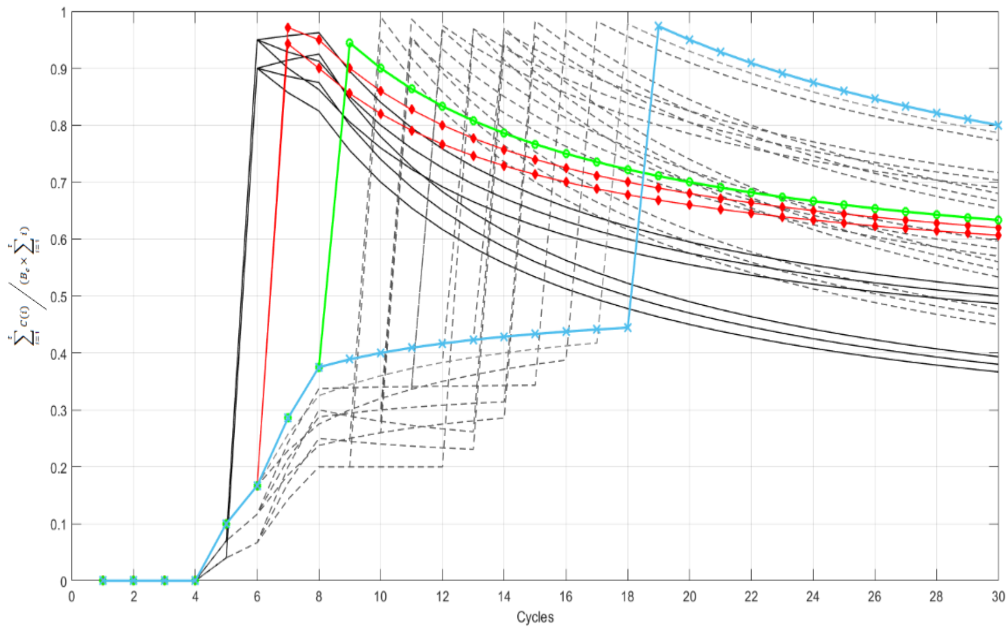

Figure 34: The ratio of the cumulative maintenance cost at each cycle t to the cumulative budget at each cycle t, for 27 cost scenarios.

The $CDF_{MD,P}$ values for different cost scenarios of Figure 34 are shown in Figure 35, with the same line styles in both Figures. The cheapest cost scenarios are related to the six cases where WL-CC is performed at cycle 6 with the solid line representing the lowest $CDF_{MD,P}$. In the remaining cases, since WL-CC is postponed due to shortage of funding, the SG is exposed to an increase of pitting-initiated SGTR scenarios and, consequently, $CDF_{MD,P}$ increases as shown in Figure 35: the diamond line represents the second cheapest two scenarios, the circled line represents the third cheapest one scenario and, finally, the crossed line represents the highest cost scenario, which also has the highest $CDF_{MD,P}$.

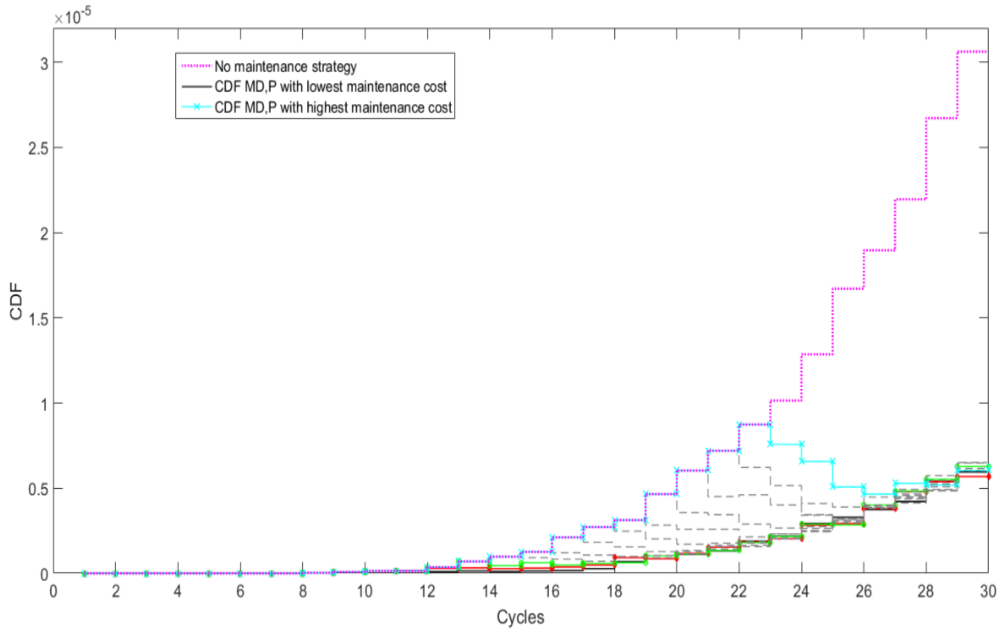

Figure 35: $CDF_{MD,P}$ values resulted from 27 maintenance cost scenarios

Figure 36 compares the cost of the NRC maintenance (solid lines) with that of our proposed method (dotted lines) in the 27 different cost scenarios, in terms of the ratio of the cumulative cost at cycle t ($\sum_{i=1}^{t} C(i)$) to the cumulative budget at cycle t ($B_c \times \sum_{i=1}^{t} i$). As it can be seen, in 12 out of 27 cases the NRC maintenance is not affordable because the available budget (dashed line) is exceeded. On the contrary, the proposed methodology manages the maintenance cost in all the possible cost scenarios.

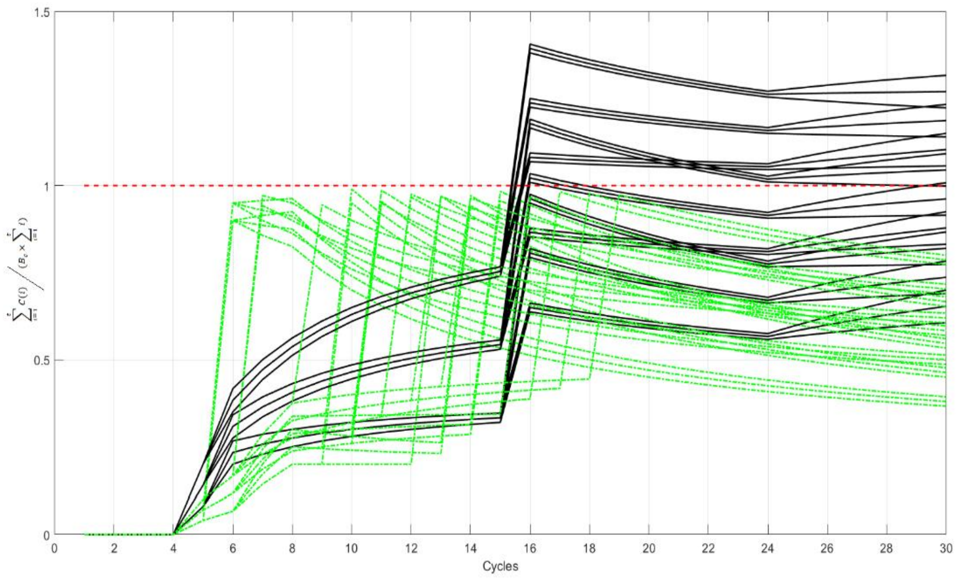

Figure 36: The ratio of the cumulative maintenance cost at each cycle t to the cumulative budget at each cycle t, for 27 cost scenarios using CB-PRA decision maintenance (dotted lines) and the NRC method (solid lines). Dashed line is the threshold when the costs exceed the budget.

Figure 37 shows the integral CDF of pitting and SCC. Only 3 out of 27 cases of very expensive maintenance costs (crossed line and two dashed lines) result in CDF values higher than for the NRC guided maintenance (dotted line), but this latter is not affordable (Figure 36). In all other cases, the total CDF is less than the NRC's value.

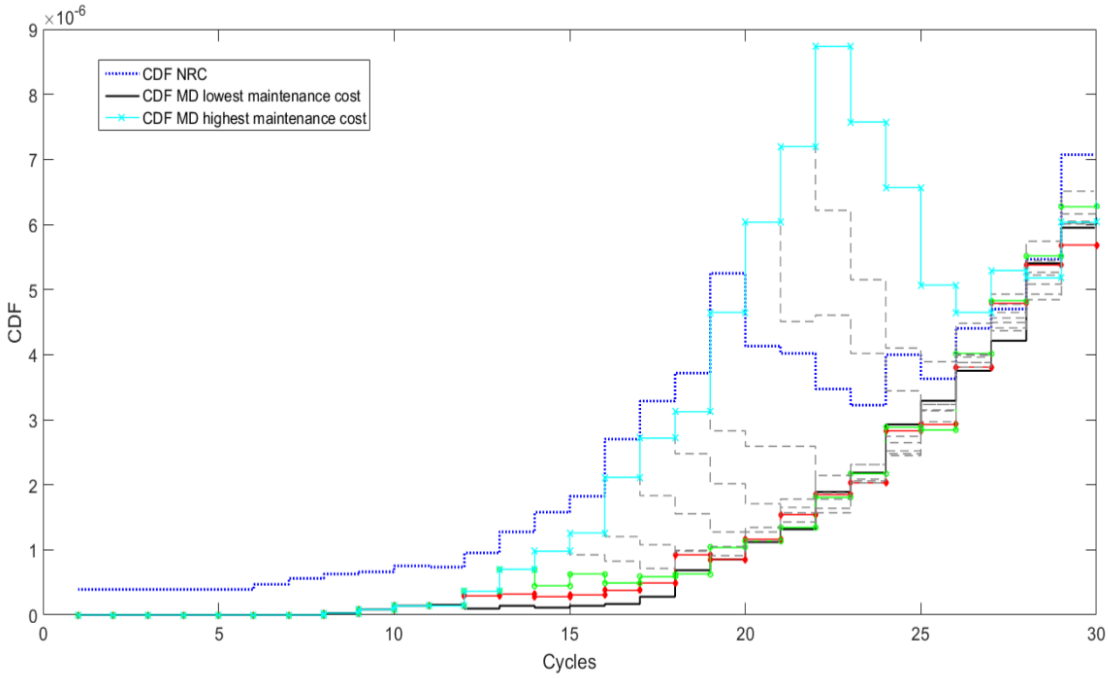

Figure 37: Comparison of CDF values of the NRC procedure with that of CB-PRA driven maintenance decisions in different cost scenarios.

3.4. Conclusions

In this chapter, optimal condition monitoring, obtained by the innovative approach of Chapter 2, is integrated in the systematic framework of PRA for updating accident probabilities and estimating their consequences based on the predicted degradation states. This allows a "living" prioritization of the risks that impact the lifecycle asset management in the short, middle, and long terms, and a proactive management of them by allowing the decision makers to take real-time decisions on the optimal maintenance strategy to prevent accidents and balance the maintenance budget expenditure. To show the methodology, the CB-PRA has been used to inform maintenance decisions (plugging and WL-CC) for controlling the risk of SGTR initiated by multiple degradation mechanisms, namely SCC and pitting.

Based on the results of the application on the case study of multiple SG tubes degradation mechanisms with Zion NPP parameters, it can be concluded that the proposed methodology can not only significantly reduce the risk of SGTR but also lower the maintenance cost.

4. CONCLUSIONS

This PhD thesis aims at introducing innovative solutions for condition-based risk-informed decision-making of energy facilities to provide a practical scheme for life extension assessment of SSCs. To this end, two different steps are identified to achieve this goal by computational approaches as described in Chapter 1 and are: 1. VoI-based data acquisition and 2. CB-PRA maintenance decision support.

Regarding VoI-based data acquisition, the issue of optimal sensor positioning for condition monitoring of aging SSCs of energy facilities is addressed by the development of VoI-based greedy and non-greedy optimization methods as well as by subset simulation approach. The pros and cons of each method in solving the problem of sensors positioning is practically presented with a case study of sensors positioning of a SG of PFBR degrading under creep. This will bring methodological and technical guidelines for cost-effective sensor positioning and data acquisition. equipment.

Firstly, the sensors positioning by the proposed greedy approach is presented and compared by the standards sensors positioning recommendations. It gives results that not only justify the positioning of the standard [52], but also require less sensors to reach the VoI_{UNI}. This can be used for developing guidelines to redeem the shortcomings that are inherent in relying on the past operational experience only, and essentially for the materials with limited past operational records.

The challenges of using greedy optimization for the VoI maximizing problems is discussed since VoI lacks the characteristic of sub-modularity. To overcome this, non-greedy optimization methods, like PSO and GA, are proposed which are not sensitive to the non-sub-modularity of the VoI. Results show that using the sensors positioning obtained by non-greedy methods not only yield better VoI, but also provides more accurate risk estimates while being computationally non-efficient and expensive.

The SS method which is typically used to find the failure probability of rare events is innovatively introduced to find the optimal sensors positioning. The proposed SS method not only does not have the greedy method's problem of the sensitivity to the non-sub-modularity of VoI but is also far more efficient than the non-greedy methods. The result of this computational work can be utilized to advance the process of data acquisition in safety related SSCs for a more profitable and reliable condition monitoring.

At the other hand, the optimal condition monitoring data, acquired as schemed in 1, can be used to estimate dynamic risk measures, by CB-PRA methodology, to provide advanced and realistic risk assessment. CB-PRA, an advanced and realistic risk assessment methodology, provides updated condition-based dynamic risk estimates of aging SSCs rather than the static risk estimates of traditional PRA. The outcome can be fed into 2 to enable condition-based risk-informed decision making.

With respect to CB-PRA maintenance decision support, in this PhD thesis, the optimal informative data provided by VoI-based data acquisition of 1 is used to address the issue of risk prioritization and maintenance decisions for multiple degradation mechanisms with cost constraints by developing computational methods for CB-PRA that provide condition-based dynamic risk estimates and cost assessment for maintenance decision-making by allowing the decision makers to take real-time decisions on the optimal maintenance strategy to prevent accidents and balance the maintenance budget expenditure.

To show the methodology, the SG of Zion NPP is selected, and the CB-PRA has been used to inform maintenance decisions (plugging and WL-CC) for controlling the risk of SGTR initiated by multiple degradation mechanisms, namely SCC and pitting. Based on the results, it can be concluded that the proposed methodology can not only significantly reduce the risk of SGTR but also lower the maintenance cost.

The outcome of this thesis with provided methodological and computational advancements, and will be useful for life extension of aging energy facilities and enables decision-making processes that are safer and cheaper.

SECTION III: REFERENCES

This Section lists all the references cited in Sections I and II of this PhD thesis.

[1] P. A. P. Ramírez and I. B. Utne, "Challenges due to aging plants," *Process Safety Progress* , vol. 30, no. 2, pp. 196-199, 2011.

[2] I. Dincer, "Renewable energy and sustainable development: a crucial review," *Renewable and sustainable energy reviews,* vol. 4, no. 2, pp. 157-175, 2000.

[3] M. Humayun, A. Safdarian, M. Z. Degefa and M. Lehtonen, "Demand response for operational life extension and efficient capacity utilization of power transformers during contingencies," *IEEE Transactions on Power Systems,* vol. 30, no. 4, pp. 2160-2169, 2014.

[4] T. Blaschke, M. Biberacher, S. Gadocha and I. Schardinger, "'Energy landscapes': Meeting energy demands and human aspirations," *biomass and bioenergy,* vol. 55, pp. 3-16, 2013.

[5] M. Shafiee and I. Animah, "Life extension decision making of safety critical systems: an overview," *Journal of Loss Prevention in the Process Industries,* vol. 47, pp. 174-188, 2017.

[6] B. R. Ellingwood, "Risk-informed condition assessment of civil infrastructure: state of practice and research issues," *Structure and infrastructure engineering* , vol. 1, no. 1, pp. 7-18., 2005.

[7] E. Zio, "Some challenges and opportunities in reliability engineering," *IEEE Transactions on Reliability,* vol. 65, no. 4, pp. 1769-1782., 2016.

[8] E. Zio, "Challenges in the vulnerability and risk analysis of critical infrastructures," *Reliability Engineering & System Safety,* vol. 152 , pp. 137-150, 2016.

[9] F. Di Maio, A. Rai and E. Zio, "A dynamic probabilistic safety margin characterization approach in support of Integrated Deterministic and Probabilistic Safety Analysis," *Reliability Engineering and System Safety,* vol. 145, pp. 9-16, 2016.

[10] A. Kamal, S. G. Al-Ghamdi and M. Koc, "Revaluing the costs and benefits of energy efficiency: A systematic review," *Energy Research & Social Science,* vol. 54, pp. 68-84, 2019.

[11] J. Xing, Z. Zeng and E. Zio, "A framework for dynamic risk assessment with condition monitoring data and inspection data," *Reliability Engineering & System Safety,* vol. 191, p. 106552, 2019.

[12] E. Zio, "The future of risk assessment," *Reliability Engineering & System Safety,* vol. 177 , pp. 176-190, 2018.

[13] M. Short and J. Twiddle, "An industrial digitalization platform for condition monitoring and predictive maintenance of pumping equipment," *Sensors,* vol. 19, no. 17, p. 3781, 2019.

[14] P. Baraldi, F. D. Maio, L. Pappaglione, E. Zio and R. Seraoui, "Condition Monitoring of Electrical Power Plant Components During Operational Transients," *Proceedings of the Institution of Mechanical Engineers, Part O: Journal of Risk and and Reliability, SAGE Publications,,* vol. 226, no. 6, pp. 568-583, 2012.

[15] Z. Tian, "An artificial neural network method for remaining useful life prediction of equipment subject to condition monitoring," *Journal of Intelligent Manufacturing,* vol. 23, no. 2, pp. 227-237, 2012.

[16] J. Xing, Z. Zeng and E. Zio, "Joint optimization of safety barriers for enhancing business continuity of nuclear power plants against steam generator tube ruptures accidents," *Reliability Engineering & System Safety,* p. 107067, 2020.

[17] N. Chen and K. L. Tsui, "Condition monitoring and remaining useful life prediction using degradation signals: Revisited," *IiE Transactions,* vol. 45, no. 9 , pp. 939-952, 2013.

[18] Z. Zeng and E. Zio, "Dynamic risk assessment based on statistical failure data and condition-monitoring degradation data," *IEEE Transactions on Reliability,* vol. 67, no. 2, pp. 609-622, 2018.

[19] Y. Wen, J. Wu and Y. Yuan, "Multiple-phase modeling of degradation signal for condition monitoring and remaining useful life prediction," *IEEE Transactions on Reliability,* vol. 66, no. 3, pp. 924-938, 2017.

[20] D. A. Dube, J. R. Chapman, K. R. Austgen and J. C. Butler, "Risk-informed prioritization of nuclear power plant issues and activities," in *International Topical Meeting on Probabilistic Safety Assessment and Analysis*, 2015.

[21] H. Kim, S.-h. Lee, J.-s. Park and H. Kim, "Reliability Data Update Using Condition Monitoring and Prognostics in Probabilistic Safety Assessment," vol. 47, pp. 204-2011, 2015.

[22] F. Di Maio, F. Antonello and E. Zio, "Condition-based probabilistic safety assessment of a spontaneous steam generator tube rupture accident scenario," *Nuclear Engineering and Design*, vol. 326, pp. 41-54, 2018.

[23] T. Aven and E. Zio, "Foundational issues in risk assessment and risk management," *Risk analysis,* vol. 34, no. 7, pp. 1164-1172, 2014.

[24] US-NRC, " PRA Procedures Guide, NUREG/CR-2300," U.S. Nuclear Regulatory Commission, Washington, DC, 1983.

[25] NRC, "Probabilistic Risk Assessment and Severe Accident Evaluation," US-NRC, California, 2011.

[26] US-NRC, "PRA Procedures Guide, NUREG/CR-2300," U.S. Nuclear Regulatory Commission, Washington, DC, 1983.

[27] P. Ramuhalli, A. Veeramany, C. A. Bonebrake, W. J. I. Jr., G. A. Coles and E. H. Hirt, "Evaluation of Enhanced Risk Monitors for Use on Advanced Reactors," in *ICONE 24*, Charlotte, USA, 2016.

[28] E. Zio, An introduction to the basics of reliability and risk analysis. Vol. 13., London: World scientific, 2007.

[29] NRC, "Reactor Safety Study: An assessment of accident risk in US commercial power plants (WASH-1400)," US Nuclear Regulatory Comission, Washington, DC, 1975.

[30] F. Di Maio, A. Rai and E. Zio, "A dynamic probabilistic safety margin characterization approach in support of Integrated Deterministic and Probabilistic Safety Analysis," *Reliability Engineering and System Safety,* vol. 145, pp. 9-16, 2016.

[31] R. Lewandowski, R. Denning, T. Aldemir and J. Zhang, "Implementation of condition-dependent probabilistic risk assessment using surveillance data on passive components," *Annals of Nuclear Energy ().,* vol. 87, pp. 1-11, 2016.

[32] W. Li, "Incorporating aging failures in power system reliability evaluation," *IEEE Transactions on Power systems* , vol. 17, no. 3, pp. 918-923, 2002.

[33] H. Kim, S.-h. Lee, J.-s. Park and H. Kim, "Reliability Data Update Using Condition Monitoring and Prognostics in Probabilistic Safety Assessment," *Nuclear Engineering and Technology,* vol. 47, pp. 204-211, 2015.

[34] J. B. Coble, G. A. Coles, R. M. Meyer and P. Ramuhalli, "Incorporating Equipment Condition Assessment in Risk Monitors for AdvSMRs," Pacific Northwest National Lab.(PNNL), Richland, WA, 2013.

[35] D. M. Frangopol and Mohamed Soliman, "Life-cycle of structural systems: recent achievements and future directions," *Structure and Infrastructure Engineering*, vol. 12, 2016.

[36] E. Zio, "Prognostics and health management of industrial equipment," in *Diagnostics and prognostics of engineering systems: methods and techniques* , 2012, pp. 333-356.

[37] M. Lehtonen, "On the optimal strategies of condition monitoring and maintenance allocation in distribution systems," in *International Conference on Probabilistic Methods Applied to Power Systems,* IEEE, 2006.

[38] A. K. Jardine, D. Lin and D. Banjevic, "A review on machinery diagnostics and prognostics implementing condition-based maintenance," *Mechanical systems and signal processing,* vol. 20, no. 7, pp. 1483-1510, 2006.

[39] V. Mallardo, M. H. Aliabadi and Z. S. Khodaei, "Optimal sensor positioning for impact localization in smart composite panels," *Journal of intelligent material systems and structures,* vol. 24, no. 5, pp. 559-573, 2013.

[40] A. Khalifeh, H. Abid and K. A. Darabkh, "Sensors," *Optimal cluster head positioning algorithm for wireless sensor networks,* vol. 20, no. 13, p. 3719, 2020.

[41] G. N. Rao, "In-service inspection and structural health monitoring for safe and reliable operation of NPPs," *Procedia Engineering,* vol. 86, pp. 476-485, 2014.

[42] P. Bhattacharyya and J. Beck, "Exploiting convexification for Bayesian optimal sensor placement by maximization of mutual information," *Structural Control and Health Monitoring,* vol. 27, no. 10, p. e2605, 2020.

[43] Y. Tan and L. Zhang, "Computational methodologies for optimal sensor placement in structural health monitoring: A review," *Structural Health Monitoring,* vol. 19, no. 4, pp. 1287-1308, 2020.

[44] P. Auerkari, T. B. Brown, S. Holdsworth, R. Hales, A. Klenk, R. Patel, A. Thomas, A. Tonti and T. Vilhelmsen, "Developments in assessing creep behaviour and creep life of components," *Materials at High Temperatures \,* vol. 21, no. 1, pp. 61-64, 2004.

[45] L. Bölöni, D. Turgut, S. Basagni and C. Petrioli, "Scheduling data transmissions of underwater sensor nodes for maximizing value of information," in *IEEE Global Communications Conference (GLOBECOM),* Atlanta, GA, 2013.

[46] P. Gjanci, C. Petrioli, S. Basagni, C. A. Phillips, L. Bölöni and D. Turgut, "Path Finding for Maximum Value of Information in Multi-Modal Underwater Wireless Sensor Networks," *IEEE Transactions on Mobile Computing,* vol. 17, no. 2, pp. 404-418, 2018.

[47] F. A. Khan, S. A. Khan, D. Turgut and L. Bölöni, "Greedy path planning for maximizing value of information in underwater sensor networks," in *39th Annual IEEE Conference on Local Computer Networks Workshops,* Edmonton, 2014.

[48] C. Malings and M. Pozzi, "Value of Information for Spatially Distributed Systems: application to sensor placement," *Reliability Engineering & System Safety,* vol. 154, pp. 219-233, 2016.

[49] H. Raiffa and R. Schlaifer, Applied Statistical Decision Theory, Harvard University, 1961.

[50] C. Bisdikian, L. M. Kaplan and M. B. Srivastava, "On the quality and value of information in sensor networks," *ACM Transactions on Sensor Networks (TOSN),* vol. 9, no. 4, p. 48, 2013.

[51] A. Krause, A. Singh and C. Guestrin, "Near-optimal sensor placements in Gaussian processes: Theory, efficient algorithms and empirical studies," *Journal of Machine Learning Research,* vol. 9, pp. 235-284, 2008.

[52] UNI 11096, "Non destructive testing - Structural integrity inspection of pressure equipment under creep condition - Inspection planning and execution, results evaluation and report," UNI Standard, Rome, 2012.

[53] C. Guestrin, A. Krause and A. P. Singh, "Near-optimal sensor placements in gaussian processes," in *22nd international conference on Machine learning,* ACM, 2005.

[54] J. Valls Miro, N. Ulapane, L. Shi, D. Hunt and M. Behrens, "Robotic pipeline wall thickness evaluation for dense nondestructive testing inspection," *Journal of Field Robotics,* vol. 35, no. 8, pp. 1293-1310, 2018.

[55] A. Krause, H. B. McMahan, C. Guestrin and A. Gupta, "Robust submodular observation selection," *Journal of Machine Learning Research,* vol. 9(Dec), pp. 2761-2801, 2008.

[56] C. Malings and M. Pozzi, "Submodularity issues in value-of-information-based sensor placement," *Reliability Engineering & System Safety* , vol. 183 , pp. 93-103, 2019.

[57] G. L. Nemhauser, L. A. Wolsey and M. L. Fisher, "An analysis of approximations for maximizing submodular set functions—I," *Mathematical programming* , vol. 14, no. 1, pp. 265-294, 1978.

[58] D. Diercks, W. Shack and J. Muscara, "Overview of steam generator tube degradation and integrity issues," *Nuclear Engineering and Design,* vol. 194 , p. 19–30, 1999.

[59] J. Riznic, Steam Generators for Nuclear Power Plants, Woodhead Publishing, 2017.

[60] EPRI, "Steam Generator Reference Book,," Electric Power Research Institute, Palo Alto, CA, 1996.

[61] IAEA, "Integrated approach to optimize operation and maintenance costs for operating nuclear power plants (IAEA-TECDOC-1509)," International Atomic Energy Agency , Vienna, Austria, 2006.

[62] IAEA, "Handbook on Ageing Management for Nuclear Power Plants," International Atomic Energy Agency, Vienna, 2017.

[63] K. C. Wade, "Steam Generator Degradation and Its Impact on Continued Operation of Pressurized Water Reactors in the United States," *Energy Information Administration,* 1995.

[64] EPRI, "Steam Generator Degradation Database (SGDD), Version 5.0," Electric Power Research Institute (EPRI), Palo Alto, CA., 2003.

[65] K. Karwoski, "Steam generator tube integrity requirements and operating experience in the United States," in *6th International CNS Steam Generator Conference*, US, 2009.

[66] NUREG/CR-6365, "Steam Generator Tube Failures," U.S National Regulatory Commission, Washington D.C., 1996.

[67] D. Straub, "Value of information analysis with structural reliability methods," *Structural Safety,* vol. 49 , pp. 75-85, 2014.

[68] S. Haladuick and M. R. Dann., "Value of information-based decision analysis of the optimal next inspection type for deteriorating structural systems," *Structure and Infrastructure Engineering,* vol. 14, no. 9, pp. 1283-1292, 2018.

[69] J. Kocijan, Modelling and control of dynamic systems using Gaussian process models, Springer International Publishing, 2016.

[70] A. Svensson, A. Solin, S. Särkkä and T. Schön, "Computationally efficient Bayesian learning of Gaussian process state space models," 2016.

[71] K. P. Murphy, " Conjugate Bayesian analysis of the Gaussian distribution," University of British Columbia, Vancouver, 2007.

[72] S. Das and P. Saha, "A review of some advanced sensors used for health diagnosis of civil engineering structures," *Measurement,* vol. 129, pp. 68-90, 2018.

[73] X. Bo, A. A. Razzaqi and G. Farid, "A Review on Optimal Placement of Sensors for Cooperative Localization of AUVs," *Journal of Sensors,* 2019.

[74] G. Gomes, F. de Almeida, D. Junqueira, S. da Cunha Jr and A. Ancelotti Jr, "Optimized damage identification in CFRP plates by reduced mode shapes and GA-ANN methods," *Engineering Structures,* vol. 181, pp. 111-123, 2019.

[75] S. Cantero-Chinchilla, J. Chiachío, M. Chiachío, D. Chronopoulos and A. Jones, "Optimal sensor configuration for ultrasonic guided-wave inspection based on value of information," *Mechanical Systems and Signal Processing,* vol. 135, p. 106377, 2020.

[76] D. Zonta, B. Glisic and S. Adriaenssens, "Value of information: impact of monitoring on decision-making," *Structural Control and Health Monitoring,* vol. 21, no. 7, pp. 1043-1056, 2014.

[77] D. R. Smith, Structured Decision Making: Case Studies in Natural Resource Management, Johns Hopkins University Press, 2020.

[78] A. A. Juan, J. Faulin, S. E. Grasman, M. Rabe and G. Figueira, "A review of simheuristics: Extending metaheuristics to deal with stochastic combinatorial optimization problems," *Operations Research Perspectives,* vol. 2, pp. 62-72, 2015.

[79] R. Qu, G. Kendall and N. Pillay, "The General Combinatorial Optimization Problem: Towards Automated Algorithm Design," *IEEE Computational Intelligence Magazine,* vol. 15, no. 2, pp. 14-23, 2020.

[80] M. S. Khorshidi, M. R. Nikoo, N. Taravatrooy, M. Sadegh, M. Al-Wardy and G. A. Al-Rawas, "Pressure sensor placement in water distribution networks for leak detection using a hybrid information-entropy approach," *Information Sciences,* vol. 516, pp. 56-71, 2020.

[81] C. Malings and M. Pozzi, "Value-of-information in spatio-temporal systems: Sensor placement and scheduling," *Reliability Engineering & System Safety,* vol. 172, pp. 45-57, 2018.

[82] S. M. Hoseyni, F. D. Maio and E. Zio, "VoI-Based Optimal Sensors Positioning and the Sub-Modularity Issue," Rome, Italy, 2019.

[83] J. H. Holland, "Genetic algorithms," *Scientific american,* vol. 267, no. 1, pp. 66-73, 1992.

[84] J. Kennedy and R. Eberhart, "Particle swarm optimization," 1995.

[85] V. Feoktistov, Differential evolution, Springer US, 2006.

[86] S.-K. Au and J. L. Beck, "Estimation of small failure probabilities in high dimensions by subset simulation," *Probabilistic engineering mechanics,* vol. 16, no. 4, pp. 263-277, 2001.

[87] H.-S. Li and Z.-J. Cao, "Matlab codes of Subset Simulation for reliability analysis and structural optimization," *Structural and Multidisciplinary Optimization* , vol. 54, no. 2, pp. 391-410, 2016.

[88] S.-K. Au and Y. Wang, Engineering risk assessment with subset simulation, John Wiley & Sons, 2014.

[89] F. Di Maio, S. M. Hoseyni and E. Zio, "Stima adattativa del rischio di rottura di componenti in pressione soggetti a creep con un approccio probabilistico," Bologna, 2018.

[90] ISPESL, "Technical Procedure Concerning Calculation and Tests to Act on Creep-Operated Pressure Vessel Components Circular N.48/2003, technical procedure issued in Italian," ISPESL, Department of Certification, Italy, 2003.

[91] NIMS, "NIMS Atlas of creep deformation property. No. D-1, Creep deformation properties of 9Cr1MoVNb steel for boiler and heat exchangers," Japanese National Institute for Materials Science, Tokyo, 2007.

[92] J. Storesund, L. Samuelson and B. Klasen, "Creep life assessment of pipe girth weld repairs with recommendations," *OMMI,* vol. 1, no. 3, 2002.

[93] S. M. Hoseyni, F. Di Maio and E. Zio, "Optimal Sensors Positioning for Condition-based Risk Assessment by Particle Swarm Optimization," Venice, 2020.

[94] M. Kloos and J. Peschke, "IDPSA approach to assess the potential of a thermally induced steam generator tube rupture," Pittsburgh; United States, 2017.

[95] M. Sattison and K. Hall, "Analysis of Core Damage Frequency: Zion, Unit 1 Internal Events," NUREG/CR-4550, SAND86-2084 Vol. 7, Rev. 1 Part 1., 1990.

[96] H. Kim, S.-H. Lee, J.-S. Park, H. Kim, Y.-S. Chang and G. Heo, "Reliability data update using condition monitoring and prognostics in probabilistic safety assessment," *Nuclear Engineering and Technology* , vol. 47, no. 2, pp. 204-2011, 2015.

[97] R. Lewandowski, R. Denning, T. Aldemir and J. Zhang, "Implementation of condition-dependent probabilistic risk assessment using surveillance data on passive components," *Annals of Nuclear Energy* , vol. 87, pp. 696-706, 2016.

[98] R. Lewandowski, "Incorporation of Corrosion Mechanisms into a State-dependent probabilistic risk assessment," The Ohio State university, Ohio, 2013.

[99] K. Chatterjee and M. Modarres, "A Probabilistic Physics of Failure Approach to Prediction of Steam Generator Tube Rupture Frequency," in *ANS PSA 2011 International Topical Meeting on Probabilistic Safety Assessment and Analysis*, Wilmington, NC, 2011.

[100] L. Cizelj, B. Mavko, R.-O. H. and A. Brücker-Foit, "Propagation of stress corrosion cracks in steam generator tubes," *International journal of pressure vessels and piping,* vol. 63, no. 1, pp. 35-43, 1995.

[101] A. Turnbull, L. N. McCartney and S. Zhou, "A model to predict the evolution of pitting corrosion and the pit-to-crack transition incorporating statistically distributed input parameters," *Corrosion Science,* vol. 48, no. 8, pp. 2084-2105, 2006.

[102] NUREG/CR-6664 , "Pressure and Leak-Rate Tests and Models for Predicting Failure of Flawed Steam Generator Tubes," US Nuclear Regulatory Commission (USNRC), 2000.

[103] P. Pla, F. Reventós, M. M. Ramos and I. Sol, "Analysis of steam generator tube plugging in A PWR. influence in the emergency operating procedures," in *22nd International Conference Nucleae energy for New Europe*, Slovenia, 2013.

[104] A. Valor, F. Caleyo, L. Alfonso, D. Rivas and J. Hallen, "Stochastic modeling of pitting corrosion: A new model for initiation and growth of multiple corrosion pits," *Corrosion Science* , vol. 49, p. 559–579, 2007.

[105] S. Ishihara, Z. Nan, A. McEvily, T. Goshima and S. Sunada, "On the initiation and growth behavior of corrosion pits during corrosion fatigue process of industrial pure aluminum," *International Journal of Fatigue*, vol. 30, no. 9, pp. 1659-1668, 2008.

[106] W. Navidi and Z. Shayer, "An application of stochastic modeling to pitting of Spent Nuclear Fuel canisters," *Progress in Nuclear Energy,* vol. 107, pp. 48-56, 2018.

[107] H. P. Hong, "Application of the stochastic process to pitting corrosion," .*Corrosion 55.1,* vol. 55, no. 1, pp. 10-16, 1999.

[108] S. V. Datla, M. I. Jyrkama and M. D. Pandey, "Probabilistic modelling of steam generator tube pitting corrosion," *Nuclear Engineering and Design* , vol. 238, p. 1771–1778, 2008.

[109] X.-X. Yuan, D. Mao and M. Pandey, "A Bayesian approach to modeling and predicting pitting flaws in steam generator tubes," *Reliability Engineering and System Safety,* vol. 94, p. 1838–1847, 2009.

[110] B. Zhou and Z. Zhai, "Failure probabilistic analysis of steam generator heat-transfer tubing with pitting corrosion," *Engineering Failure Analysis,* vol. 18, no. 5, pp. 1333-1340, 2011.

[111] L. Luo, Y. Huang, ShuoWeng and F.-Z. Xuan, "Mechanism-related modelling of pit evaluation in the CrNiMoV steel in simulated environment of low pressure nuclear steam turbine," *Materials and Design* , vol. 105, p. 240–250, 2016.

[112] P.J.Millett and C. Welty, "REVIEW of EPRI's steam generator R&D program," Electric Power Institute, Palo Alto, CA, 2012.

[113] P. R. Burgmayer, "Method of sludge removal in pressurized water nuclear reactors". Patent WO2001011935 A2, 22 Februaury 2001.

SECTION IV: PUBLICATIONS

This Section provides the papers related to this PhD research activity. The research activity has led to the acceptance (2), the submission (1) and the work in progress (1) of 4 manuscripts at international peer-reviewed journals and books (see Table 16), and the acceptance of 3 papers presented at the international academic conferences (see Table 17).

These publications which introduce the core techniques of this PhD thesis are attached in this Section.

Table 16: Publications in international peer-reviewed journals and books

No.	Title	Authors	Status
1[J]	Optimal sensor positioning on pressurized equipment based on value of information	S.M. Hoseyni, F. Di Maio, E. Zio	**Journal Article** – *Proceedings of the Institution of Mechanical Engineers, Part O: Journal of Risk and Reliability, January 2021, 1748006X21989661*
2[J]	Subset simulation for optimal sensors positioning based on value of information	S.M. Hoseyni, F. Di Maio, E. Zio	**Journal Article –** in progress
3[J]	Condition-based probabilistic safety assessment for maintenance decision making regarding a nuclear power plant steam generator undergoing multiple degradation mechanisms	S.M. Hoseyni, F. Di Maio, E. Zio	**Journal Article** - *Reliability Engineering and System Safety 191, November 2019, 106583*
1[B]	Stima adattiva del rischio di rottura di attrezzature in pressione, sulla base dei dati di monitoraggio.	F. Antonello, P. Bragatto, F. Di Maio, S.M. Hoseyni, E. Zio	**Book** – ISBN: 978-88-7484-174-5

Table 17: Publications in international conferences

No.	Title	Authors	Status
1[C]	Optimal Sensors Positioning for Condition-based Risk Assessment by Particle Swarm Optimization	S.M. Hoseyni, F. Di Maio, E. Zio	**Conference Proceeding**- *ESREL2020PSAM15*, Venice, 1,6 Nov. 2020
2[C]	VoI-Based Optimal Sensors Positioning and the Sub-Modularity Issue	S.M. Hoseyni, F. Di Maio, E. Zio	**Conference Proceeding** - *International Conference on System Reliability and Safety*, ICSRS, Rome, Nov. 2019
3[C]	Stima probabilistica del rischio di rottura di componenti in pressione soggetti a creep e monitoraggio continuo delle condizioni	F. Di Maio, S.M.. Hoseyni, E. Zio	**Conference Proceeding** - *SAFAP 2018- Sicurezza ed affidabilità delle attrezzature a pressione*, Bologna, Nov. 2018.

PAPER 1[J]: OPTIMAL SENSOR POSITIONING ON PRESSURIZED EQUIPMENT BASED ON VALUE OF INFORMATION

SAGE Publishing

Seyed Mojtaba Hoseyni, Francesco Di Maio, and Enrico Zio

Proceedings of the Institution of Mechanical Engineers, Part O: Journal of Risk and Reliability, January 2021, 1748006X21989661

https://doi.org/10.1177%2F1748006X21989661

PAPER 2[J]: SUBSET SIMULATION FOR OPTIMAL SENSORS POSITIONING BASED ON VALUE OF INFORMATION

Seyed Mojtaba Hoseyni, Francesco Di Maio, and Enrico Zio

In progress

PAPER 3[J]: CONDITION-BASED PROBABILISTIC SAFETY ASSESSMENT FOR MAINTENANCE DECISION MAKING REGARDING A NUCLEAR POWER PLANT STEAM GENERATOR UNDERGOING MULTIPLE DEGRADATION MECHANISMS

ScienceDirect

Seyed Mojtaba Hoseyni, Francesco Di Maio, and Enrico Zio

Reliability Engineering and System Safety 191, November 2019, 106583
https://doi.org/10.1016/j.ress.2019.106583

BOOK 1[B]: STIMA ADATTIVA DEL RISCHIO DI ROTTURA DI ATTREZZATURE IN PRESSIONE, SULLA BASE DEI DATI DI MONITORAGGIO.

Federico Antonello, Paolo Bragatto, Francesco Di Maio, Seyed Mojtaba Hoseyni, and Enrico Zio

ISBN 978-88-7484-174-5

https://www.researchgate.net/publication/338079072_Stima_adattiva_del_rischio_di_rottura_di_attrezzature_in_pressione_sulla_base_dei_dati_di_monitoraggio

PAPER 1[C]: OPTIMAL SENSORS POSITIONING FOR CONDITION-BASED RISK ASSESSMENT BY PARTICLE SWARM OPTIMIZATION

Seyed Mojtaba Hoseyni, Francesco Di Maio, and Enrico Zio

In the 30th European Safety and Reliability Conference and 15th Probabilistic Safety Assessment and Management Conference (ESREL2020 PSAM15)

Venice, Italy, 1–5 November 2020

 E-proceedings of the 30th European Safety and Reliability Conference and 15th Probabilistic Safety Assessment and Management Conference (ESREL2020 PSAM15)

Editors: Piero Baraldi, Francesco Di Maio and Enrico Zio

ISBN: 978-981-14-8593-0

https://www.rpsonline.com.sg/proceedings/esrel2020/pdf/5146.pdf

PAPER 2[C]: THE SUB-MODULARITY ISSUE WITH VOI-BASED OPTIMAL SENSORS LOCATION IDENTIFICATION

Seyed Mojtaba Hoseyni, Francesco Di Maio, and Enrico Zio

IEEE Xplore® Digital Library

In the 4th International Conference on System Reliability and Safety, ICSRS
Rome, Italy, November 2019

DOI: 10.1109/ICSRS48664.2019.8987650

PAPER 3[C]: STIMA PROBABILISTICA DEL RISCHIO DI ROTTURA DI COMPONENTI IN PRESSIONE SOGGETTI A CREEP E MONITORAGGIO CONTINUO DELLE CONDIZIONI

Francesco Di Maio, Seyed Mojtaba Hoseyni, and Enrico Zio

In the *SAFAP 2018- Sicurezza ed affidabilità delle attrezzature a pressione*
Bologna, Italy, 28-29 November 2018
Pages 14-20

 Proceedings of the SAFAP 2018

Editors: Francesca Ceruti, Daniela Gaetana Cogliani

ISBN: 978-88-7484-139-4

[This page intentionally left blank.]

POLITECNICO DI MILANO
DIPARTIMENTO DI ENERGIA

POLITECNICO MILANO 1863

ARCHIVES
AND LIBRARY SYSTEM